FACULTY
OF MATHEMATICS
AND PHYSICS
Charles University

MASTER THESIS

Filip Klimovič

Terahertz Radiation in Nanostructures

Department of Chemical Physics and Optics

Supervisor of the master thesis: doc. RNDr. Tomáš Ostatnický, Ph.D.

Study programme: Physics

Study branch: Optics and Optoelectronics

Prague 2019

I declare that I carried out this master thesis independently, and only with the cited sources, literature and other professional sources.

I understand that my work relates to the rights and obligations under the Act No. 121/2000 Sb., the Copyright Act, as amended, in particular the fact that the Charles University has the right to conclude a license agreement on the use of this work as a school work pursuant to Section 60 subsection 1 of the Copyright Act.

In Prague on 3 January 2019   signature of the author

Title: Terahertz Radiation in Nanostructures

Author: Filip Klimovič

Department: Department of Chemical Physics and Optics

Supervisor: doc. RNDr. Tomáš Ostatnický, Ph.D., Department of Chemical Physics and Optics

Abstract: In this theoretical work, we study quantum mechanical phenomena exhibited by electrons confined in nanocrystals. First, a model of quantum dots as potential wells is derived. We argue that only the volume, not shape, is a significant parameter of the model in scope of terahertz spectroscopy. The studied geometries are interchangeable and we may choose among them in order to simplify given problems to solve. Then we choose the spherical symmetry for investigating depolarization effects, which are reflected in Maxwell Garnett effective medium theory by a depolarization factor. Within the first order perturbation, Poisson's equation is solved for electrons distributed according to wavefunction. We show that while reproducing the same value in the classical limit, the depolarization factor increases for nanocrystals. Maximum is reached in non-degenerate regime when only the ground state is occupied. Increasing the depolarization factor shifts plasmonic resonances towards higher frequencies.

Keywords: terahertz conductivity, quantum dot, depolarization factor, effective medium theory

I would like to express my sincere thanks and gratitude to Dr. Tomáš Ostatnický for his patience and very kind supervision of my thesis.

Acknowledged should be the UNESCO's promotions during the International Year of Light 2015 that strengthened my decision to pursue my master studies in the field of optics and optoelectronics.

I would like to thank to my relatives and close friends for their support.

Contents

Table of constants

$e = 1.602 \times 10^{-19}$ C .... elementary charge

$m_0 = 9.109 \times 10^{-31}$ kg .... free electron rest mass

$\varepsilon_0 = 8.854 \times 10^{-12}$ F m^{-1} .... vacuum permittivity

$\hbar = 6.582 \times 10^{-16}$ eV s rad^{-1} .... reduced Planck's constant

$k_B = 8.61733 \times 10^{-5}$ eV K^{-1} .... Boltzmann's constant

1 eV $= e$ J C$^{-1} = 1.602 \times 10^{-19}$ J .... one *electronvolt*, unit of energy

General notation

The upper index asterisk * denotes complex cojugation.

Symbol c.c. stands for a complex conjugate term.

The hat ˆ sign indicates an operator.

The imaginary unit $\sqrt{-1}$ is represented by symbol i.

1. Introduction

Introduction to THz conductivity

Terahertz spectroscopy is a rapidly developing field over the last decades thanks to novel materials and techniques that allow for better generation and detection of terahertz pulses. It can provide us with great amounts of information on phenomena concerning charge transport on nanometric distances, LLOYD-HUGHES AND JEON [1]. The electron scattering rate in solids is often higher than the probing field frequency around 1 THz $\sim$ 4.1 meV or in multiterahertz spectral ranges. Quantum dots and various other semiconductor nanostructures are under investigation for their potential to be at the core of nanoelectronic devices. However corresponding theoretical models of microscopic conductivity are far behind experimental obtaining of complex permittivity spectra. Far-field terahertz spectroscopy is a potent method for probing large ensembles of nanostructures, NĚMEC ET AL. [2]. In such case, one obtains spectra proprietary to the effective material parameters of the composite materials. Microscopic theories to fully describe and explain all phenomena are yet to be derived.

Objectives

We are interested in theoretical models for effective permittivity of a composite material in the THz spectral range. The main aim of our work is to address the depolarization effects in semiconductor nanostructures with quantum mechanical approach, for classical electrostatics don't apply. We do two major changes to the classical approach:

- We use quantum mechanical formula for the microscopic conductivity of the nanoparticles within linear response regime instead of bulk Drude conductivity.

- We look closely at expressions for the local field inside the nanoparticles within the quantum perturbation theory.

In Part one of our work, we summarize relevant theoretical background. We give the basic quantum mechanical formalism we use throughout the work and we present the classical effective medium theory for composite materials.

In Part two, we address the geometry of our model of nanoparticles. We compare asymptotic behaviour of density of states, of dipole moments and conductivity spectra for cubic and spherical geometries. We show that while not equivalent, the geometries are interchangeable in the scope of THz spectroscopy, as long as we keep volume the same. This is handy for solving different problems.

In Part three, we apply the first order perturbation theory in order to find the electric field generated by electrons displaced by the external field as a perturbation. We recreate the self-consistent condition for a local electric intensity inside spherical nanoparticles. Based on that, we derive the depolarization factor, whose values differ from those given by the classical electrostatics. The depolarization factor is an important element in the effective medium approximation.

Part I

Theoretical Background

2. Quantum Mechanics Formalism

In this chapter sumarize the general description of interaction of electrons with external electromagnetic radiation and we give a basic model of nanostructures. First we address density of states and distribution of electrons over the energy levels. Then we derive the semi-classical interaction hamiltonian within the dipole approximation. We find first order perturbation stationary states of density matrix of the system and we inspect its response to the electric field within linear response formalism.

2.1 Electron states

Possible quantum-mechanical states $|k\rangle$ of the system and their energy are found by solving the time-independent Schrödinger equation. That is finding the eigensystem of the hamiltonian $\hat{\mathcal{H}}$ of an electron in the nanostructure.

$$\hat{\mathcal{H}}|k\rangle = \mathcal{E}_k|k\rangle \tag{2.1}$$

Due to confinement of the electrons, we assume a discrete spectrum of bound single-electron states. The energy of state $|k\rangle$ is $\mathcal{E}_k = \hbar\omega_k$. The form of the hamiltonian is

$$\hat{\mathcal{H}} = \frac{\hat{p}^2}{2m} + V(\mathbf{r}) \tag{2.2}$$

within the effective mass approximation and $V(\mathbf{r})$ is the potential confining the electron.

Occupation of states

The electrons are fermions and as such, they obey the Pauli exclusion principle. The equilibrium or *thermal* distribution of the electrons over the energy levels follows the Fermi-Dirac statistics, see e.g. CALLEN [3]. The occupation of a state with energy $\mathcal{E}$ is given by

$$f(\mathcal{E}, \mu_F, T) = \frac{1}{\mathrm{e}^{\frac{\mathcal{E}-\mu_F}{k_B T}} + 1} \tag{2.3}$$

where μ_F is the chemical potential, in semiconductor science often called the *Fermi level*, and T is the absolute temperature.

The total number of particles in the system can be formally expressed as

$$N = \int_{-\infty}^{+\infty} f(\mathcal{E}, \mu_F, T) n(\mathcal{E}) \, \mathrm{d}\mathcal{E} \tag{2.4}$$

where $n(\mathcal{E})$ is the density of states or explicitly for discrete levels

$$N = \sum_{\text{states } k} f_k = \sum_{\text{levels } l} g_l f_l \tag{2.5}$$

for f_k and f_l denote $f(\mathcal{E}_k, \mu_F, T)$, $f(\mathcal{E}_l, \mu_F, T)$ respectively and g_l is the degeneracy factor of the level $\mathcal{E}_l$, due to which we must distinguish between levels and states. The spin degeneracy factor of 2 is included in the summation over all of the states k and in the degeneracy factor g_l.

Suppose a certain density of carriers is injected e.g. by photoexcitation by a pump of controlled intensity into the system. In order to accommodate a given number of electrons N in the quantum dot, one needs to solve the implicit equation (2.5) for the chemical potential μ_F. For this purpose, numerical methods are employed.

2.2 Dynamics of the system

We apply external electric field to the system. The interaction strength between the system and magnetic part of the electromagnetic radiation is of lower order of magnitude. We suppose that the electric field doesn't affect the original system substantially, i.e. the system retains the structure of energy levels and the interaction with the external field can be viewed as a perturbation.

Interaction hamiltonian

We follow MARDER [4]. The hamiltonian of minimal coupling[1]is

$$\hat{\mathcal{H}} = \frac{(\hat{\mathbf{p}} - e\mathbf{A})^2}{2m} + V(\mathbf{r}) \tag{2.6}$$

where $\hat{\mathbf{p}}$ is the momentum operator and $\mathbf{A}$ is the vector potential of the field. By performing the second power we obtain

$$\hat{\mathcal{H}} = \frac{\hat{p}^2}{2m} + V(\mathbf{r}) - \frac{e}{2m}\left(\hat{\mathbf{p}} \cdot \mathbf{A} + \mathbf{A} \cdot \hat{\mathbf{p}}\right) - \frac{e^2 A^2}{2m} \tag{2.7}$$

The first two terms on the right hand side form the hemiltonian $\hat{\mathcal{H}}_0$ of the unperturbed system. The rightmost term is of second order in the perturbation $\propto A^2$ and therefore can be neglected. We choose the x-representation to further simplify the rest. The momentum operator is $\hat{\mathbf{p}} = -i\hbar\nabla$. Hence

$$
\begin{aligned}
\left(\hat{\mathbf{p}} \cdot \mathbf{A} + \mathbf{A} \cdot \hat{\mathbf{p}}\right)\psi(\mathbf{r}) &= -i\hbar\left(\nabla \cdot \mathbf{A}\psi(\mathbf{r}) + \mathbf{A} \cdot \nabla\psi(\mathbf{r})\right) \\
&= -i\hbar\left[\left(\nabla \cdot \mathbf{A}\right)\psi(\mathbf{r}) + 2\mathbf{A} \cdot \nabla\psi(\mathbf{r})\right] \\
&= 2\mathbf{A} \cdot \hat{\mathbf{p}}\ \psi(\mathbf{r})
\end{aligned} \tag{2.8}
$$

In the last step we exploited the Coulomb calibration of the vector potential $\nabla \cdot \mathbf{A} = 0$. The hamiltonian is now

$$\hat{\mathcal{H}} = \hat{\mathcal{H}}_0 - \frac{e}{m}\mathbf{A} \cdot \hat{\mathbf{p}} \tag{2.9}$$

The electric field intensity $\mathbf{E}$ is given by

$$\mathbf{E} = -\frac{\partial \mathbf{A}}{\partial t} - \nabla\Phi \tag{2.10}$$

---

[1]The hamiltonian of interaction does not account for non-zero spin effects.

Let us suppose the gradient of the scalar potential Φ is zero and a harmonic time dependence of the field $\mathbf{E} = \widetilde{\mathbf{E}} e^{-i\omega t} + \text{c.c.}$ and $\mathbf{A} = \widetilde{\mathbf{A}}_0 e^{-i\omega t} + \text{c.c.}$ with $\widetilde{\mathbf{E}}$ and $\widetilde{\mathbf{A}}$ constant amplitudes. Therefore $\mathbf{A} = -\frac{i}{\omega}\mathbf{E}$ which leads to

$$\hat{\mathcal{H}} = \hat{\mathcal{H}}_0 + \frac{ie}{m\omega}\left(\widetilde{\mathbf{E}} \cdot \hat{\mathbf{p}}\, e^{-i\omega t} - \text{c.c.}\right) \tag{2.11}$$

The matrix elements of the hamiltonian are

$$\left\langle f \left| \hat{\mathcal{H}} \right| i \right\rangle = \left\langle f \left| \hat{\mathcal{H}}_0 \right| i \right\rangle + \frac{ie}{m\omega}\left(\left\langle f \left| \widetilde{\mathbf{E}} \cdot \hat{\mathbf{p}} \right| i \right\rangle e^{-i\omega t} - \text{c.c.}\right) \tag{2.12}$$

We consider the field homogeneous on a scale larger than the entire quantum dot. For the interaction is strictly local, we may apply the *dipole approximation*:

$$\left\langle f \left| \widetilde{\mathbf{E}} \cdot \hat{\mathbf{p}} \right| i \right\rangle = \widetilde{\mathbf{E}} \cdot \left\langle f \left| \hat{\mathbf{p}} \right| i \right\rangle \tag{2.13}$$

It can be shown that

$$-\frac{i\hbar}{m}\left\langle f \left| \hat{\mathbf{p}} \right| i \right\rangle = \left\langle f \left| \left[\hat{\mathcal{H}}_0, \mathbf{r}\right] \right| i \right\rangle = \frac{\hbar\omega_{fi}}{e}\left\langle f \left| e\mathbf{r} \right| i \right\rangle \tag{2.14}$$

where square brackets $\left[\hat{\alpha}, \hat{\beta}\right]$ denote a commutator of operators $\hat{\alpha}$ and $\hat{\beta}$. ω_{fi} stands for $\omega_f - \omega_i$. The hamiltonian elements can be expressed as

$$\left\langle f \left| \hat{\mathcal{H}} \right| i \right\rangle = \hbar\omega_i \delta_{fi} - \frac{\omega_{fi}}{\omega}\left\langle f \left| e\mathbf{r} \right| i \right\rangle \cdot \widetilde{\mathbf{E}} e^{-i\omega t} \tag{2.15}$$

We also applied the *rotating wave approximation*, eliminating the complex conjugate term oscillating on high frequencies of $\omega + \omega_{fi}$ compared to the frequencies $\omega - \omega_{fi}$ of the term we are left with. The unperturbed hamiltonian $\hat{\mathcal{H}}_0$ is diagonal in the eigenstates basis, as expressed by the Kronecker delta symbol δ_{fi}. The interaction hamiltonian is off-diagonal in such basis. The bra-ket $\left\langle f \left| -e\mathbf{r} \right| i \right\rangle$ is called the *dipole moment* for transitions of electrons between states $|i\rangle$ and $|f\rangle$.

Density matrix

The density matrix $\hat{\rho}$, also called the statistical operator, is used to describe a quantum system in a *mixed state*. An expectation value of an operator $\hat{A}$ over the entire system is calculated using the density matrix

$$\left\langle \hat{A} \right\rangle = \text{Tr}\left(\hat{\rho}\hat{A}\right) \tag{2.16}$$

by evaluating the trace of their product. For instance the total number of particles in the system is $N = \text{Tr}\,\hat{\rho}$.

The equation of motion for the density matrix is given by the Liouville-von Neumann equation

$$i\hbar\frac{\partial\hat{\rho}(t)}{\partial t} = \left[\hat{\mathcal{H}}(t), \hat{\rho}(t)\right] \tag{2.17}$$

Let us define the hamiltonian and the density matrix of the system responding to external field in the following way: $\hat{\mathcal{H}} = \hat{\mathcal{H}}_0 + \hat{\mathcal{H}}_{\text{int}}$ and $\hat{\rho} = \hat{\rho}_0 + \hat{\rho}_1$, where index 'int' stands for interaction and the 1 for the first order perturbation term[2]. We may then expand the commutator in eq. (2.17) as

$$\left[\hat{\mathcal{H}}, \hat{\rho}\right] = \left[\hat{\mathcal{H}}_0, \hat{\rho}_0\right] + \left[\hat{\mathcal{H}}_{\text{int}}, \hat{\rho}_0\right] + \left[\hat{\mathcal{H}}_0, \hat{\rho}_1\right] + \left[\hat{\mathcal{H}}_{\text{int}}, \hat{\rho}_1\right] \tag{2.18}$$

The rightmost term is of the second order of magnitude of the perturbation and will be neglected henceforth.

The density matrix of the system in thermal equilibrium, which is an incoherent mixture of states, is

$$\hat{\rho}_0 = \sum_{\text{states } k} f_k \, |k\rangle\langle k| \tag{2.19}$$

Within the perturbation theory the occupation of states doesn't change over time and for the equilibrium part of the density matrix holds $\frac{\partial}{\partial t}\hat{\rho}_0 = 0$. Therefore we are left with the equation of motion for the first order perturbation:

$$\frac{\partial \hat{\rho}_1(t)}{\partial t} = -\frac{i}{\hbar}\left[\hat{\mathcal{H}}_{\text{int}}(t), \hat{\rho}_0(t)\right] - \frac{i}{\hbar}\left[\hat{\mathcal{H}}_0(t), \hat{\rho}_1(t)\right] - \gamma\hat{\rho}_1(t) \tag{2.20}$$

where the last term represents a relaxation of correlation or a *thermalization* of the system. $\gamma = 1/\tau$ is the dephasing rate, τ being the relaxation time. The relaxation mechanism was not included in the hamiltonian, so it must have been introduced to the Liouville-von Neumann equation *a posteriori*.

The formal solution is

$$\hat{\rho}_1(t) = \frac{1}{i\hbar} \int_{-\infty}^{+\infty} \Theta(t - t') \left\{ \left[\hat{\mathcal{H}}_{\text{int}}(t'), \hat{\rho}_0(t')\right] + \left[\hat{\mathcal{H}}_0(t'), \hat{\rho}_1(t')\right] - i\hbar\gamma\hat{\rho}_1(t') \right\} \mathrm{d}t' \tag{2.21}$$

where $\Theta(t - t')$ is the Heaviside step function to preserve the causality. The explicit stationary solution to the equation of motion for the correlation part of the density matrix within the first order perturbation theory is

$$\boxed{(\hat{\rho}_1)_{kl}(t) = \frac{f_{kl}}{\hbar}\frac{\langle k \,|e\mathbf{r}|\, l\rangle \cdot \widetilde{\mathbf{E}}\mathrm{e}^{-i\omega t}}{\omega - \omega_{kl} + i\gamma}\, |k\rangle\langle l|} \tag{2.22}$$

where f_{kl} stands for the difference in occupation of the two states in terms of the Fermi-Dirac distribution function $f_{kl} = f(\hbar\omega_k) - f(\hbar\omega_l)$.

2.3   Electric conductivity

Within the linear response regime, we study the material by probing it using external (e.g. electric) field of sufficiently weak intensity, so that it doesn't alter the material's properties under investigation. Throughout the derivation below, we follow Pushkarev et al. [5] and apply first order perturbation theory.

The (linear) electric conductivity $\boldsymbol{\sigma}$ is defined by the Ohm's law as follows:

$$\mathbf{j} = \boldsymbol{\sigma} \cdot \mathbf{E} \tag{2.23}$$

or explicitly in components:

$$j_\lambda(\omega) = \sum_{\mu=1}^{3} \sigma_{\lambda\mu}(\omega) E_\mu(\omega) \tag{2.24}$$

---

[2]We suppose the probing terahertz pulse doesn't affect the equilibrium distribution of electrons over states k. The perturbation term is off-diagonal, describing *correlation*.

where $\mathbf{j}$ is the electric current density and $\mathbf{E}$ the electric intensity. Due to the vectorial character of both $\mathbf{j}$ and $\mathbf{E}$ the conductivity is a second rank tensor. Within the first order perturbation theory the current density is

$$j_\lambda(\omega) = -\frac{e}{V}\frac{\partial}{\partial t}\langle x_\lambda \rangle = -\frac{e}{V}\frac{\partial}{\partial t}\operatorname{Tr}\left(\hat{\rho}_1 x_\lambda\right) \tag{2.25}$$

Recalling the explicit solution to the Liouville-von Neumann equation (2.22), we can evaluate the trace:

$$j_\lambda(\omega) = -\frac{e}{V}\frac{\partial}{\partial t}\sum_{n,k,l}\langle n|k\rangle\,\frac{f_{kl}}{\hbar}\frac{\langle k\,|e\mathbf{r}|\,l\rangle \cdot \widetilde{\mathbf{E}}\mathrm{e}^{-i\omega t}}{\omega - \omega_{kl} + i\gamma}\,\langle l\,|x_\lambda|\,n\rangle \tag{2.26}$$

By the orthogonality relation $\langle n|k\rangle = \delta_{nk}$ and performing the derivative we get

$$j_\lambda(\omega) = \frac{i\omega e}{V}\sum_{k,l}\frac{f_{kl}}{\hbar}\frac{\langle k\,|e\mathbf{r}|\,l\rangle \cdot \widetilde{\mathbf{E}}\mathrm{e}^{-i\omega t}}{\omega - \omega_{kl} + i\gamma}\,\langle l\,|x_\lambda|\,k\rangle \tag{2.27}$$

In order to obtain the conductivity components, we apply a projector $\hat{P}_\mu$ in the direction of μ to the vectors on the right side and divide the current by electric intensity $\sigma = j/E$.

$$\sigma_{\lambda\mu}(\omega) = \frac{i\omega e^2}{V}\sum_{k,l}\frac{f_{kl}}{\hbar}\frac{\left\langle k\,|x_\mu|\,l\right\rangle\left\langle l\,|x_\lambda|\,k\right\rangle}{\omega - \omega_{kl} + i\gamma} \tag{2.28}$$

Within the linear response regime, the response function (conductivity in this case) depends only on the properties of the material. It does not depend on any external fields. We see the dipole moments are of crucial importance to the electric conductivity.

2.4 Quantum dots

Semiconductor nanostructures are heterostructures of semiconductor materials whose characteristic scale is nanometric in at least one or up to all three dimensions. In this work, we address the elementary type of nanostructures: single nanocrystals, also called nanoparticles or *quantum dots.*

Charge carriers are confined in such structures on scales which are typically smaller than Bohr radius of an exciton. This leads to so called *strong confinement regime* where quantum properties of electrons broadly manifest. In particular, we need to take into account the quantization of energy of the electron, as the band structure breaks into discrete levels. In this regime we can also neglect the Coulomb interaction between the electron and a hole within the exciton and we can look at the electron in the nanocrystal as a particle subjected only to the confining potential $V(\mathbf{x})$. Let us choose a form of a rectangular potential well, see fig. 2.1. Geometry and potential barrier height of the well will be addressed later.

We will neglect the holes in the valence band. We assume the holes' effective mass is of higher order than that of an electron and hence the holes can be ignored
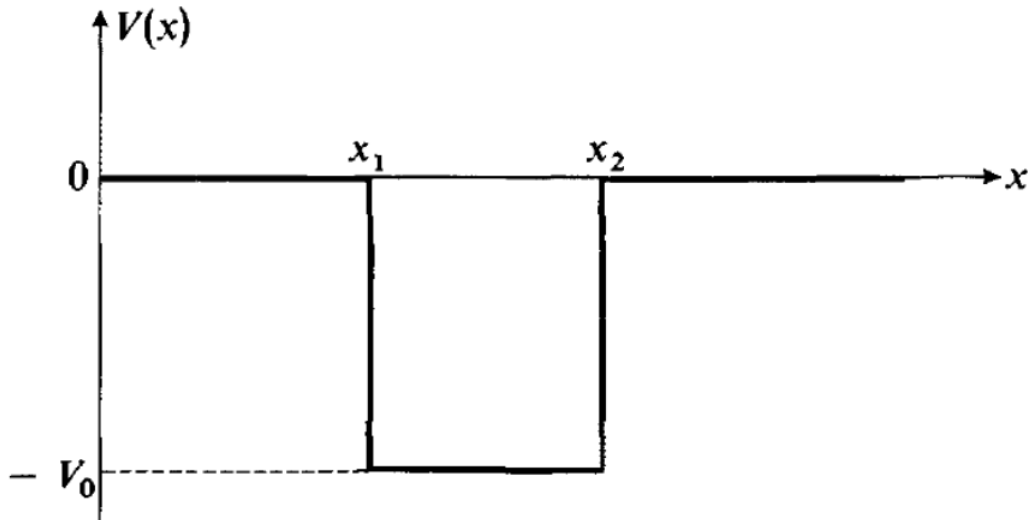
Figure 2.1: A scheme of a one-dimensional potential well. From
Cohen-Tannoudji et al. [6].

completely or described by classical models. However, the primary reason here is
simplicity. One can handle electrons and holes as two separate systems and add
their contributions afterwards.

We choose GaAs as an example of a semiconductor material with direct band
gap. The dispersion in the near vicinity of the Γ-point allows for the effective mass
approximation. Other qualities of the material include high conductivity among
semiconductors and its general accessibility for experimental measurements. For
the relevant material properties of GaAs refer to tab. 2.1.

property	value
relative permittivity (static)	$\varepsilon_r = 12.85$
electron effective mass	$m_e^* = 0.067\, m_0$
hole effective mass	$m_h^* = 0.47\, m_0$
el. momentum scattering time	$\tau = 270$ fs
electron mobility (bulk)	$\mu_0 = 7200$ cm^2 V^{-1} s^{-1}

Table 2.1: Relevant material properties of GaAs. From Chelikowsky and
Louie [7].

3. Effective Medium Theory

A composite medium is a structure of either metal or dielectric inclusions in a dielectric matrix. The electromagnetic field inside the inclusions can be considered as homogeneous due to the characteristic dimensions much smaller than applicable radiation wavelengths. It was shown by Maxwell Garnett that such medium can be described by an effective dielectric function, see GARNETT [8]. Other *effective medium approximations* are represented e.g. by Bruggeman's model BRUGGEMAN [9] for percolated mixtures. In this chapter we summarize the classical approach to composite materials adopting Maxwell Garnett's mixing formula.

3.1 Effective permittivity

We consider a composite medium made of semiconductor inclusions which are not percolated and are sparsely distributed in a dielectric matrix with the permittivity ε_d. The semiconductor is undoped, i.e. in the *ground state* it is characterized by a real frequency-independent permittivity ε_s in the THz spectral range. The effective permittivity ε_g of the composite can be found as a function of the *filling fraction f*, i.e. the portion of total volume occupied by the inclusions.

Let $\mathbf{E}_s$ be local electric intensity inside the semiconductor inclusions and $\mathbf{E}_d$ intensity in the dielectric matrix. We suppose the materials are isotropic. From the constitutive relation for mean electric induction $\mathbf{D}$ and electric intensity $\mathbf{E}$

$$\mathbf{D} = \varepsilon_0 \varepsilon_g \mathbf{E} \tag{3.1}$$

following LANDAU ET AL. [10] one obtains

$$\varepsilon_g = \frac{D}{\varepsilon_0 E} = \frac{f \varepsilon_s E_s + (1-f) \varepsilon_d E_d}{f E_s + (1-f) E_d}. \tag{3.2}$$

Subject to an external electric field E_0, the material becomes polarized. The local electric intensity E_{loc} is hence lowered by a depolarization term

$$\mathbf{E}_{\text{loc}} = \mathbf{E}_0 - L \frac{\mathbf{P}}{\varepsilon_0} \tag{3.3}$$

where L is depolarization factor describing the shape of the inclusion and $\mathbf{P}$ is the polarization

$$\mathbf{P} = \varepsilon_0 \varepsilon_r \mathbf{E}_{\text{loc}} - \varepsilon_0 \mathbf{E}_{\text{loc}}. \tag{3.4}$$

which makes the equation for the local field (3.3) self-consistent. We find that

$$\mathbf{E}_{\text{loc}} = \mathbf{E}_0 \frac{\varepsilon_d}{\varepsilon_d (1-L) + L \varepsilon_s} \tag{3.5}$$

when $\varepsilon_r = \frac{\varepsilon_s}{\varepsilon_d}$ for the inclusions inside the matrix. Inserting the local field electric intensities[1] $\mathbf{E}_d = \mathbf{E}_0$ and $\mathbf{E}_s = \mathbf{E}_{\text{loc}}$ into (3.2) we find the Maxwell Garnett mixing formula:

$$\varepsilon_g = \varepsilon_d \frac{f \varepsilon_s + (1-f) \left[\varepsilon_d (1-L) + \varepsilon_s L \right]}{f \varepsilon_d + (1-f) \left[\varepsilon_d (1-L) + \varepsilon_s L \right]}. \tag{3.6}$$

---

[1]The depolarization factor for the matrix is $L = 0$.

Depolarization factor

We refer to LANDAU ET AL. [10]. The depolarization factor L describes depolarization effects in a polarized body. It depends solely on the geometry (shape and orientation) of the body, not on its size. Its values may range between 0 and 1. The sum of the depolarization factors in three perpendicular directions of the body must be unity

$$L_x + L_y + L_z = 1 \tag{3.7}$$

An analytic expression of the depolarization factor L can be found for any ellipsoid. For some specific geometries, the factor can be found easily based on some physical insight and symmetry. Some values are shown in tab. 3.1.

geometry	value
desk (perpendicular to the field)	1
sphere	$\frac{1}{3}$
cylinder (axis perpendicular to the field)	$\frac{1}{2}$
cylinder (axis parallel to the field)	0

Table 3.1: Depolarization factor values for selected geometries.

Photoexcited conductivity

Let us now consider free electrons injected into the semiconductor inclusions (e.g. by photoexcitation). They provide an additional contribution to the (otherwise zero) far-infrared conductivity. For bulk crystals, Drude model DRUDE [11] is usually applied to describe the conductivity. The Drude-like character is of form:

$$\Delta\sigma_p = \frac{\sigma_0}{1 + i\omega\tau} \tag{3.8}$$

with $\sigma_0 = ne^2\tau/m$ where n is the concentration, $-e$ the charge of an electron, τ momentum scattering time and m the effective mass of the electrons. We introduce the *plasma frequency* ω_p

$$\omega_p = \sqrt{\frac{ne^2}{m\varepsilon_0}} \tag{3.9}$$

exploiting which, the conductivity $\Delta\sigma_p$ can be expressed as

$$\Delta\sigma_p = \frac{\omega_p^2\varepsilon_0\tau}{1 + i\omega\tau}. \tag{3.10}$$

The normalized conductivity per electron (electron mobility) $\mu = \frac{\sigma}{en}$ is shown in fig. 3.1. The complex relative permittivity of the photoexcited semiconductor is

$$\varepsilon_p(\omega) = \varepsilon_s + \Delta\varepsilon_p = \varepsilon_s + \frac{i\Delta\sigma_p}{\omega\varepsilon_0} \tag{3.11}$$

or the additional contribution explicitly, with $\gamma = \frac{1}{\tau}$

$$\Delta\varepsilon_p = \frac{\omega_p^2}{i\gamma\omega - \omega^2} \tag{3.12}$$
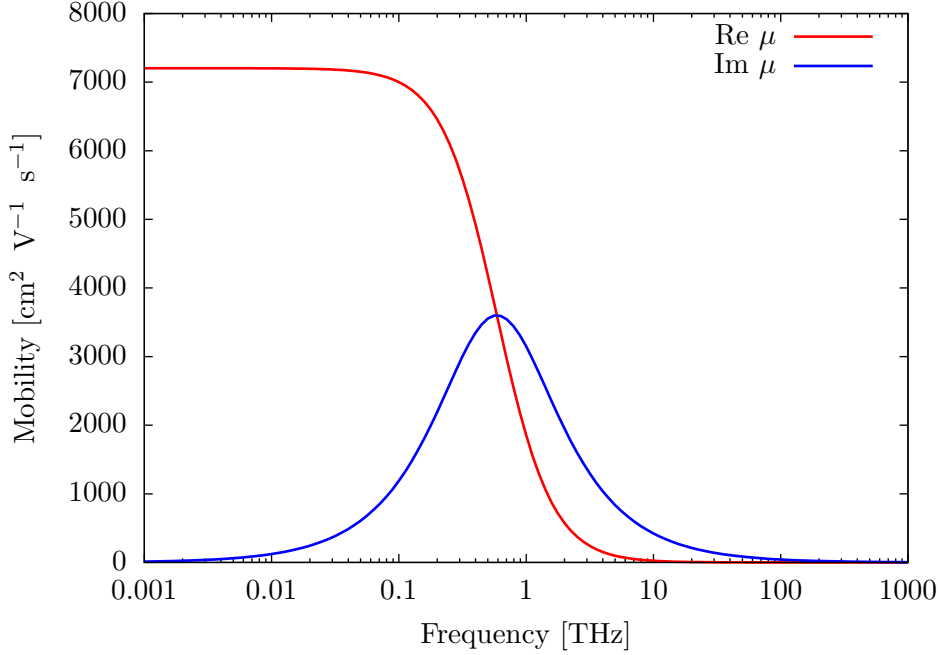
Figure 3.1: Normalized Drude conductivity (mobility) of photoexcited bulk GaAs.

The Drude model, which is over a hundred years old, yields good results for bulk materials. The note that the conductivity has its maximum at zero frequency. However, we may easily argue that the DC-conductivity of a nanoparticle must be equal to zero. In external electric field, the localized electrons cannot drift towards infinity. These different qualitative features of nanostructures' response spectra are appointed to plasmon resonances, NIENHUYS AND SUNDSTRÖM [12], PITARKE ET AL. [13]. The appearance of a plasmonic resonance is explained in the following section. However, other microscopic theories of conductivity were introduced as well, e.g. Drude-Smith phenomenological extension of the model, SMITH [14]. Its physical foundation has been improved recently, COCKER ET AL. [15], based on diffusive restoring current. For another example, Monte Carlo simulation method, see NĚMEC ET AL. [16]. In our work we will use the quantum mechanical formula (2.28) for electron conductivity presented in the preceding chapter.

3.2 Plasmonic resonance

Let us assume spherical shape of the conducting inclusions. The depolarization factor for a sphere is $L = \frac{1}{3}$. It can be shown from elementary electrostatics that the field outside a polarized or conductive sphere in a homogeneous external electric field has form as if caused by a dipole of a moment $\mathbf{p} = \frac{4\pi}{3} R^3 \mathbf{P}$, where R is the radius of the sphere. Due to boundary condition of continuity of the potential, the field inside the sphere is homogeneous. For spherical inclusions (3.5) therefore becomes

$$\mathbf{E}_{\text{loc}} = \mathbf{E}_0 \frac{3\varepsilon_d}{2\varepsilon_d + \varepsilon_s} \tag{3.13}$$

which simplifies the general mixing formula (3.6) in the following.

The effective permittivity $\varepsilon_{\mathrm{eff}}(\omega)$ of the composite of the photoexcited semiconductor inclusions and the dielectric matrix within the Maxwell Garnett model is now a complex-valued function:

$$\varepsilon_{\mathrm{eff}} = \varepsilon_d \frac{(2-2f)\varepsilon_d + (1+2f)\varepsilon_p}{(2+f)\varepsilon_d + (1-f)\varepsilon_p}. \tag{3.14}$$

The contribution $\Delta\varepsilon_{\mathrm{eff}}(\omega)$ of the free carriers to this effective permittivity is given as the difference between the permittivities of the photoexcited and ground state

$$\varepsilon_{\mathrm{eff}} = \varepsilon_g + \Delta\varepsilon_{\mathrm{eff}} \tag{3.15}$$

and can be expressed as follows

$$\Delta\varepsilon_{\mathrm{eff}} = \Delta\varepsilon_p \frac{(1+2f)\varepsilon_d - (1-f)\varepsilon_g}{(2+f)\varepsilon_d + (1-f)\varepsilon_s + (1-f)\Delta\varepsilon_p} \tag{3.16}$$

or explicitly

$$\Delta\varepsilon_{\mathrm{eff}} = \frac{(1+2f)\varepsilon_d - (1-f)\varepsilon_g}{(2+f)\varepsilon_d + (1-f)\varepsilon_s} \frac{\omega_p^2}{\frac{(1-f)}{(2+f)\varepsilon_d + (1-f)\varepsilon_s}\omega_p^2 - \omega^2 + i\gamma\omega} \tag{3.17}$$

where we can observe the form of the spectral dependence, see fig. 3.2. The spectrum of the response of the free carriers in the composite to far-infrared field has a form of response of a *damped harmonic oscillator*. The damping is caused by the scattering term $i\gamma\omega$. Opposed to the Drude-like character (3.12) of the contribution of the free carriers to the permittivity of the semiconductor
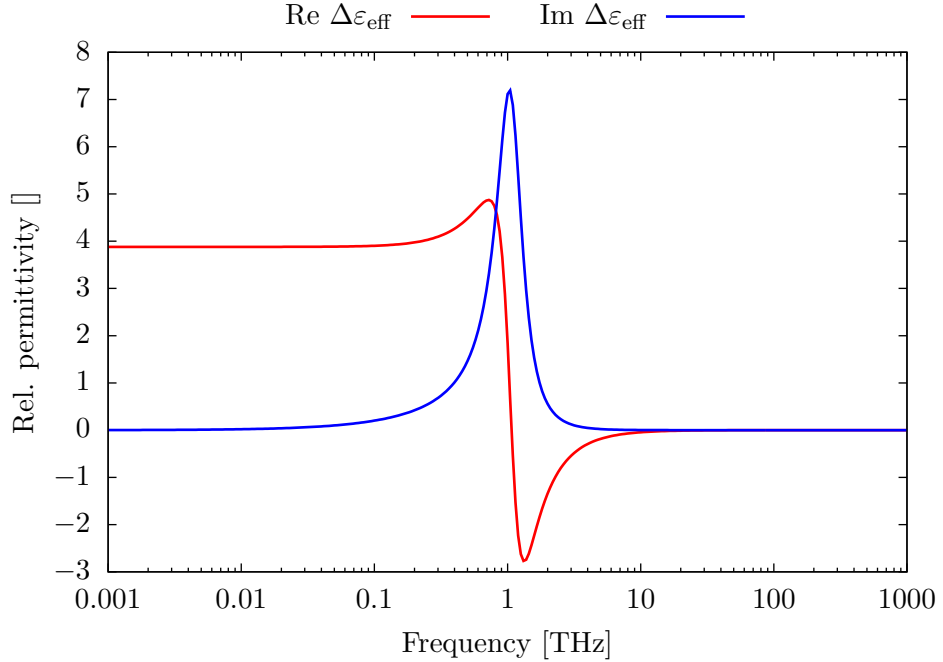

Figure 3.2: Contribution of the photoexcited free charge carriers to permittivity $\Delta\varepsilon_{\mathrm{eff}}$ of a composite material. $\varepsilon_s = 12.85$, $\varepsilon_d = 11.7$, $f = 0.1$, $n = 10^4$ μm^{-3}

15

itself, here we can identify an effective restoring force in the term including ω_p^2, hence the oscillator analogy. Such restoring force is introduced to the system due to the localization of plasmonic oscillations and consequent screening of the external field, whence the depolarization term in (3.3). The plasma frequency is the resonant frequency of plasmonic oscillations.

Part II

Model of Nanoparticles

4. Density of States

In this chapter, we find the bound states for a cube (or a cuboid prism) and a sphere by solving the time-independent Schrödinger equation. Although the wavefunctions differ dramatically for cubic and spherical geometries, we show that the volume is the only important parameter when it comes to asymptotic behaviour of densities of states. We also show that decrease in height of potential barrier of a finite potential well acts as an increase in the *effective* volume. In this chapter we omit the spin degeneracy factor of 2.

4.1 Cubic symmetry

Infinite potential well

The hamiltonian of a free particle is

$$\hat{\mathcal{H}} = -\frac{\hbar^2}{2m}\Delta \tag{4.1}$$

where m is the effective mass of the electron. Let the potential $V(x, y, z)$ be equal to 0 for $x \in (0, A)$, $y \in (0, B)$, $z \in (0, C)$ and equal to $+\infty$ otherwise. It forms a box for the electron to occupy. The time-independent Schrödinger equation for this problem is

$$\left[-\frac{\hbar^2}{2m}\Delta + V(x, y, z) \right] \Psi(x, y, z) = \mathcal{E}_n\Psi(x, y, z) \tag{4.2}$$

The wavefunction must obey the normalization condition

$$\int \Psi^*\Psi \, \mathrm{d}^3x = 1 \tag{4.3}$$

For the cubic symmetry, the wavefunction can be separated as follows:

$$\Psi(x, y, z) = \psi_x(x)\psi_y(y)\psi_z(z) \tag{4.4}$$

which allows us to look for the solutions of the 1D problem only. The wavefunction needs to be normalized and must be equal to zero outside of the box with zero potential. The solution to the particle in a box problem is:

$$\Psi(x, y, z) = \sqrt{\frac{2}{A}} \sin(k_x x)\sqrt{\frac{2}{B}} \sin(k_y y)\sqrt{\frac{2}{C}} \sin(k_z z) \tag{4.5}$$

where $k_x = \frac{n\pi}{A}$, $k_y = \frac{m\pi}{B}$, $k_z = \frac{l\pi}{C}$ and n, m, l are positive integers with the energy

$$\mathcal{E} = \frac{\hbar^2 k^2}{2m} \tag{4.6}$$

where $k^2 = k_x^2 + k_y^2 + k_z^2$ is the square of the wavevector. Therefore the energy levels are:

$$\mathcal{E}_{nml} = \frac{\hbar^2\pi^2}{2m}\left(\frac{n^2}{A^2} + \frac{m^2}{B^2} + \frac{l^2}{C^2} \right) \tag{4.7}$$

We could choose $A = B = C$ in which case we would be dealing with a cube.

Finite potential well

Now we proceed to a potential well with finite height V_0 of the barrier. Let the potential be equal to 0 for $x, y, z \in (-\frac{L}{2}, \frac{L}{2})$ and equal to V_0 otherwise. The electron can now tunnel into the barrier. That is described by fast-decaying however non-zero wavefunction inside the barrier region. Attention must be paid to more complicated boundary conditions. We neglect intricate behaviour of the wavefunction beyond edges and vertices of the cube, hence the wavefunction can still be factorized

$$\psi(x, y, z) = \psi_x(x)\psi_y(y)\psi_z(z). \tag{4.8}$$

For bound states ($\mathcal{E} < V_0$) the 1D wavefunction is of form:

$$
\begin{aligned}
\psi_x(x) = \psi_1(x) &= A_1 e^{Qx} \quad \text{for } x < -\frac{L}{2} \\
&= \psi_2(x) = A_2 \cos(qx) \quad \text{for } -\frac{L}{2} < x < \frac{L}{2} \text{ symmetric solution} \\
&= \psi_2(x) = A_2 \sin(qx) \quad \text{for } -\frac{L}{2} < x < \frac{L}{2} \text{ antisymmetric solution} \\
&= \psi_3(x) = A_3 e^{-Qx} \quad \text{for } x > \frac{L}{2}
\end{aligned}
\tag{4.9}
$$

where $q = \frac{\sqrt{2m\mathcal{E}}}{\hbar}$ and $Q = \frac{\sqrt{2m(V_0-\mathcal{E})}}{\hbar}$. From boundary conditions

$$\psi_1\left(-\frac{L}{2}\right) = \psi_2\left(-\frac{L}{2}\right) \tag{4.10}$$

$$\left.\frac{\mathrm{d}}{\mathrm{d}x}\psi_1(x)\right|_{x=-\frac{L}{2}} = \left.\frac{\mathrm{d}}{\mathrm{d}x}\psi_2(x)\right|_{x=-\frac{L}{2}} \tag{4.11}$$

and likewise at $x = \frac{L}{2}$ we find implicit equations for the wavevector k

$$\sqrt{u_0^2 - v^2} = +v \tan v \quad \text{symmetric solution} \tag{4.12}$$

$$\sqrt{u_0^2 - v^2} = -v \cot v \quad \text{antisymmetric solution,} \tag{4.13}$$

which can be further simplified by introducing *dimensionless* wavevectors

$$
\begin{aligned}
v &= \frac{qL}{2} \\
u &= \frac{QL}{2} \\
u_0 &= \frac{\sqrt{2mV_0}L}{2\hbar}
\end{aligned}
\tag{4.14}
$$

The energy of nth bound state is then:

$$\mathcal{E}_n = \frac{\hbar^2 q_n^2}{2m} = \frac{2\hbar^2 v_n^2}{mL^2} \tag{4.15}$$

where v_n is the solution of either (4.12) or (4.13).

Furthermore from the boundary conditions we find that the wavefunction constant factors are in the following relations:

$$A_1 = +A_2 \frac{\cos\left(q\frac{L}{2}\right)}{\exp\left(-Q\frac{L}{2}\right)} = +A_3 \qquad \text{symmetric solution} \qquad (4.16)$$
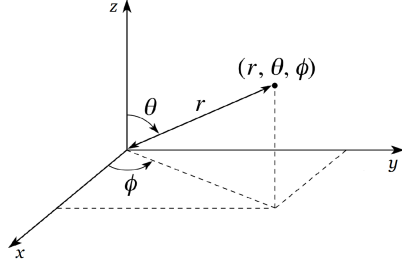
$$A_1 = -A_2 \frac{\sin\left(q\frac{L}{2}\right)}{\exp\left(-Q\frac{L}{2}\right)} = -A_3 \qquad \text{antisymmetric solution} \qquad (4.17)$$

The absolute value of these factors is to be found using the normalization condition.

4.2 Spherical symmetry

Infinite potential well

Addressing spherical quantum dots, we perform the analysis in the spherical coordinates: radial distance r, polar angle or *inclination* $\theta \in (0, \pi)$ and azimuthal angle $\phi \in (0, 2\pi)$. Given the geometry, the transformation relations are given as:

$$r = \sqrt{x^2 + y^2 + z^2}$$

$$\theta = \arccos\left(\frac{z}{r}\right) \qquad (4.18)$$

$$\phi = \arctan\left(\frac{y}{x}\right)$$

It can be handy to express ϕ as $\arg(x + iy)$ for it returns the angle $\phi \in (0, 2\pi)$.

Let the potential be equal to 0 for $r \in (0, R)$ and equal to $+\infty$ otherwise. The wavefunction can be separated into a radial and an angular part:

$$\psi(r, \theta, \phi) = \mathcal{R}_{nl}(r)\mathcal{Y}_{lm}(\theta, \phi) = \mathcal{N}_{nl}j_l(k_{nl}r)Y_{lm}(\theta, \phi). \qquad (4.19)$$

The quantum numbers are $n = 1, 2, 3...$, $l = 0, 1, 2...$ and $m = -l, ..., +l$. The wavevector satisfies: $k_{nl}R = z_{nl}$ where z_{nl} is the n-th zero of the spherical Bessel function $j_l(z)$:

$$j_l(z) = \sqrt{\frac{\pi}{2z}}J_{l+\frac{1}{2}}(z) \qquad (4.20)$$

which is defined using the Bessel function $J_\alpha(z)$ of the first kind. The normalization factor of the radial part $\mathcal{N}_{nl}$ is

$$\mathcal{N}_{nl} = \sqrt{\int_0^R j_l^2(k_{nl}r)r^2 \, dr}^{-1} = \sqrt{\frac{2}{a^3}}j_{l+1}^{-1}(z_{nl}) \qquad (4.21)$$

under the zero-value boundary condition.

$Y_{lm}(\theta, \phi)$ is the spherical harmonic function of degree l and order m. The sphercial harmonics are normalized and orthogonal

$$\int_0^{2\pi}\int_0^\pi Y_{lm}^*(\theta, \phi)Y_{l'm'}(\theta, \phi)\sin(\theta) \, d\theta \, d\phi = \delta_{ll'}\delta_{mm'} \qquad (4.22)$$

where we exploited the Kronecker δ-symbol. The energy levels are:

$$\mathcal{E}_{nl} = \frac{\hbar^2 z_{nl}^2}{2mR^2} \qquad (4.23)$$

By inspecting the dependence of the radial part of the wavefunction on the angular momentum quantum number l, we see that the probability density for the particle is shifting towards the outer boundary of the quantum dot as the angular momentum increases. That is caused by the *centrifugal barrier* term in the Schrödinger's equation. The total effective potential can be seen in fig. 4.1.
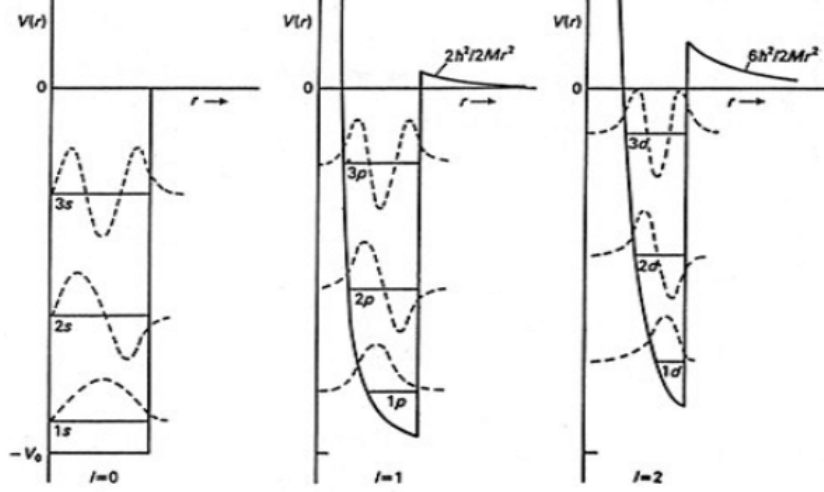

Figure 4.1: A rectangular potential well with the addition of the centrifugal barrier. From DUNLAP [17].

Finite potential well

Let the potential be equal to 0 for $r \in (0, R)$ and equal to V_0 otherwise. The angular part remains unchanged $Y_{lm}(\theta, \phi)$. The solution to the equation for the radial part of the bound states is

$$\begin{aligned}
\mathcal{R}(r) = \mathcal{R}_1(r) &= A_1 j_l(qr) \quad \text{for } r < R \\
= \mathcal{R}_2(r) &= A_2 k_l(Qr) \quad \text{for } r > R
\end{aligned} \tag{4.24}$$

where $q = \frac{\sqrt{2m\mathcal{E}}}{\hbar}$ and $Q = \frac{\sqrt{2m(V_0 - \mathcal{E})}}{\hbar}$. $j_l(r)$ is the lth spherical Bessel function of the first kind and $k_l(r)$ is the lth modified spherical Bessel function of the second kind.

The boundary conditions are

$$\mathcal{R}_1(R) = \mathcal{R}_2(R) \tag{4.25}$$

$$\frac{\mathrm{d}}{\mathrm{d}r}\mathcal{R}_1(r)\bigg|_{r=R} = \frac{\mathrm{d}}{\mathrm{d}r}\mathcal{R}_2(r)\bigg|_{r=R} \tag{4.26}$$

or explicitly, employing the recurrence formulas for the derivatives of the (modified) spherical Bessel functions, see e.g. OLVER ET AL. [18]

$$A_1 j_l(qR) = A_2 k_l(QR) \tag{4.27}$$

$$q A_1 \left[\frac{l}{qR} j_l(qR) - j_{l+1}(qR) \right] = Q A_2 \left[\frac{l}{QR} k_l(QR) - k_{l+1}(QR) \right] \tag{4.28}$$

By eliminating A_1, A_2 we get implicit equation for the wavevector q (or dimensionless number qR) to be solved numerically:

$$qR \, \frac{j_{l+1}(qR)}{j_l(qR)} = \sqrt{G^2 - q^2} R \, \frac{k_{l+1}\left(\sqrt{G^2 - q^2}R\right)}{k_l\left(\sqrt{G^2 - q^2}R\right)} \tag{4.29}$$

where $G = \frac{\sqrt{2mV_0}}{\hbar}$, $\sqrt{G^2 - q^2} = Q$. The condition (4.29) is, applying some Bessel functions identities, in agreement with results from LEYRONAS AND COMBESCOT [19]. The constant factors A_1, A_2 are then to be determined by combining the boundary (4.27), (4.28) and the normalization (4.3) conditions.

4.3 Comparison of densities

The energy spectra of confined electrons systems are discrete. A comparison of densities of such states (represented by Dirac δ-functions) wouldn't be very clear. Instead, we compare total count of states with energy smaller or equal to given energy level.

The volume of a cube of size a is $V = a^3$, whereas the volume of a sphere of radius r is $V = \frac{4\pi}{3}r^3$. We want to show that the asymptotic behaviour of the densities does not depend on the geometry as long as the volume of the quantum dot is kept the same. However we are used to describe the nanoparticles by their linear dimensions. Therefore we choose notation that 'cube(s)' stands for a cube with size $a = s$ nm and volume $V = s^3$ nm^3 and 'sphere(s)' stands for a sphere with the same volume $V = s^3$ nm^3 and thus radius $R = s\left(\frac{3}{4\pi}\right)^{1/3}$ nm, unless explicitly stated otherwise.

For an infinite depth potential well we compare total counts of states for a given energy level for cubes of size 20 nm and 30 nm with spheres of the corresponding radius, see fig. 4.2. We observe that even though the densities are different (with different distributions of δ-functions), they are equivalent on a sufficiently large intervals of energies. The total states counts visualized by steps scale in the same manner with the current energy level. Furthermore we add two densities of states for a cube and a sphere with the same linear dimensions to the comparison. The condition of the same volume is therefore broken and the resulting densities' asymptotes vary significantly. We observe that the smaller the volume of the quantum dot, the greater the separation of energy levels is. That leads to lower density of the states.

We may inspect closely the detailed structure of the density of states in fig. 4.3 where we added an asymmetric cuboid of dimensions $a = 20$ nm, $b = 20\sqrt{\pi}$ nm, $c = 20\left(\sqrt{\pi}\right)^{-1}$ nm with volume $V = 20^3$ nm^3 in addition to the cube(20) and the sphere(20) with the same volume. High steps in the total states count indicate a random degeneracy of the energy level. We can see that a sphere has the highest degeneracy $g = 2l + 1$ where l is the orbital quantum number of the given level. The projection quantum number m has no effect on the resulting energy. The cube also shows degeneracy given either by a permutation of the quantum numbers n, m, l or by coincidence of the sums of the squares of the quantum numbers, i.e. the energy only depends on the absolute value of the wavevector and not on its direction in case of isotropic effective mass. No such
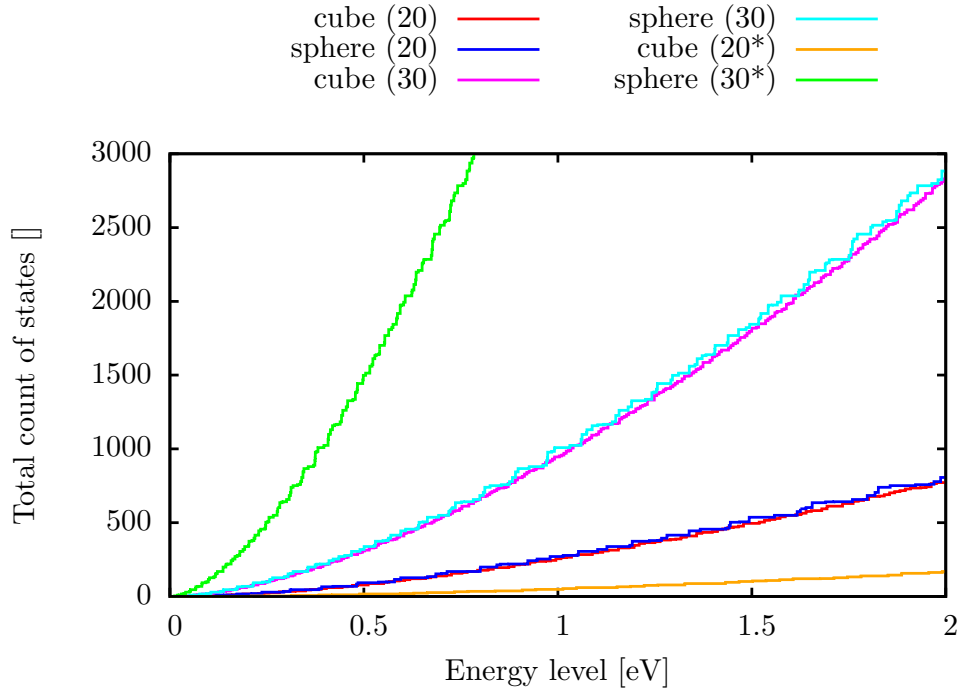
Figure 4.2: Comparison of densities of states for an infinite potential well. 'cube(20*)' stands for a cube with size of radius of sphere(20), i.e. $a = \left(\frac{3}{4\pi}\right)^{1/3} 20$ nm resulting in smaller volume than cube(20), and 'sphere(30*)' stands for a sphere with radius equal to the size of cube(30), i.e. $r = 30$ nm that yields greater volume than sphere(30).
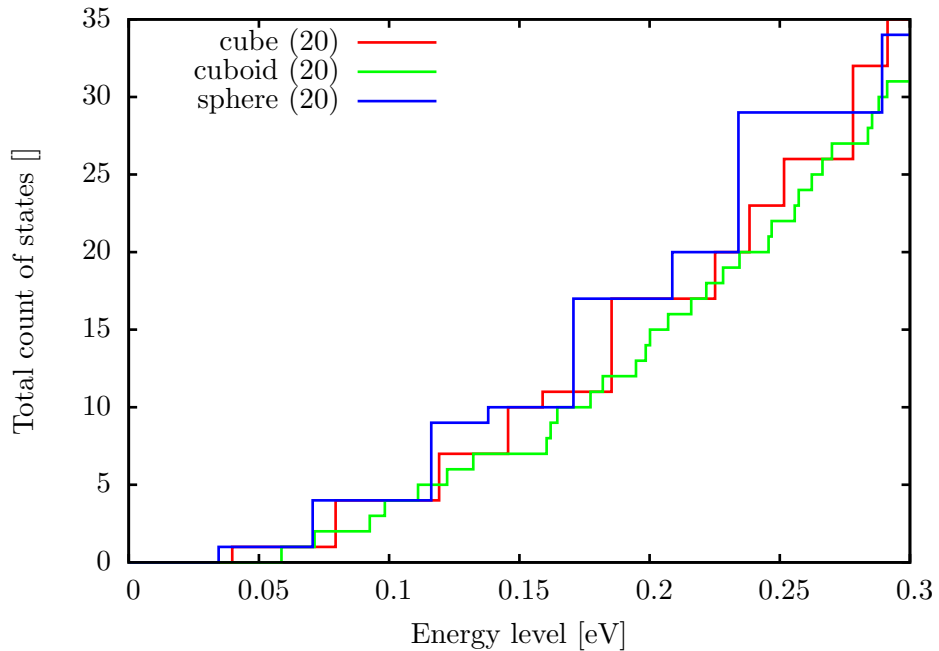

Figure 4.3: Densities of states or a cube, an asymmetric cuboid and a sphere of the same volume. We observe different degeneracies of levels. However the asymptotic behaviour of the densities is the same.

degeneracy can be observed within the cuboid with the choice of the dimensions stated above.
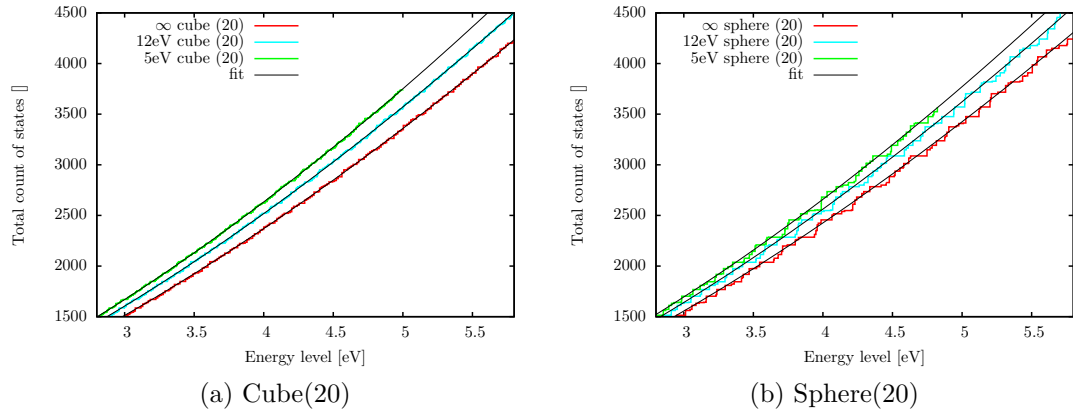

(a) Cube(20)

(b) Sphere(20)

Figure 4.4: Comparison of densities of states in quantum dots with the same real volume V but different potential barrier height V_0: infinite, 12 eV, 5 eV. The densities vary as the effective volume effective volume V_{eff} changes.

In case of finite height of the potential barrier of the quantum dot we witness decreasing of the separation between energy level as if an *effective volume* of the nanocrystal was increasing. See fig. 4.4a and 4.4b for finite barrier cubes and spheres respectively. The phenomenon can be explained by the possibility of an electron to penetrate into the walls of the well to a certain depth given by the exponential decay of the wavefunction inside the barrier, see eq. (4.9). Density of states of a free particle in three dimensions per unit volume is given as

$$n(\mathcal{E}) = \frac{m^{\frac{3}{2}}}{\hbar^3 \pi^2 \sqrt{2}} \sqrt{\mathcal{E}} \tag{4.30}$$

The total count of states in volume V is then

$$N(\mathcal{E}) = V \frac{m^{\frac{3}{2}}}{\hbar^3 \pi^2 \sqrt{2}} \frac{2}{3} \mathcal{E}^{\frac{3}{2}} \tag{4.31}$$

We expect the same functional form for scaling of the densities and total counts of bound states for a quantum dot. Therefore we can estimate the effective volume for a finite potential barrier from fitting the densities of states with functions $N(\mathcal{E}) = \alpha \mathcal{E}^{3/2}$ where the parameter is proportional the volume $\alpha \propto V$. In particular let α be the fitted parameter for an infinite barrier sphere(20) and β belong to a finite height $V_0 = 5$ eV barrier sphere(20). The effective volume of the latter can be estimated as

$$V_{\text{eff}} = V \frac{\beta}{\alpha} \tag{4.32}$$

In this case of a finite height $V_0 = 5$ eV barrier the effective volume V_{eff} of the sphere seems to be ca. 8% greater than the real volume V.

This allows us to proceed with infinite height potential barrier in further calculations, even though we cannot expect infinite barrier in raelity. Despite

the strong confinement regime, the material properties of the nanocrystals and surrounding matrix are quite similar. However the finite barrier height can be compensated by increasing the effective volume in our calculations.

A note on GaAs

We have chosen GaAs as demonstration material. We use its material properties and we don't pay much attention to real shapes of GaAs quantum dots being fabricated. They can be grown in a pyramidal shape (BAUHUIS ET AL. [20]) either by epitaxial growth or by self-assembly methods such as Stranski-Krastnow procedure. In VOROBIEV ET AL. [21] energy spectrum is computed for a pyramid with square base of size a and height $a/2$ using even mirror boundary condition. It is stated that energy levels separation appears to be larger for a pyramid compared to prism geometry. However such pyramid has six times lesser volume than a cube of the same size. Also the even mirror boundary condition corresponds to weak confinement of the electron. Therefore the asymptotic behaviour of the energy spectrum is not directly comparable with our results.

5. Dipole Moments

The interaction of our electronic system with external electric field is characterized by dipole moments for the electron transitions between individual states. In this chapter, we calculate the dipole moments for cubic and spherical geometry. We show that while selection rules differ in the two geometries, the *total amount* of transitions is the same.

5.1 Selection rules

Cubic symmetry

Let us assume x-polarization of the electric intensity component of the radiation. For reasons of symmetry, the parity of the system's state must change during a dipole transition. The group analysis can be found in the appendix [A.2]. The parity change defines the dipole selection rules. Furthermore, we know the wavefunction can be separated, see eq. (4.4), and therefore we obtain

$$\langle klm \left| x \right| k'l'm' \rangle = \langle k \left| x \right| k' \rangle \langle l | l' \rangle \langle m | m' \rangle \tag{5.1}$$

Due to the orthogonality of the states we may write $\langle l|l' \rangle \langle m|m' \rangle = \delta_{ll'}\delta_{mm'}$ using the Kronecker δ-symbol. We also know that for increasing quantum number n_x denoting energy levels, there are alternating symmetric (odd n_x) and antisymmetric (even n_x) solutions for the wavefunction, see eq. (4.9). This is exactly the change in parity required by the symmetries. Hence the selection rules in terms of quantum numbers n_x, n_y, n_z are

$$\begin{aligned}
\Delta n_x &= 2k + 1 \qquad k \in \mathbb{Z} \\
\Delta n_y &= 0 \\
\Delta n_z &= 0
\end{aligned} \tag{5.2}$$

Let us now evaluate the non-zero dipole moments. For an infinite potential well we have

$$\langle k \left| x \right| k' \rangle = \frac{2}{A} \int_0^A \sin\left(\frac{n\pi}{A}x\right) \sin\left(\frac{m\pi}{A}x\right) x \, \mathrm{d}x \tag{5.3}$$

By substitution $\xi = x/A$ we obtain

$$\langle k \left| x \right| k' \rangle = 2A \int_0^1 \sin(n\pi\xi) \sin(m\pi\xi) \, \mathrm{d}\xi \tag{5.4}$$

An analytical expression for the integral can be found:

$$\langle k \left| x \right| k' \rangle = \frac{A}{\pi^2} \left\{ \frac{\pi(m-n)\sin[\pi(m-n)] + \cos[\pi(m-n)] - 1}{(m-n)^2} - \right.$$
$$\left. - \frac{\pi(m+n)\sin[\pi(m+n)] + \cos[\pi(m+n)] - 1}{(m+n)^2} \right\} \tag{5.5}$$

For a finite height potential barrier the analytic expression is possible as well. It greatly reduces time complexity of computational algorithms compared to numerical integration. We won't show the integral here, but we mention the need to integrate over the three domains in (4.9) separately. For the potential barrier high enough, which corresponds to the strong confinement regime, we can use an approximation of the dipole moments by the formula for infinite barrier given above.
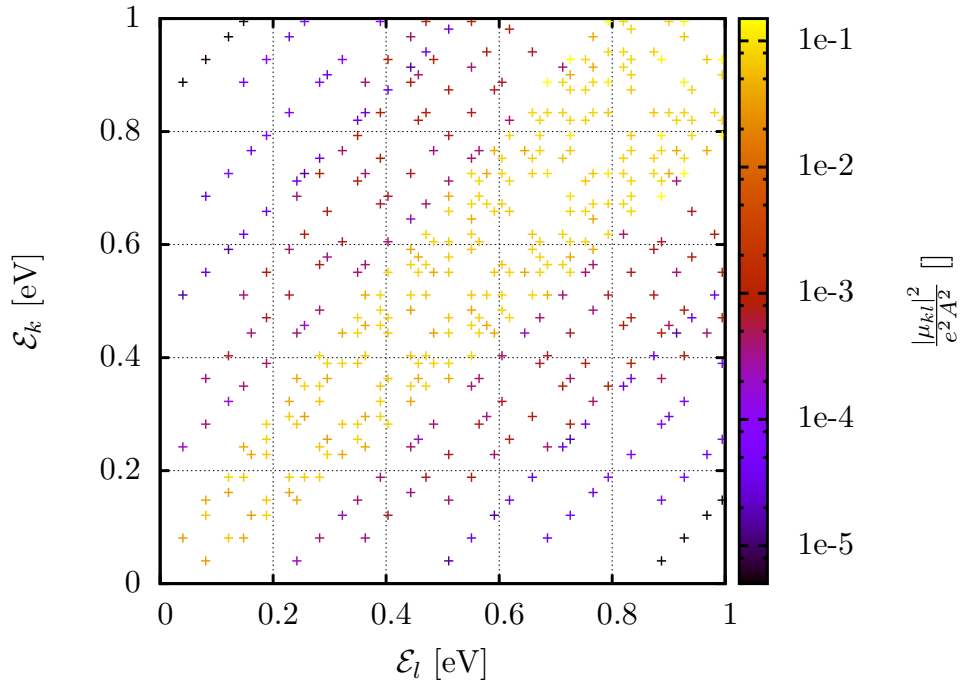

Figure 5.1: A map of normalized dipole transition rates for cube(20).

In fig. 5.1 we show a map of dipole moments squared $|\mu_{kl}|^2 = |\langle k|ex|l\rangle|^2$ between energy levels in a cube of size of 20 nm, for those are included in the diagonal elements of the conductivity tensor we are interested in. The values are normalized to unit size and unit charge. The distance from the diagonal of the figure represents the energy difference $\mathcal{E}_{kl}$ between levels k,l. We observe that no transitions lay on the diagonal and that the transitions are aligned to lines parallel to the diagonal due to the periodicity of the sine function and hence the constant separation between energy levels. Degeneracy of the levels has been summed over.

Spherical symmetry

For x-polarization the dipole selection rules for spherical symmetry are as follows. Derivation based on symmetry analysis is presented in the appendix [A.2].

$$\begin{aligned}
\Delta n &= k \quad k \in \mathbb{Z} \\
\Delta l &= \pm 1 \\
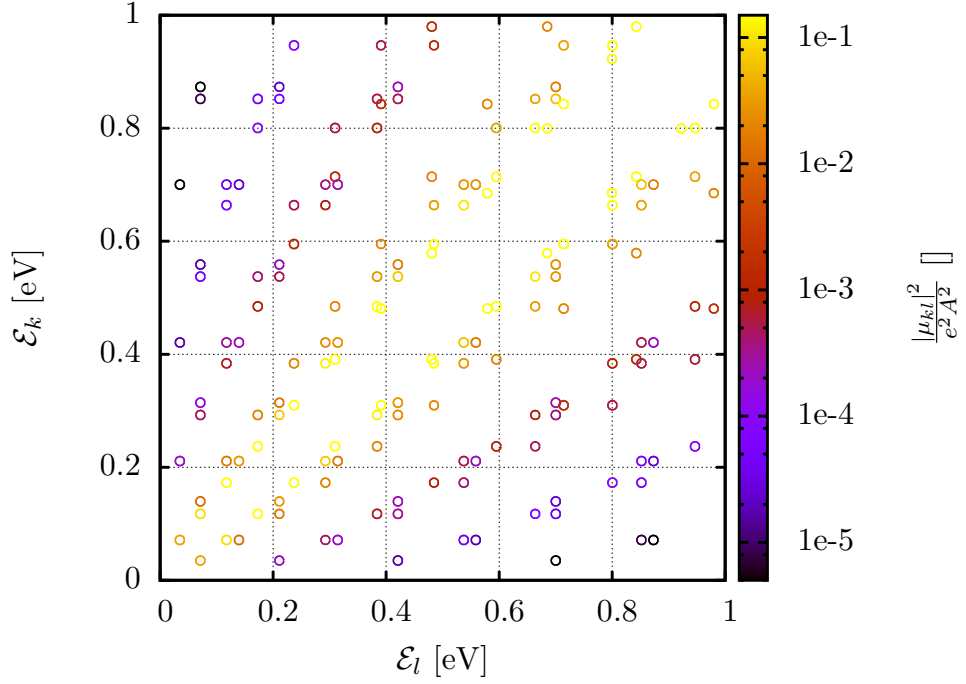\Delta m &= \pm 1
\end{aligned} \tag{5.6}$$

Figure 5.2: A map of normalized dipole transition rates for sphere(20).

While evaluating the dipole moments, we can separate the radial and the angular parts (4.19) of the wavefunctions

$$\Psi_{nlm}(r, \theta, \phi) = \mathcal{R}_{nl}(r)\mathcal{Y}_{lm}(\theta, \phi) \tag{5.7}$$

The operator of the dipole moment transforms to spherical coordinates as $x = r\sin(\theta)\cos(\phi)$. Therefore

$$\langle n'l'm' |x| nlm \rangle = \int_0^\infty \mathcal{R}_{n'l'}^*(r)\mathcal{R}_{nl}(r)r^3 \, \mathrm{d}r \times$$
$$\times \int_0^{2\pi} \int_0^\pi Y_{l'm'}^*(\theta, \phi)Y_{lm}(\theta, \phi)\sin^2(\theta)\cos(\phi) \, \mathrm{d}\theta \, \mathrm{d}\phi \tag{5.8}$$

The integral of the angular part $\langle l'm' |x| lm \rangle_\Omega$ can be expressed explicitly. The selection rules (5.6) give four possibilities:

$$\langle l+1, m+1 |x| lm \rangle_\Omega = +\frac{1}{2}\sqrt{\frac{(l+m+1)(l+m+2)}{(2l+1)(2l+3)}} \tag{5.9}$$

$$\langle l-1, m+1 |x| lm \rangle_\Omega = -\frac{1}{2}\sqrt{\frac{(l-m-1)(l-m)}{(2l-1)(2l+1)}} \tag{5.10}$$

$$\langle l+1, m-1 |x| lm \rangle_\Omega = -\frac{1}{2}\sqrt{\frac{(l-m+1)(l-m+2)}{(2l+1)(2l+3)}} \tag{5.11}$$

$$\langle l-1, m-1 |x| lm \rangle_\Omega = +\frac{1}{2}\sqrt{\frac{(l+m-1)(l+m)}{(2l-1)(2l+1)}} \tag{5.12}$$

28

The radial part integral

$$\langle n'l' \,|x|\, nl \rangle_r = \mathcal{N}_{n'l'} \mathcal{N}_{nl} \int_0^R j_{l'}(q_{n'l'}r) j_l(q_{nl}r) r^3 \,\mathrm{d}r \tag{5.13}$$

is to be evaluated numerically. We employ the adaptive Gauss-Kronrod quadrature integration algorithm, SHAMPINE [22]. Squares of dipole moments $|\mu_{kl}|^2$ between states k and l for sphere(20) are depicted in fig. 5.2. As opposed to a cube, the transitions don't form parallel lines, for the distances between consecutive zeros of the Bessel functions are not the same. They do however approach the parallel pattern for high energies due to the asymptotic form of the spherical Bessel function of the first kind $j_l(z)$ for large z:

$$j_l(z) \rightarrow \frac{\sin\left(z - l\frac{\pi}{2}\right)}{z} \tag{5.14}$$

We note that a dipole moment also has its phase. The moments' phases depend on the phases of the wavefunctions of the states $\langle k \,|x|\, l \rangle = \langle k_0 \,|x|\, l_0 \rangle \, \mathrm{e}^{i\varphi_k} \mathrm{e}^{-i\varphi_l}$. The phase is not, however, an observable physical quantity. Therefore the phase is either compensated by the wavefunctions' phase itself when computing e.g. density of particles: $\rho_{kl}(x) = \langle k \,|x|\, l \rangle \langle x|k\rangle \langle l|x\rangle$, or a square of the size of the moment is taken, as e.g. in the Fermi golden rule for the transition rates

$$\Lambda_{k \rightarrow l} = \frac{2\pi}{\hbar} \left| \left\langle k \left| e\mathbf{r} \right| l \right\rangle \cdot \mathbf{E} \right|^2 n_l \tag{5.15}$$

where n_l is the density of final states. As expected, the transition rate $\Lambda_{k \rightarrow l}$ is real-valued and its dimension is $[s^{-1}]$.

5.2 Comparison of dipole moments

Same as for the comparison of the densities of states for cubic and spherical geometries of the quantum dot, we want to show that, despite apparent differences in the dipole transition maps, the dipole moments are *equivalent in an integral sense* for the two geometries. In this sense of equivalence, if the dephasing rate is high enough, one cannot tell the difference between distinct transitions and the overall dipole moments are the same for cubic and spherical geometries.

Therefore we compute densities of the transitions in the energy-energy plane and take an average over a certain area. The two averaged maps for cube(20) and sphere(20) can be seen in fig. 5.3 and fig. 5.4 respectively. The moments were averaged by weighting the contributions by a Gauss function. The greater the variance, the better the correspondence of both maps. However we are interested in rather small scales. The chosen standard deviation is $\sigma = 0.04$ eV[1]. It can be seen that on a sufficiently large scale, the intensities of dipole moments are equivalent for both geometries.

---

[1]The dephasing rate in GaAs corresponds to $\gamma = 0.00244$ eV. If such is our resolution of distinct transitions (i.e. $\sigma = \gamma$), one can distinguish between different transitions in both cube(20) and sphere(20). The averaged maps become the same at ca. 60 nm.
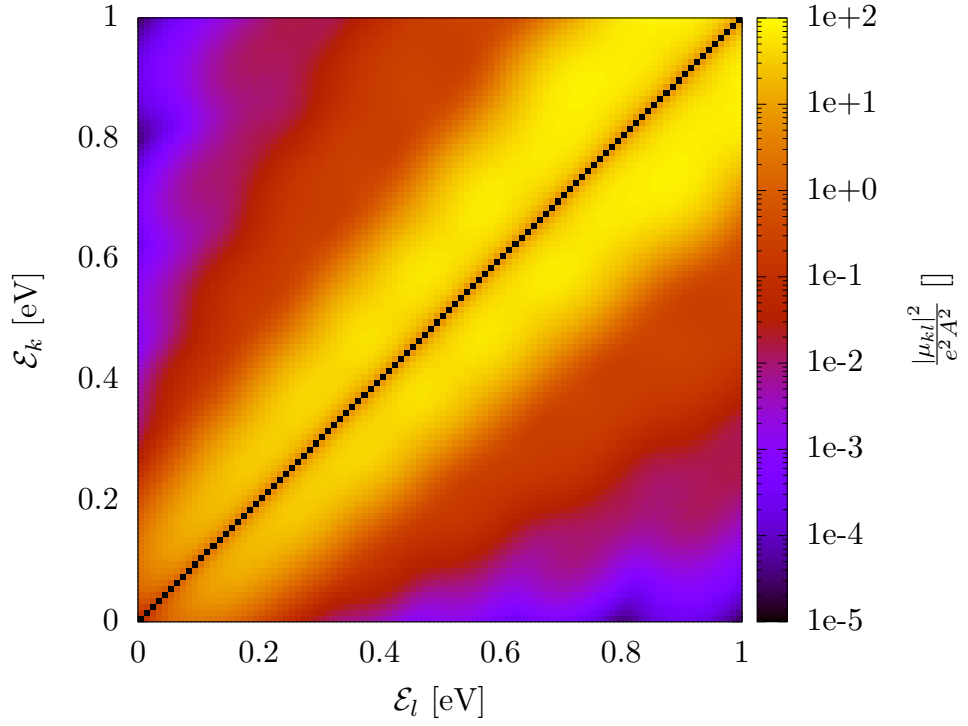
Figure 5.3: Averaged normalized dipole moments for cube(20).
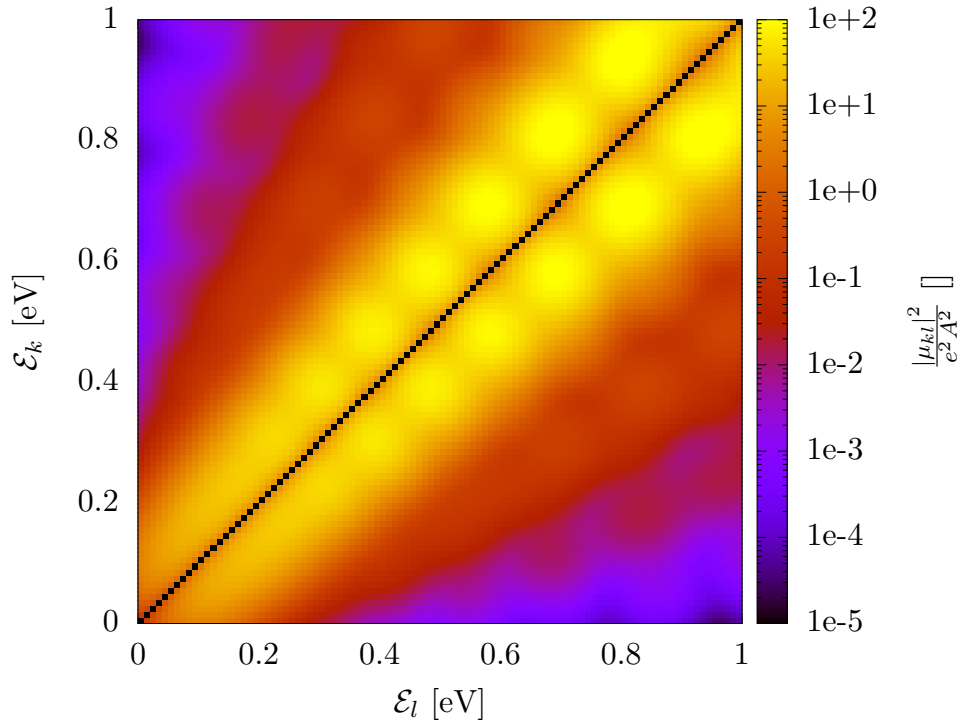Average weighted by a Gaussian, $\sigma = 0.04$ eV.

Figure 5.4: Averaged normalized dipole moments for sphere(20).
Average weighted by a Gaussian, $\sigma = 0.04$ eV.

6. Terahertz Conductivity

In this chapter we will see electric conductivity spectra in terahertz range obtained within the linear response theory. We have already derived the expression (2.28) for the conductivity tensor elements in chapter 2. In linear regime, only the diagonal elements in directions of significance to symmetry are nonzero. It is shown within the symmetry group analysis in the appendix [A.3]. The conductivity in the direction of x is

$$\sigma_x(\omega) = \frac{i\omega e^2}{V} \sum_{k,l} \frac{f_{kl}}{\hbar} \frac{|\langle k\,|x|\,l \rangle|^2}{\omega - \omega_{kl} + i\gamma} \tag{6.1}$$

where k and l denote states of the system. Obviously, this simple model of conductivity neglects many incoherent phenomena[1]. All incoherent effects are substituted by the phenomenological dephasing rate γ in the formula above.

6.1 Mobility spectra

We continue the comparison of cubic and spherical geometries. This time we compare the mobility spectra for the two geometries, again with the same volume. We mention that the spectra belong to quantum dots as a whole, not only the material they consist of (GaAs in our example). The mobility represents the *microscopic* conductivity[2].

For small dimensions of the quantum dot, the dipole transitions contributing to the mobility spectrum are resonant at multiterahertz frequencies, as seen in fig. 6.1. We can also notice that the separation of transitions between distinct pairs of energy levels is wide, so that distinct peaks are formed. In spite of the fact the response of cube(20) and sphere(20) varies in shape, we may find some similarities. The tails of the spectra are basically at the same frequencies and the total area under the curve is very similar for both geometries. This reflects the same asympototical behaviour of the densities of states and the dipole moments from previous chapters.

For increasing dimensions of the nanocrystal, the number of peaks in the spectra increases while their separation decreases. Eventually, the distinct peaks join together, as observed in fig. 6.2. In a cube, multiple transitions contribute to the same peaks, therefore the apparent lesser density of peaks in the spectrum than in a sphere. Recall fig. 5.1 and 5.2 of dipole moments for a cube and a sphere respectively, where the distance of the mark from the diagonal shows the energy of the dipole transition. The marks form straight lines in case of a cube.

---

[1]Scattering processes play an important role throughout condensed matter physics, charge transport in particular. Within a band structure, an accelerating particle can get into a neighbouring Brillouin zone, where it acquires negative velocity while gaining momentum. This phenomenon is known as the Bloch oscillations. Casually it is prevented by scattering mechanisms, that also let us remain within the effective mass approximation.

[2]Although the nanoparticles are conductive on the microscopic level, they become polarized in external field as they are isolated and therefore they act as dielectric on the macroscopic scale.

(a) Real part.

(b) Imaginary part.
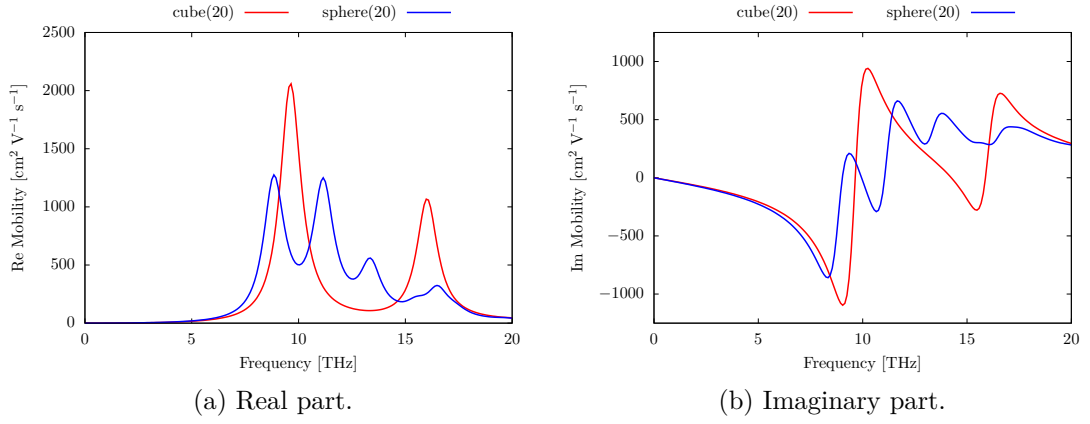
Figure 6.1: Comparison of mobility spectra for cubic and spherical geometries of the quantum dot with the same volume. Size of the cube is 20 nm.

(a) Real part.

(b) Imaginary part.

Figure 6.2: Mobility spectra for cubic and spherical quantum dots with the same volume. Size of the cube is 50 nm.

(a) Real part.

(b) Imaginary part.
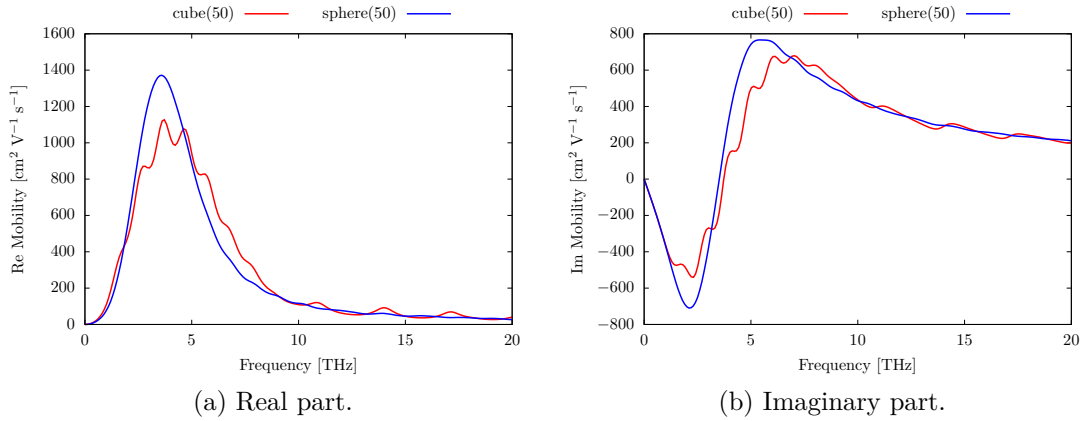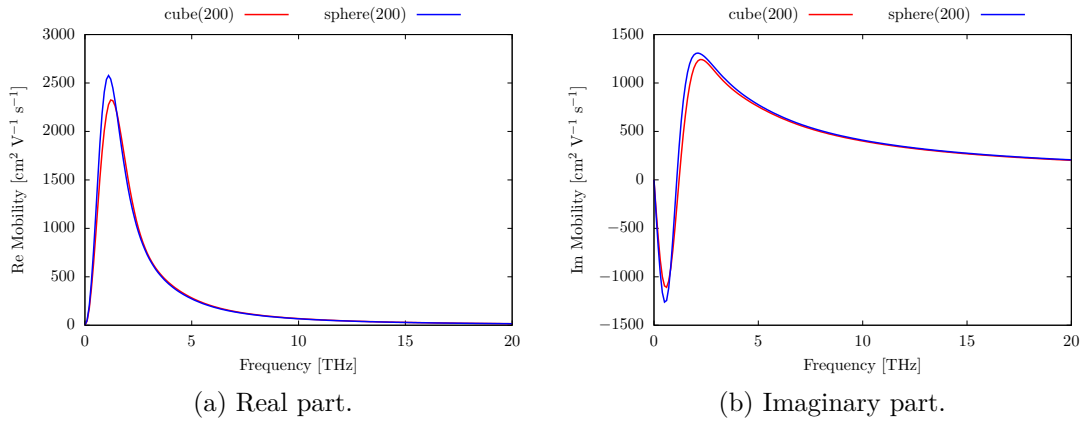
Figure 6.3: Mobility spectra for cubic and spherical quantum dots with the same volume. Size of the cube is 200 nm

For quantum dots large enough, we do not observe any qualitative differences in the shapes of the mobility spectra for the two geometries. For electron mobilities in cube(200) and sphere(200), see fig. 6.3 The response of the cube only appears a little smaller then that of a sphere. For increasing volume of the crystal, the spectrum shift towards lower frequencies. That is enabled by higher density of energy levels the electrons may occupy. Later in this chapter, this will also be commented upon further.

Temperature dependence

The contributions of individual dipole transitions are weighted by the difference in population of the participating levels f_{kl}. The difference depends on the shape of Fermi-Dirac distribution, which is affected by temperature and number of electrons in the system, hence altering the temperature and/or electron density results in a change of the mobility spectrum. The temperature dependence is demonstrated in fig. 6.4. We can see that at low temperature (10 K) only the ground level is occupied and only the transition to the first excited level may occur, while at high temperature (300 K) the thermal distribution covers more levels and a transition from the first to the second excited level can be seen. The density of electrons is $n = 10^4\ \mu m^{-3}$. Cube(20) has been chosen because there we can observe the individual transitions form distinct peaks in the spectrum.

(a) Real part.

(b) Imaginary part.
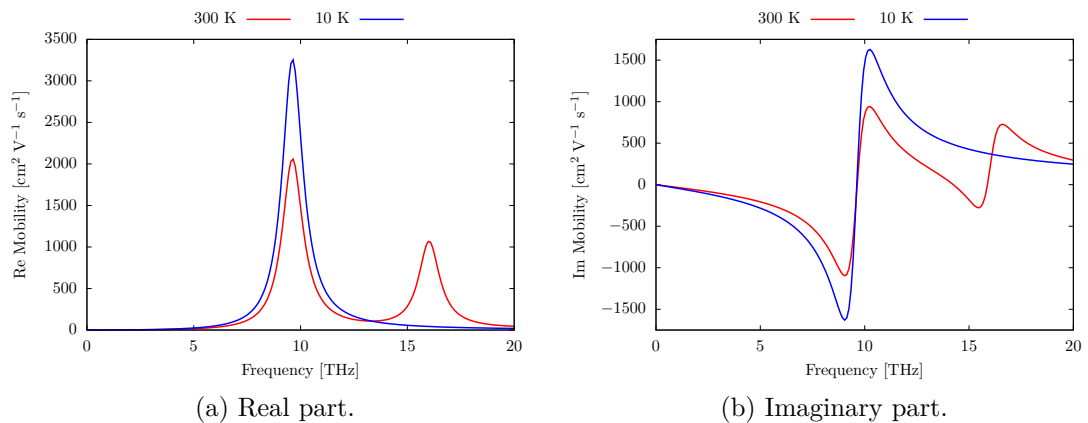
Figure 6.4: Comparison of mobility spectra for the same cubic quantum dot at temperatures 10 K and 300 K.

Finite potential well

In chapter 4 we have argued that the finite height of the energy barrier forming the potential well acts effectively as increasing of volume of an infinite potential well, as the wavefunction penetrates into the barrier. However the density of carriers doesn't reflect the larger effective volume and the dipole moments are slightly different due to overlap of the exponential decaying parts of the wavefunction inside the barrier region. Fig. 6.5 illustrates that the decreasing energy barrier of the potential well shifts the spectrum towards the one of a larger volume quantum dot with the infinite barrier. Therefore the increasing effective volume approximation is reasonable and applicable.

(a) Real part.

(b) Imaginary part.
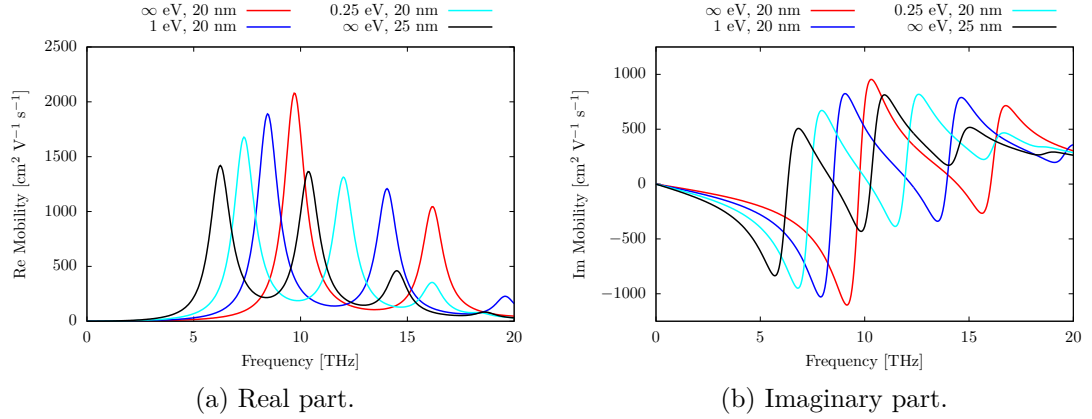
Figure 6.5: Mobility spectra for various effective volumes due to the finite potential well. $T = 300$ K, $n = 10^4$ μm^{-3}.

Large volume limit

In fig. 6.6 we compare mobility spectra of larger nanocrystals with bulk Drude mobility. We observe the spectra are nearing the Drude model for increasing volume, but they remain zero for zero frequency. In order to reproduce the non-zero conductivity for DC case, we would need to prevent the electrons from restoring of the initial distribution on loss of coherence in the equations of motion.

(a) Real part.

(b) Imaginary part.
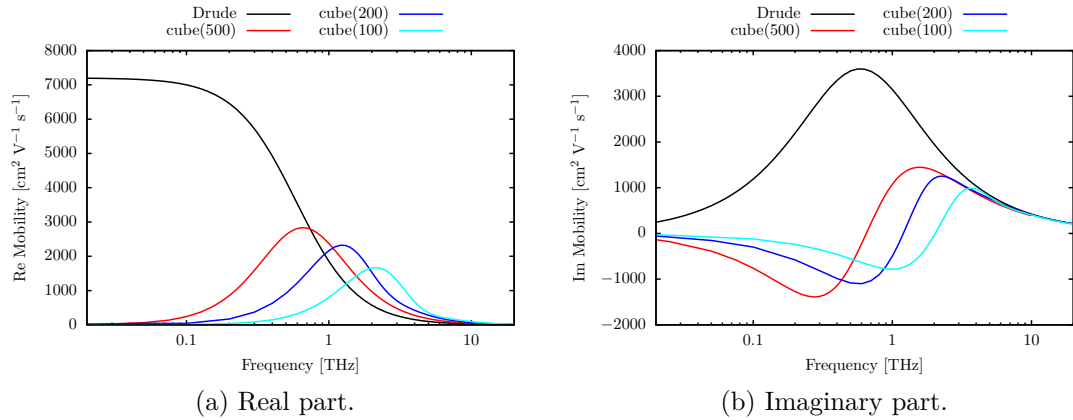
Figure 6.6: Comparison of mobilities obtained by using the quantum mechanical linear response theory with the classical Drude model.

6.2 Further comments

Another parameter with influence on the mobility spectra is the dephasing rate γ. It controls the width of the distinct Lorentzian spectral lines corresponding to resonant frequencies. However in our work we have chosen a fixed value of the dephasing energy $\hbar\gamma = 0.00244$ eV, corresponding to $\tau = 270$ fs for GaAs.

Alternate approach: Kubo formula

The electric conductivity tensor can be also obtained as a response function within the linear response formalism using the Kubo formula, see RÖSSLER [23],

$$\sigma_{\lambda\mu}(\omega) = \frac{i}{\hbar\omega} \int_0^{+\infty} e^{i\omega t} \, \mathrm{Tr}\left(\hat{\rho}_0 \left[j_\lambda(t), j_\mu(0)\right]\right) \mathrm{d}t \qquad (6.2)$$

which yields result

$$\sigma_x(\omega) = -\frac{ie^2}{V} \sum_{k,l} \omega_{kl} \frac{f_{kl}}{\hbar} \frac{|\langle k\,|x|\,l\rangle|^2}{\omega - \omega_{kl} + i\gamma} \qquad (6.3)$$

as in MARDER [4]. Comparing our formula for conductivity (6.1) to the expression (6.3), one can see the latter does not vanish in the DC limit $\omega = 0$, which doesn't fit the model of confined carriers. Close to equilibrium, the dephasing term has been neglected in the Kubo formula. Such approximation does not pose any problems in translation invariant bulk materials, where the electrons satisfy the equilibrium distribution right after a scattering event. However, in nanostructures, a diffusive restoration current, which is present due to broken translational symmetry of the system, must be taken into account, OSTATNICKÝ ET AL. [24], COCKER ET AL. [15].

We have not neglected the dephasing term in the derivation of conductivity tensor (6.1) in chapter 2, therefore the restoring of the equilibrium distribution (mathematically extinction of $\hat{\rho}_1$) is accounted for. We only have to bear in mind that the dephasing rate γ does not correspond to the pure momentum scattering time τ, but the carriers also need some time to return to their initial thermal distribution. By setting $\gamma = 1/\tau$ we assume the electrons return to their equilibrium distribution upon scattering *instantaneously*.

Momentum conservation principle

We can notice that for small quantum dots dipole transitions occur for large energy gaps corresponding to multiterahertz frequencies. For large quantum dots the contribution of high energy transitions is negligible, even though pairs of levels with these gaps obviously do exist. However it is the dipole moments that extinguish these transitions. The electrons must obey the momentum conservation principle, although it does not explicitly enter the equations of motion. The incident photons carry enough energy for the transitions between levels happen, but by far not enough momentum. This inconvenience is counteracted by the uncertainty principle

$$\sigma_x \sigma_p \geq \frac{\hbar}{2} \qquad (6.4)$$

The more precise the localization of the electron within the confining potential is, the greater the momentum uncertainty becomes. The momentum conservation principle then needs to be satisfied within the momentum uncertainty, which allows for larger momentum differences between levels participating in transitions for smaller quantum dots. Mathematically the dipole moments, the energy gaps and the momentum uncertainty are tied together.

6.3 Shape discussion conclusion

We have compared properties of cubic and spherical geometries of our model of a quantum dot. We have seen the same asymptotic behaviour of densities of states for cubes and spheres of the same volume in chapter 4 as well as the same averaged dipole moment density in chapter 5. Now we have compared the mobility spectra.

In this chapter we have seen, that for small quantum dots the mobility spectra for a cube and a sphere differ in detailed structure of the dipole transition resonance peaks, while still having some similar features. Increasing the size makes the differences less apparent and eventually the shape of the spectra becomes the same. Moreover if we consider a real sample, we must take into account imperfections and distributions of sizes of the nanoparticles that cause non-homogeneous broadening of the spectral lines. Therefore the fine structure of the spectrum will never be observable and we will not be able to tell the difference between the response of composite materials consisting of spheres or cubes. The geometry plays a certain role, but only the volume of quantum dot is a significant parameter. At least in cases where the conductivity tensor is symmetric, that is. We conclude that in the scope of terahertz spectroscopy we may choose a geometry of quantum dots that simplifies solving equations of given problems, while the results are still relevant for other geometries as well.

Also the finite height of energy barrier of the potential well can be approached by the increasing effective volume approximation.

Part III

Depolarization Effects

7. Depolarization Field

Exposed to external electric field, the material becomes polarized. Displacement of the electrons inside the nanostructures causes screening of the external field. The inclusions respond to different *local field* than the matrix. The depolarization field has been known from classical electrostatics. However in quantum mechanical approach, the electrons do not form a surface charge but are distributed in the volume according to the wavefunction. In this chapter, we will provide a general derivation of the local electric field from the charge distribution. For solving Poisson's equation is generally a formidable task, we will also derive a *depolarization factor* depending on the inclusions' parameters in order to simplify later calculations of effective response functions of composite materials.

7.1 Electric charge distribution

The density function in x-representation is obtained from the density matrix

$$n(\mathbf{r}) = \sum_{k,l} \langle x | \hat{\rho}_{kl} | x \rangle \tag{7.1}$$

Let us write explicit forms of the equilibrium density and the perturbation term separately based on (2.19) and (2.22)

$$n_0(\mathbf{r}) = \sum_k f_k \, \Psi_k^*(\mathbf{r}) \Psi_k(\mathbf{r}) \tag{7.2}$$

$$n_1(\mathbf{r}) = \sum_{k,l} \frac{f_k - f_l}{\hbar} \frac{\langle k \, | e\mathbf{r} \, | \, l \rangle \cdot \widetilde{\mathbf{E}} \, e^{-i\omega t}}{\omega - (\omega_k - \omega_l) + i\gamma} \Psi_l^*(\mathbf{r}) \Psi_k(\mathbf{r}) \tag{7.3}$$

The densities obey

$$\int n_0(\mathbf{r}) \, \mathrm{d}\mu = N_0 \tag{7.4}$$

$$\int n_1(\mathbf{r}) \, \mathrm{d}\mu = 0 \tag{7.5}$$

while μ being measure.

The equilibrium radial density of electrons is plotted in fig. 7.1 for sphere(20) and sphere(100). We remind the notation from chapter 4: sphere(t) stands for a sphere with radius $r = \left(\frac{3}{4\pi}\right)^{1/3} t$ so that it has the same volume as a cube of size t. The angular dependence of equilibrium density is trivial, for the ground state is fully symmetric. It is evident from the figure that the electrons are not allowed to occupy the space near the surface. The larger the volume, the flatter the distribution is and the smaller is the vacant area. In the large scale limit, the distribution is uniform. That is in correspondence with the classical image. Positive-charge holes we neglected earlier due to very large effective mass obey this uniform distribution.

The density of electric charge is

$$\rho(\mathbf{r}) = -en_{\mathrm{e}}(\mathbf{r}) + en_{\mathrm{h}}(\mathbf{r}) \tag{7.6}$$
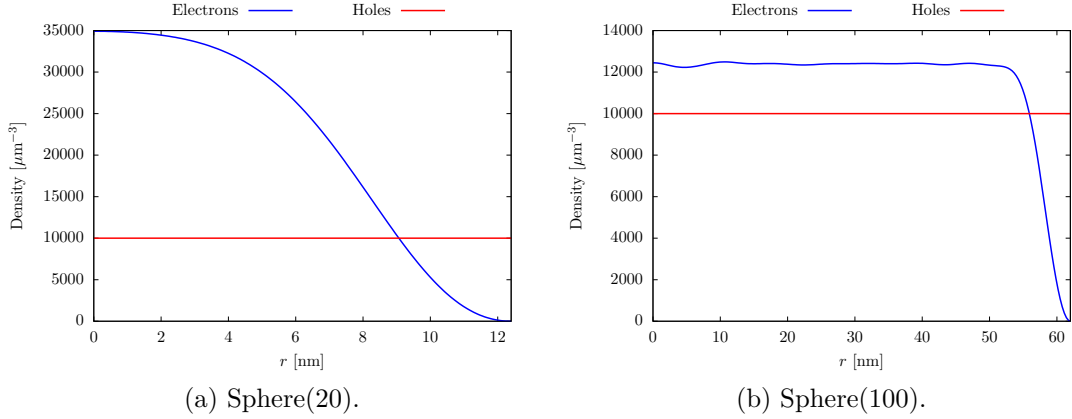
Figure 7.1: The equilibrium radial distribution of electrons and holes for sphere(20) and sphere(100) at given temperature and carrier density $T = 300$ K, $n = 10^4$ μm^{-3}.

where n_{e} and n_{h} represent densities of electrons and holes respectively. Obviously, an electric field must arise from the difference between positive and negative charge distributions. However, in the equilibrium state no net force is driving the electrons. Thus the electric force must be compensated by a 'quantum force' of the potential well. We will ignore this equilibrium contribution to electric field.

Contribution of the perturbation electric charge density will be of larger significance. From eq. (7.3) can be seen that the perturbation density $n_1(\mathbf{r})$ is complex-valued and frequency-dependent.

Poisson's equation

In order to find the electric intensity $\mathbf{E}_1$ of the depolarization field caused by displaced electric charge distributed in volume of a body, one needs to solve the Poisson's equation for the electric potential Φ

$$\Delta\Phi(\mathbf{r}) = \frac{\rho_1(\mathbf{r})}{\varepsilon_0} \tag{7.7}$$

Note that the classical Poisson's equation makes use of the permittivity of the material $\varepsilon = \varepsilon_r\varepsilon_0$. That is a self-consistent feature, which is not however in compliance with our first order perturbation theory approach and we proceed with the vacuum permittivity only.

For now, suppose we have found a formal solution to the equation. The electric intensity of the depolarization field is then obtained by taking the gradient of the potential

$$\mathbf{E}_1(\mathbf{r}) = -\nabla\Phi(\mathbf{r}) \tag{7.8}$$

7.2 Depolarization factor

Ultimately, we will employ an effective medium approximation for our composite material. The Maxwell Garnett theory presented in chapter 3, assumes uniform electric field. Note that the susceptibility obtained from linear response formalism

in chapter 6 is also an average for the whole nanocrystal. Therefore we are looking for a way to find an effective uniform field magnitude instead of its spatial distribution and then how to derive it from susceptibility itself.

Mean electric field

A classical way to find the average field over given volume is

$$\langle \mathbf{E}_1 \rangle_c = \frac{1}{V} \int \mathbf{E}_1(\mathbf{r}) \, \mathrm{d}\mu \tag{7.9}$$

However, the electric field in a given point is only relevant when it acts (locally) on a charged particle. Therefore the averaged field is being weighted by probability of finding an electron in the area. The mean field is

$$\langle \mathbf{E}_1 \rangle = \frac{1}{N_0} \int \mathbf{E}_1(\mathbf{r}) n_0(\mathbf{r}) \, \mathrm{d}\mu \tag{7.10}$$

to the first order of perturbation theory. The weight taken into account is the equilibrium single electron probability density. N_0 is the total number of electrons. Note that in classical limit, i.e. the equilibrium distribution of electrons is uniform $n_0(\mathbf{r}) = \frac{N_0}{V}$, the two mean values yield the same result $\langle \mathbf{E}_1 \rangle = \langle \mathbf{E}_1 \rangle_c$. Similarly, if the field $\mathbf{E}_1(\mathbf{r})$ is homogeneous, the two mean values yield the same result as well. However opposed to classical approach, when the electrons are distributed according to their wavefunctions, neither the density nor the field is homogeneous.

Depolarization factor

As mentioned before, the inclusions respond to the local field $\mathbf{E}_{\mathrm{loc}}$ inside. It is given by a self-consistent condition

$$\mathbf{E}_{\mathrm{loc}} = \mathbf{E}_0 + \mathbf{E}_1(\mathbf{E}_{\mathrm{loc}}) \tag{7.11}$$

The depolarization field, to the first order of perturbation, E_1 is caused by the electrons displaced by the local field $\mathbf{E}_{\mathrm{loc}} = \widetilde{\mathbf{E}} \, \mathrm{e}^{-i\omega t}$ driving them, density given by (7.3). In order for us to be able to exploit the classical effective medium theory, we take the average of the depolarization field

$$\mathbf{E}_{\mathrm{loc}} = \mathbf{E}_0 + \langle \mathbf{E}_1 \rangle \tag{7.12}$$

For finding the field $\mathbf{E}_1$ by solving Poisson's equation is a formidable task in general and for we need the mean value only, we introduce a depolarization factor L in order to simplify the self consistent condition for the local electric field $\mathbf{E}_{\mathrm{loc}}$.

$$\mathbf{E}_{\mathrm{loc}} = \mathbf{E}_0 - L\frac{\mathbf{P}}{\varepsilon_0} \tag{7.13}$$

where $\mathbf{P} = \varepsilon_0 \Delta\chi \mathbf{E}_{\mathrm{loc}}$ is (linear) polarization of the material due to the displacement of free electrons. The depolarization factor L is defined as a ratio of the actual screening field (induction) $\varepsilon_0 \langle E_1 \rangle$ to the polarization P

$$\boxed{L = -\frac{\varepsilon_0 \langle E_1(E_{\mathrm{loc}}) \rangle}{P(E_{\mathrm{loc}})} = -\frac{\langle E_1(E_{\mathrm{loc}}) \rangle}{\Delta\chi E_{\mathrm{loc}}}} \tag{7.14}$$

The free electrons contribution to electric susceptibility $\Delta\chi(\omega)$ can be obtained from the conductivity spectra $\sigma(\omega)$ we calculated in chapter 6 using formula (3.11).

In order to prevent ambiguity in the depolarization factor interpretation, in the following we show that within the linear response regime it gives both the first order perturbation E' to the external field E_0 as well as the depolarization field E_1 fulfilling the self-consistent condition for the local field E_{loc}. We assume a linear dependence of the depolarization field E_1 on the local field E_{loc}

$$E_1 = -\alpha E_{\text{loc}} \tag{7.15}$$

Then it follows from eq. (7.11) that

$$E_{\text{loc}} = \frac{E_0}{1 + \alpha} \tag{7.16}$$

Now let us introduce the first order perturbation E' caused by the external field E_0

$$E' = -\beta E_0 \tag{7.17}$$

Higher orders of perturbation are obtained by reapplying this relation to itself. The depolarization field is then given by the sum of the perturbation series to infinity, whence the local field is

$$E_{\text{loc}} = E_0 + \sum_{k=1}^{\infty} (-\beta)^k E_0 = E_0 \sum_{k=0}^{\infty} (-\beta)^k = \frac{E_0}{1 + \beta} \tag{7.18}$$

By comparison of eq. (7.16) and (7.18) we see that $\alpha = \beta$. Relation to the depolarization factor is $\alpha = L\Delta\chi$.

In the following chapters, we will calculate the depolarization factor in a one-dimensional case and for a sphere.

8. 1D Case

In this chapter, we study one-dimensional case for it is rather simple and in order to acquire some insight before addressing the three-dimensional problem in the following chapter. We will find the electric field caused by the displaced conductive electrons and we will calculate the depolarization factor.

8.1 Desk analogy

The general approach to solving the Poisson's equation (as any other partial differential equation defined on the entire space) is the Fourier transform. In one-dimensional case, one needs not to solve the Poisson's equation at all in order to find the electric intensity. It can be obtained by a single integration

$$\mathbf{E}_1(x) = -\int \frac{\rho_1(x)}{\varepsilon_0} \mathrm{d}x \tag{8.1}$$

That is not however instructive with respect to the three-dimensional case. Also in the 1D universe, the dimension of the electric intensity is [Vm] instead of [Vm^{-1}]. To fix this, we present the analogy to an infinite perpendicular desk in three-dimensional space. In both cases, the Poisson's equation is mathematically equivalent. Due to reasons of symmetry, the partial derivatives in y and z directions are zero.

Fig. 8.1 explains the way to construct the perpendicular desk using one-dimensional rods. The equidistant spacing of the rods must be as follows, so that the equilibrium volumetric density n of electrons is isotropic from a macroscopic point of view. Say there are N_0 electrons in a rod of length A. The linear density

(a) Single 1D rod.   (b) Array of rods.   (c) Perpendicular desk.
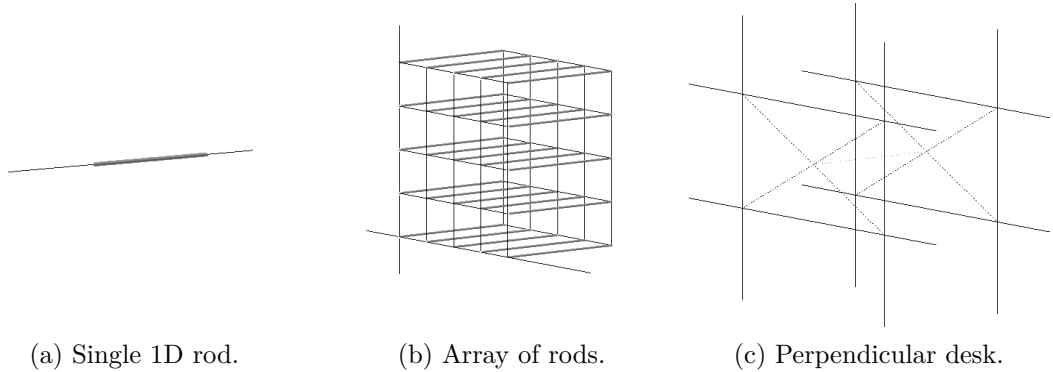
Figure 8.1: Construction of an infinite perpendicular desk in three-dimensional space using an array of equidistantly spaced one-dimensional rods. *Courtesy of Vojtěch Klimovič.*

of electrons is then $\lambda = N_0/A$. It holds for densities that

$$n = \lambda^3 = \frac{N_0^3}{A^3} \tag{8.2}$$

and so the surface density of the rods must be

$$\sigma = \frac{N_0^2}{A^2} \tag{8.3}$$

or equivalently their spacing in the grid must be $a = A/N_0$.

Now that we operate in the three-dimensional space with electrostatics well defined, we can exploit the Gauss law of electrostatics to simplify the problem. Same as within the classical electrostatics, any charged infinite layer creates a field constant in the space. The electric field outside the desk is zero, for the entire desk is electrically neutral. Furthermore in the quantum mechanical approach, where the electrons are distributed in the volume according to the wavefunction, the charge at the boundaries of the desk is zero. From that we can see that not only outside, but also at the boundary the field is zero and therefore we can derive a zero-derivative boundary condition for the potential $\Phi(x)$. We are thus enabled to use a discrete Fourier series expansion.

The physics of the one-dimensional rod and the perpendicular desk is however not exactly the same. In the desk we would discover sub-bands emerging in the dispersion relation of a band structure caused by unrestrained movement of electrons in the perpendicular directions. This also leads to different densities of states. These two physical models are not equivalent, although we can justify this analogy from the point of view of electrostatics.

8.2   Poisson's equation

We are left with the task of finding the electric intensity inside the desk. Hence we solve the Poisson's equation for the potential with the aforementioned zero-derivative boundary condition.

The wavefunctions with the zero-value boundary condition have the form

$$\Psi_k(x) = \sqrt{\frac{2}{A}} \sin\left(\frac{k\pi}{A}x\right) \tag{8.4}$$

In order to solve the Poisson's equation, we will perform a Fourier series expansion of the electron density distribution (7.2) and (7.3):

$$n_0(x) = \sum_N \mathcal{A}_N \varphi_N(x) \tag{8.5}$$

$$n_1(x) = \sum_N \mathcal{B}_N \xi_N(x) \tag{8.6}$$

Once we know the expansion coeficients $\mathcal{B}_N$, we can easily solve the Poisson's equation

$$\Delta\Phi(x) = -\frac{e}{\varepsilon_0} \sum_N \mathcal{B}_N \xi_N(x) \tag{8.7}$$

using the eigenvalue relation

$$\Delta\xi_N(x) = \lambda_N \xi_N(x) \tag{8.8}$$

The solution is given by

$$\Phi(x) = -\frac{e}{\varepsilon_0} \sum_N \frac{\mathcal{B}_N}{\lambda_N} \xi_N(x) \tag{8.9}$$

The expansion basis is to be chosen as an orthogonal set among the eigenfunctions of the "one-dimensional Laplace operator" $\frac{\mathrm{d}^2}{\mathrm{d}x^2}$ by the boundary condition.

Differing from the wavefunction, the dimension of the electron density $n(x)$ is $[\mathrm{m}^{-1}]$. Such must be also the dimension of the expansion basis functions and the expansion coefficients must be dimensionless numbers. For the coefficients are given by scalar product, it must be defined as follows:

$$\langle \varphi | \psi \rangle = A \int_0^A \varphi^*(x)\psi(x)\,\mathrm{d}x \tag{8.10}$$

The normalized expansion basis is then

$$\varphi_N(x) = \frac{\sqrt{2}}{A}\cos\left(\frac{N\pi}{A}x\right) \qquad \text{for } N = 0, 2, 4, \dots \tag{8.11}$$

$$\xi_N(x) = \frac{\sqrt{2}}{A}\cos\left(\frac{N\pi}{A}x\right) \qquad \text{for } N = 1, 3, 5, \dots \tag{8.12}$$

φ_N with N even for the equilibrium density n_0, while ξ_N with odd N for the first order perturbation density n_1. It follows from the non-trivial Fourier series coefficients

$$S_{|k-l|} = A \int_0^A \varphi^*_{|k-l|}(x)\Psi^*_k(x)\Psi_l(x)\,\mathrm{d}x = \frac{1}{\sqrt{2}} \tag{8.13}$$

$$S_{k+l} = A \int_0^A \varphi^*_{k+l}(x)\Psi^*_k(x)\Psi_l(x)\,\mathrm{d}x = -\frac{1}{\sqrt{2}} \tag{8.14}$$

for the density matrix has only non-zero elements for $m = n$ in equilibrium while in the first order of perturbation only pairs of wavefunctions of opposite parity are allowed by the dipole selection rules. Hence the expansion coefficients for the densities are

$$\mathcal{A}_N = \sum_k \frac{f_k}{\sqrt{2}}\left(\delta_{N,0} - \delta_{N,2k}\right) \tag{8.15}$$

$$\mathcal{B}_N = \sum_{k,l} \frac{\alpha_{kl}}{\sqrt{2}}\left(\delta_{N,|k-l|} - \delta_{N,k+l}\right) \tag{8.16}$$

where we used the Kronecker-δ symbol and where

$$\alpha_{kl} = \frac{f_k - f_l}{\hbar}\frac{\langle k\,|e\mathbf{r}\,|\,l\rangle \cdot \tilde{\mathbf{E}}\,\mathrm{e}^{-i\omega t}}{\omega - (\omega_k - \omega_l) + i\gamma} \tag{8.17}$$

The explicit forms of the expansion of the densities are

$$n_0(x) = \sum_k f_k\left[\frac{1}{\sqrt{2}}\varphi_0(x) - \frac{1}{\sqrt{2}}\varphi_{2k}(x)\right] \tag{8.18}$$

$$n_1(x) = \sum_{k,l} \alpha_{kl}\left[\frac{1}{\sqrt{2}}\xi_{|k-l|}(x) - \frac{1}{\sqrt{2}}\xi_{k+l}(x)\right] \tag{8.19}$$

The eigenvalues of the expansion basis functions are

$$\lambda_N = -\frac{N^2\pi^2}{A^2} \tag{8.20}$$

and the explicit form of the solution for the potential $\Phi(x)$ is

$$\Phi(x) = \frac{e}{\varepsilon_0}\sum_N \frac{\sqrt{2}A}{N^2\pi^2}\mathcal{B}_N\cos\left(\frac{N\pi}{A}x\right) \tag{8.21}$$

Electric field

The electric intensity $E_1(x)$ is obtained by taking the gradient of the potential

$$E_1(x) = -\nabla\Phi(x) = -\frac{e}{\varepsilon_0}\sum_N \frac{\sqrt{2}}{N\pi}\mathcal{B}_N \sin\left(\frac{N\pi}{A}x\right) \tag{8.22}$$

As it was noted before, in 1D case the dimension of the electric intensity is [Vm]. To fix this issue, we multiply the field by the surface density σ of the rods given by (8.3). $E_1(x) \rightarrow \sigma E_1(x)$.

The mean electric field according to the classical averaging over the length can be integrated analytically

$$\langle E_1 \rangle_c = \frac{1}{A}\int_0^A E_1(x)\mathrm{d}x = -\frac{e}{\varepsilon_0}\sigma\sum_N \frac{2\sqrt{2}}{N^2\pi^2}\mathcal{B}_N \tag{8.23}$$

which holds for N odd. This is fine for the first order perturbation expansion has non-zero coefficients just only for odd N. The mean value weighted by electron probability density is as follows.

$$\langle E_1 \rangle = \frac{1}{N_0}\int_0^A E_1(x)n_0(x)\mathrm{d}x = \frac{1}{N_0}\int_0^A E_1(x)\sum_k f_k \left|\Psi_k(x)\right|^2 \mathrm{d}x \tag{8.24}$$

The integral of a product of three sines can be expressed analytically as well

$$\int_0^A \sin\left(\frac{N\pi}{A}x\right)\frac{2}{A}\sin^2\left(\frac{k\pi}{A}x\right)\mathrm{d}x = \frac{8k^2}{N\pi(4k^2 - N^2)} \tag{8.25}$$

again well defined for odd N and hence

$$\langle E_1 \rangle = -\frac{e}{\varepsilon_0}\sigma\sum_N\sum_k \frac{8\sqrt{2}k^2}{N^2\pi^2(4k^2 - N^2)}\frac{f_k}{N_0}\mathcal{B}_N \tag{8.26}$$

8.3   Depolarization factor

For unitary local electric intensity $\mathbf{E}_{\mathrm{loc}} = 1$ (at given frequency ω), the definition relation of the depolarization factor L (7.14) simplifies to

$$L = -\frac{\langle E_1 \rangle}{\Delta\chi} \tag{8.27}$$

We have already calculated the mean depolarization field $\langle E_1 \rangle$ above. The free electrons' contribution to the susceptibility $\Delta\chi$ can be obtained from the conductivity $\sigma(\omega)$ as in (6.1) through relation (3.11):

$$\Delta\chi(\omega) = \frac{i\sigma(\omega)}{\omega\varepsilon_0} \tag{8.28}$$

The mean electric field $\langle E_1 \rangle$ turns out to have the same spectral dependence as the susceptibility $\Delta\chi$. That means the depolarization factor, as their ratio, is real-valued and frequency-independent. We shall distinguish between L and L_c,

depending on the averaging used to calculate the mean field. The value of the depolarization factor while using the classical averaging is

$$L_c = 1 \tag{8.29}$$

independent of size of the 1D quantum dot or any other parameters. This result matches the classical theory.

The values of the depolarization factor obtained utilizing the weighted averaging, however, differ. Dependence on the size, temperature and excitation is observed. Results for the depolarization factor L are plotted in fig. 8.2. It takes
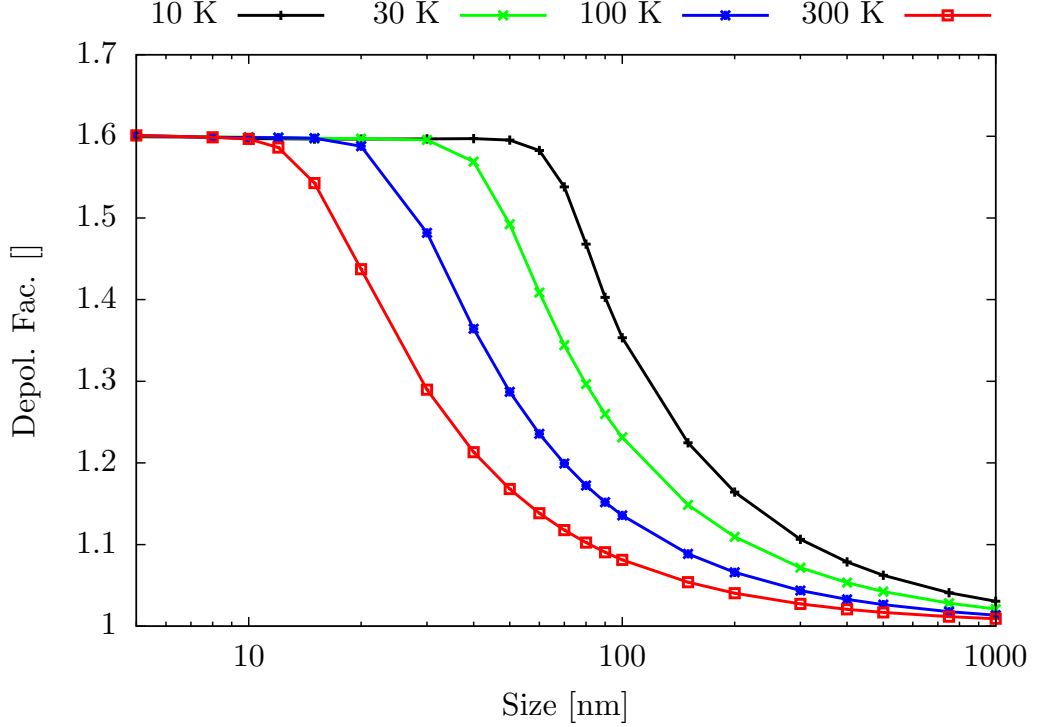

Figure 8.2: Dependence of the depolarization factor L on size of the quantum dot for various temperatures. Density of electrons $n = 10^4 \ \mu\text{m}^{-3}$.

upon values between 1 and $\frac{8}{5}$. The unity is the classical limit for large dimensions of the structure, high concentrations of electrons and high temperatures. On the other hand, the $\frac{8}{5}$ is the ratio of $\langle E_1 \rangle$ to $\langle E_1 \rangle_c$ in the most non-classical case, when only the ground level is occupied and only the transition from the ground to the first excited level occurs. In such case, the only non-zero expansion coefficients for the perturbation density are $\mathcal{B}_1 = \frac{1}{\sqrt{2}}(\alpha_{12} + \alpha_{21})$ and $\mathcal{B}_3 = -\frac{1}{\sqrt{2}}(\alpha_{12} + \alpha_{21})$. Then we get

$$\langle E_1 \rangle = -\frac{e\sigma}{\varepsilon_0 \pi^2} \frac{16}{9}(\alpha_{12} + \alpha_{21}) \tag{8.30}$$

$$\langle E_1 \rangle_c = -\frac{e\sigma}{\varepsilon_0 \pi^2} \frac{128}{45}(\alpha_{12} + \alpha_{21}) \tag{8.31}$$

and the result of the division is

$$\frac{\langle E_1 \rangle}{\langle E_1 \rangle_c} = \frac{8}{5} \tag{8.32}$$

In this chapter, we have seen that for obtaining the true depolarization factor for nanostructures within the quantum theory, it is necessary to take into consideration both the non-uniform equilibrium distribution of electrons in the volume of the quantum dot and the non-homogeneous electric field inside caused by the electrons displaced in volume as well. Neither of these phenomena is accounted for within the classical electrostatics.

9. Sphere

We proceed analogically to the 1D case. We are focused on finding the values of depolarization factor applicable for nanometric spherical inclusions. We will employ the corrected depolarization factor within the Maxwell Garnett effective medium approximation.

9.1 Multipole expansion

Also in the three-dimensional case, the Poisson's equation on the entire space is generally solved by applying the Fourier analysis. In the spherical coordinate system, one expands the angular part in the spherical harmonic series[1] and performs the Fourier-Bessel transform (also known as Hankel transform) on the radial part.

We are primarily interested in the electric intensity inside of the polarized conductive sphere. The electric field outside is not of much importance to us, but it can be found rather easily utilizing the multipole expansion. The knowledge of the field outside will enable us to formulate boundary conditions for the Poisson's equation to be solved inside the sphere and therefore will allow us to use the discrete Fourier-Bessel series (also known as Dini series) expansion of the radial part.

The densities of the electrons (7.2) and (7.3) are

$$n_0(\mathbf{r}) = \sum_{nlm} f_{nl} \, \mathcal{N}_{nl}^2 j_l^2(k_{nl}r) \, |Y_{lm}|^2 \tag{9.1}$$

$$n_1(\mathbf{r}) = \sum_{nlmn'l'm'} \alpha_{nlmn'l'm'} \, j_l(k_{nl}r) \, j_{l'}(k_{n'l'}r) Y_{l'm'}^*(\theta, \phi) Y_{lm}(\theta, \phi) \tag{9.2}$$

where

$$\alpha_{nlmn'l'm'} = \frac{e}{\hbar} \frac{(f_{n'l'} - f_{nl})\mathcal{E}_0 e^{-i\omega t}}{\omega - (\omega_{n'l'} - \omega_{nl}) + i\gamma} \, \langle n'l'm'|x|nlm \rangle \, \mathcal{N}_{n'l'}\mathcal{N}_{nl} \tag{9.3}$$

We exploit that the displaced electric charge $\rho_1(\mathbf{r}') = -en_1(\mathbf{r}')$ is confined inside the sphere of radius R to obtain a valid multipole expansion of the potential $\Phi(\mathbf{r})$ in terms of the spherical harmonics outside the sphere, Lacava [26]

$$\Phi(\mathbf{r}) = \frac{1}{4\pi\varepsilon_0} \left[4\pi \sum_{LM} \frac{1}{2L+1} \frac{1}{r^{L+1}} q_{LM} Y_{LM}(\theta, \phi) \right] \tag{9.4}$$

where

$$q_{LM} = \int Y_{LM}^*(\theta', \phi')(r')^l \rho_1(\mathbf{r}') \, \mathrm{d}^3 r' \tag{9.5}$$

For the densities represent sums of products of two wavefunctions, which are eigenfunctions of the Laplace's operator as well[2], we will need to evaluate integrals

---

[1] *The general spherical harmonics transform can be done on concentric spherical surfaces of different radii independently, but it fails to represent the radial dependence effectively*, Kazhdan et al. [25]. However from the separated structure of solution to the Schrödinger equation, we know the angular dependence is the same for any radius.

of products of three spherical harmonics, ARFKEN ET AL. [27]:

$$\int_0^{2\pi} \int_0^{\pi} Y_{LM}^*(\theta, \phi) Y_{l_1 m_1}(\theta, \phi) Y_{l_2 m_2}(\theta, \phi) \sin(\theta) \, \mathrm{d}\theta \, \mathrm{d}\phi =$$
$$= \sqrt{\frac{(2l_1 + 1)(2l_2 + 1)}{4\pi(2L + 1)}} \langle l_1 \, l_2 \, 0 \, 0 | L \, 0 \rangle \langle l_1 \, l_2 \, m_1 \, m_2 | L \, M \rangle \tag{9.6}$$

where $\langle l_1 \, l_2 \, m_1 \, m_2 | L \, M \rangle$ are the Clebsch-Gordan coefficients for coupling of angular momenta, COHEN-TANNOUDJI ET AL. [6]. The formula holds for 'physical' degrees l and orders m of the spherical harmonics. For the wavefunctions are solutions to the Schrödinger equation, they indeed are physical. The identity

$$Y_{l,m}^*(\theta, \phi) = (-1)^m Y_{l,-m}(\theta, \phi) \tag{9.7}$$

is another utile formula. Applying (9.7) to (9.5), due to properties of the Clebsh-Gordan coefficients one finds that

$$q_{LM} \neq 0 \qquad \text{only for } L = 1 \tag{9.8}$$

It is not a surprising result, since the dipole selection rules only allow transitions with $\Delta l = \pm 1$. The explicit form of the potential $\Phi(\mathbf{r})$ outside is

$$\Phi(\mathbf{r}) = \frac{1}{3\varepsilon_0} \frac{1}{r^2} q_{11} \left[Y_{11}(\theta, \phi) - Y_{1-1}(\theta, \phi) \right] \tag{9.9}$$

We employed relation $q_{11} = -q_{1-1}$ which follows from reasons of symmetry. The potential $\Phi(\mathbf{r})$ is that of a dipole aligned with x-axis. Alas the field outside the sphere generated by the first order perturbation density of charge has form as if induced by an electric dipole in the center of the sphere.

The situation is the same in classical electrostatics. The field outside of a polarized sphere has a dipole component only. However from the surface charge density and continuity condition of the potential, one can find the electric field inside the sphere is homogeneous. This does not hold in our quantum approach, as the charge remains displaced in the volume rather than on the surface. The surface charge is zero. Therefore the formula for potential outside the sphere must also hold at the surface. Electric intensity, which can be obtained by taking the gradient of the potential, is then also defined on the surface. These observations allow us to formulate a boundary condition for the radial part of the potential $\Phi(\mathbf{r})$ to be found as a solution to the Poisson's equation inside the sphere. The potential on the surface is

$$\Phi(\mathbf{r})\Big|_{r=R} = \frac{1}{3\varepsilon_0} q_{11} \left[Y_{11}(\theta, \phi) - Y_{1-1}(\theta, \phi) \right] \frac{1}{R^2} \tag{9.10}$$

and its derivative with respect to the radial coordinate r is

$$\frac{\partial \Phi(\mathbf{r})}{\partial r}\Big|_{r=R} = -\frac{2}{3\varepsilon_0} q_{11} \left[Y_{11}(\theta, \phi) - Y_{1-1}(\theta, \phi) \right] \frac{1}{R^3} \tag{9.11}$$

By comparing the two, one gets the boundary condition

$$r \frac{\partial \Phi(\mathbf{r})}{\partial r}\Big|_{r=R} = -2 \, \Phi(\mathbf{r})\Big|_{r=R} \tag{9.12}$$

for the radial part of the potential inside the sphere.

---

[2]Consider the structure of the time-independent Schrödinger equation (4.2).

9.2 Poisson's equation

We will perform the expansion of the electron density distribution (9.1) and (9.2) to their respective eigenfunction bases:

$$n_0(x) = \sum_N \mathcal{A}_N \varphi_N(x) \tag{9.13}$$

$$n_1(x) = \sum_N \mathcal{B}_N \xi_N(x) \tag{9.14}$$

Once we know the expansion coeficients $\mathcal{B}_N$, we can easily solve the Poisson's equation

$$\Delta\Phi(x) = -\frac{e}{\varepsilon_0} \sum_N \mathcal{B}_N \xi_N(x) \tag{9.15}$$

using the eigenvalue relation

$$\Delta\xi_N(x) = \lambda_N \xi_N(x) \tag{9.16}$$

The solution is given by

$$\Phi(x) = -\frac{e}{\varepsilon_0} \sum_N \frac{\mathcal{B}_N}{\lambda_N} \xi_N(x) \tag{9.17}$$

Expansion basis

The eigenfunctions are the spherical harmonics $Y_{l,m}(\theta,\phi)$ for the angular part and the spherical Bessel functions of the first kind $j_l(z)$ for the radial part of the Laplace's operator. The generally known procedure of expansion to the Fourier-Bessel series, also known as Dini series, is modified for the spherical coordinates, CHEN [28].

We will choose degree l and order m of the spherical harmonics of the expansion basis by reasoning on symmetry. The spherical harmonic for expanding the equilibrium density $n_0(\mathbf{r})$ will be $Y_{0,0}$ for both are totally symmetric. For the electric field $\mathbf{E}$ is x-polarized, the angular part of the basis for expanding the perturbation density $n_1(\mathbf{r})$ will be $Y_{1,1}(\theta,\phi) - Y_{1,-1}(\theta,\phi)$. We refer to (A.9) in order to comply with the choice of basis we made, under which we obtained the dipole selection rules (5.6).

The type l of the basis spherical Bessel function must correspond to the spherical harmonics chosen for basis, therefore $j_0(z)$ form the basis for expansion of the radial part of $n_0(\mathbf{r})$ and $j_1(z)$ for $n_1(\mathbf{r})$. The orthogonal set of the spherical Bessel functions on interval $[0,R]$ will be specified by the boundary condition.

The dimension of the electron density $n(\mathbf{r})$ is $[\text{m}^{-3}]$. Such must be also the dimension of the expansion basis functions and the expansion coefficients must be dimensionless numbers. For the coefficients are given by the scalar product, it must be defined as follows:

$$\langle\varphi|\psi\rangle = V \int \varphi^*(\mathbf{r})\psi(\mathbf{r}) \, \mathrm{d}^3r \tag{9.18}$$

We can express the basis functions φ_N and ξ_N:

$$\varphi_N(\mathbf{r}) = \frac{1}{\sqrt{V}} \mathcal{N}_N \, j_0(q_N r) \, Y_{0,0}(\theta,\phi) \tag{9.19}$$

$$\xi_N(\mathbf{r}) = \frac{1}{\sqrt{V}} \mathcal{M}_N \, j_1(k_N r) \frac{1}{\sqrt{2}} [Y_{1,1}(\theta,\phi) - Y_{1,-1}(\theta,\phi)] \tag{9.20}$$

where $\mathcal{N}_N$ and $\mathcal{M}_N$ are normalization factors of the corresponding spherical Bessel functions. Wavevectors q_N and k_N are to be determined from the boundary condition. For $\varphi_N(\mathbf{r})$ are not used as a basis to differential equation solutions, we may choose arbitrary boundary condition for the expansion basis. We proceed with zero-value boundary condition[3]

$$j_0(q_N R) = 0 \tag{9.21}$$

which, considering the explicit form of $j_0(z)$

$$j_0(z) = \frac{\sin(z)}{z} \tag{9.22}$$

gives

$$q_N R = N\pi \tag{9.23}$$

for integer $N > 0$. The normalization is given by

$$\mathcal{N}_N = N\pi\sqrt{\frac{2}{R^3}} \tag{9.24}$$

Concerning basis functions $\xi_N(\mathbf{r})$, we apply the condition (9.12) to the radial part $j_1(k_N r)$:

$$\left. r\frac{\partial j_1(k_N r)}{\partial r}\right|_{r=R} = -2\,j_1(k_N r)\Big|_{r=R} \tag{9.25}$$

We use one of the recurrence formulas, OLVER ET AL. [18], for differentiation of the spherical Bessel functions

$$\frac{\mathrm{d}}{\mathrm{d}z}j_l(z) = \frac{l}{z}j_l(z) - j_{l+1}(z) \tag{9.26}$$

to perform the derivative on the boundary condition. We obtain

$$3\,j_1(k_N R) - k_N R\,j_2(k_N R) = 0 \tag{9.27}$$

Using another recursive identity for spherical Bessel functions

$$j_{l-1}(z) + j_{l+1}(z) = \frac{2l+1}{z}j_l(z) \tag{9.28}$$

we simplify the boundary condition to

$$k_N R\,j_0(k_N R) = 0 \tag{9.29}$$

which holds for the zeros given by

$$k_N R = N\pi \tag{9.30}$$

for integer $N > 0$. The normalization is given by $\mathcal{M}_N = \mathcal{D}_N^{-1/2}$ where

$$\mathcal{D}_N = \frac{R^3}{2}\left\{(j_l')^2(k_N R) + \frac{1}{k_N R}j_l(k_N R)j_l'(k_N R) + \left[1 - \frac{l(l+1)}{k_N^2 R^2}\right]j_l^2(k_N R)\right\} \tag{9.31}$$

---

[3]We will see that this choice is handy later, when we calculate the mean electric field. Due to (9.23) and (9.30), some of the expressions will turn out as orthogonality relations.

according to LEBEDEV AND SILVERMAN [29]. Note that the prime symbol j'_l here stands for a derivative with respect to the entire argument. For $l = 1$ it can be simplified to

$$\mathcal{D}_N = \frac{R^3}{2} \left\{ j_1^2(k_N R) - j_0(k_N R) j_2(k_N R) \right\} \tag{9.32}$$

The rightmost term is zero due to the boundary condition. Exploiting the explicit formula for $j_1(z)$:

$$j_1(z) = \frac{\sin(z)}{z^2} - \frac{\cos(z)}{z} \tag{9.33}$$

one finds that also

$$\mathcal{M}_N = N\pi \sqrt{\frac{2}{R^3}} \tag{9.34}$$

The eigenvalues λ_N for eigenfunctions $\xi_N(\mathbf{r})$ of the Laplace's operator are

$$\lambda_N = -k_N^2 \tag{9.35}$$

The potential Φ can be then expressed

$$\Phi(\mathbf{r}) = \frac{e}{\varepsilon_0} \sum_N \frac{\mathcal{B}_N}{k_N^2} \xi_N(\mathbf{r}) \tag{9.36}$$

Now we are left with expansion coefficients $\mathcal{B}_N$ to be evaluated.

Expansion coefficients

Let us perform the expansions. The formal expressions for the coefficients are:

$$\mathcal{A}_N = \langle \varphi_N | n_0 \rangle \tag{9.37}$$
$$\mathcal{B}_N = \langle \xi_N | n_1 \rangle \tag{9.38}$$

Coefficients $\mathcal{A}_N$ are

$$\mathcal{A}_N = \sum_{nlm} f_{nl} V \int \varphi_N^*(\mathbf{r}) \Psi_{nlm}^*(\mathbf{r}) \Psi_{nlm}(\mathbf{r}) \, \mathrm{d}^3 x =$$
$$= \sum_{nl} f_{nl} \sqrt{V} \int_0^R \mathcal{N}_N \mathcal{N}_{nl}^2 j_0(q_N r) \, j_l^2(k_{nl} r) r^2 \mathrm{d}r \times \tag{9.39}$$
$$\times \sum_m \int_0^{2\pi} \int_0^\pi Y_{00}^*(\theta, \phi) Y_{lm}^*(\theta, \phi) Y_{lm}(\theta, \phi) \sin(\theta) \, \mathrm{d}\theta \, \mathrm{d}\phi$$

Using the explicit form of $Y_{00}(\theta, \phi) = \frac{1}{\sqrt{4\pi}}$, the angular part integration reduces to orthogonality relation for the spherical harmonics. We get

$$\mathcal{A}_N = \sqrt{V} \sum_{nl} f_{nl} \frac{2l+1}{\sqrt{4\pi}} \mathcal{N}_N \mathcal{N}_{nl}^2 \int_0^R j_0(q_N r) \, j_l^2(k_{nl} r) r^2 \mathrm{d}r \tag{9.40}$$

The radial part is to be integrated numerically using the adaptive Gauss-Kronrod quadrature, SHAMPINE [22].

The situation is a little more complicated for the perturbation density expansion.

$$\mathcal{B}_N = \sum_{nlmn'l'm'} \alpha_{nln'l'} \langle n'l'm'|x|nlm\rangle V \int \xi_N^*(\mathbf{r})\Psi_{n'l'm'}^*(\mathbf{r})\Psi_{nlm}(\mathbf{r})\mathrm{d}^3 x =$$

$$= \sum_{nln'l'} \alpha_{nln'l'} \mathcal{M}_N \mathcal{N}_{n'l'}\mathcal{N}_{nl}\sqrt{V} \int_0^R j_1(k_N r)\, j_l(k_{nl} r)\, j_{l'}(k_{n'l'} r)r^2\mathrm{d}r\times$$

$$\times \sum_{mm'} \langle n'l'm'|x|nlm\rangle \int_0^{2\pi}\int_0^\pi \frac{1}{\sqrt{2}}\left[Y_{1,1}^*(\theta,\phi) - Y_{1,-1}^*(\theta,\phi)\right]\times$$

$$\times Y_{l'm'}^*(\theta,\phi)Y_{lm}(\theta,\phi)\sin(\theta)\,\mathrm{d}\theta\,\mathrm{d}\phi \tag{9.41}$$

where $\alpha_{nln'l'}$ is

$$\alpha_{nln'l'} = \frac{e}{\hbar}\frac{(f_{n'l'} - f_{nl})\widetilde{E}_0 e^{-i\omega t}}{\omega - (\omega_{n'l'} - \omega_{nl}) + i\gamma} \tag{9.42}$$

We apply (9.7) to either $Y_{1,\pm 1}^*(\theta,\phi)$ or $Y_{l'm'}^*(\theta,\phi)$ in the angular part integral, so that we can exploit (9.6) directly. Then we evaluate the Clebsch-Gordan coefficients using method from THOMPSON [30] along with the rest of the expression.

We have computed the expansion coefficients $\mathcal{B}_N$. The perturbation density can be then expressed in terms of eigenfunctions as

$$n_1(\mathbf{r}) = \frac{1}{\sqrt{V}}\sum_N \mathcal{B}_N\mathcal{M}_N\, j_1(k_N r)\frac{1}{\sqrt{2}}\left[Y_{1,1}(\theta,\phi) - Y_{1,-1}(\theta,\phi)\right] \tag{9.43}$$

and we may proceed to the solution of the Poisson's equation (9.36) for the electric potential Φ

$$\Phi(\mathbf{r}) = \sum_N \mathcal{C}_N\, j_1(k_N r)\left[Y_{1,1}(\theta,\phi) - Y_{1,-1}(\theta,\phi)\right] \tag{9.44}$$

where we introduced

$$\mathcal{C}_N = \frac{1}{\sqrt{2V}}\frac{e}{\varepsilon_0 k_N^2}\mathcal{B}_N\mathcal{M}_N \tag{9.45}$$

Electric intensity

The electric intensity $\mathbf{E}_1(\mathbf{r})$ is obtained by taking the gradient of the potential

$$\mathbf{E}_1(\mathbf{r}) = -\nabla\Phi(\mathbf{r}) \tag{9.46}$$

Formulas for the derivative of the spherical harmonics with respect to ϕ is

$$\frac{\partial Y_{lm}(\theta,\phi)}{\partial\phi} = imY_{lm}(\theta,\phi) \tag{9.47}$$

and with respect to θ the first for $m \geq 0$:

$$\frac{\partial Y_{lm}(\theta,\phi)}{\partial\theta} = m\cot(\theta)Y_{lm}(\theta,\phi) + \sqrt{(l-m)(l+m+1)}\,e^{-i\phi}Y_{l,m+1}(\theta,\phi) \tag{9.48}$$

$$\frac{\partial Y_{lm}(\theta,\phi)}{\partial\theta} = -m\cot(\theta)Y_{lm}(\theta,\phi) - \sqrt{(l+m)(l-m+1)}\,e^{i\phi}Y_{l,m-1}(\theta,\phi) \tag{9.49}$$

and the second for $m < 0$, Abramowitz and Stegun [31]. Performing the gradient and using explicit forms for the spherical harmonics we find the electric intensity in spherical coordinates

$$E_r = \sqrt{\frac{3}{2\pi}} \sin(\theta) \cos(\phi) \sum_N \mathcal{C}_N \left[\frac{1}{r} j_1(k_N r) - k_N j_2(k_N r) \right] \qquad (9.50)$$

$$E_\theta = \sqrt{\frac{3}{2\pi}} \cos(\theta) \cos(\phi) \sum_N \mathcal{C}_N \frac{1}{r} j_1(k_N r) \qquad (9.51)$$

$$E_\phi = -\sqrt{\frac{3}{2\pi}} \sin(\phi) \sum_N \mathcal{C}_N \frac{1}{r} j_1(k_N r) \qquad (9.52)$$

Now we know the distribution of the electric field inside the spherical quantum dot due to perturbation in the distribution of electrons. For the distribution of the field, see fig. 9.1. The field inside the sphere is the solution to the Poisson's equation with the boundary condition, the field outside is given by the multipole expansion.
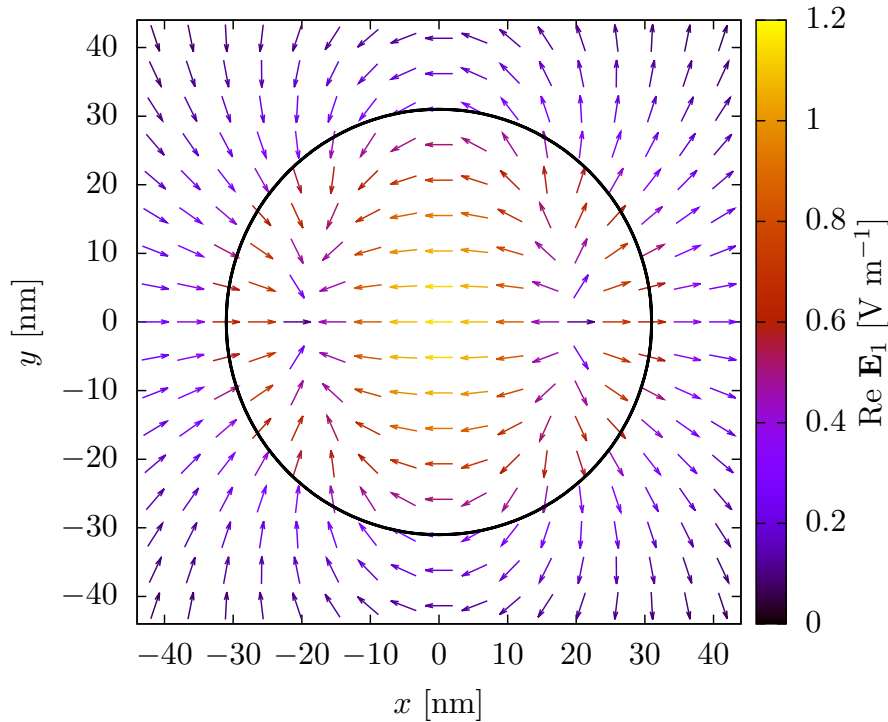

Figure 9.1: The electric field $\mathbf{E}_1$ in x, y plane inside sphere(20) caused by perturbation of unitary driving field $\mathbf{E}_{\text{loc}}(\omega = 0)$.

Mean electric field

The mean electric intensity will have only the x-component non-zero. y and z-components will vanish for reasons of symmetry. The x-component of the field is obtained from the spherical ones (9.50) as

$$E_x(r, \theta, \phi) = \sin(\theta)\cos(\phi)E_r + \cos(\theta)\cos(\phi)E_\theta - \sin(\phi)E_\phi =$$

$$= \sqrt{\frac{3}{2\pi}} \sum_N \mathcal{C}_N \left[\frac{j_1(k_N r)}{r} - \sin^2(\theta)\cos^2(\phi)k_N j_2(k_N r) \right] \tag{9.53}$$

where we exploited the trigonometric unity identity. Let us recall the expansion of the equilibrium density

$$n_0(\mathbf{r}) = \sum_N \mathcal{A}_N \frac{\mathcal{N}_N}{\sqrt{V}} j_0(q_N r) Y_{00}(\theta, \phi) \tag{9.54}$$

The explicit form of the angular dependence is $Y_{00}(\theta, \phi) = \frac{1}{\sqrt{4\pi}}$. Let us define $\mathcal{A}'_N = \mathcal{A}_N \mathcal{N}_N / \sqrt{V}$. The mean electric intensity is then

$$\langle E_x \rangle = \frac{1}{2\pi N_0} \sqrt{\frac{3}{2}} \sum_N \sum_M \mathcal{A}'_N \mathcal{C}_M \left[\int_0^R \frac{j_0(q_N r)j_1(k_M r)}{r} r^2 \mathrm{d}r \int_0^{2\pi} \int_0^\pi \sin(\theta)\mathrm{d}\theta\mathrm{d}\phi - \right.$$

$$\left. - \int_0^R k_M\, j_0(q_N r)j_2(k_M r)r^2\mathrm{d}r \int_0^{2\pi} \int_0^\pi \sin^3(\theta)\cos^2(\phi)\mathrm{d}\theta\mathrm{d}\phi \right] \tag{9.55}$$

We evaluate the angular integrals

$$\int_0^{2\pi} \int_0^\pi \sin(\theta)\mathrm{d}\theta\mathrm{d}\phi = 4\pi \tag{9.56}$$

$$\int_0^{2\pi} \int_0^\pi \sin^3(\theta)\cos^2(\phi)\mathrm{d}\theta\mathrm{d}\phi = \frac{4}{3}\pi \tag{9.57}$$

yielding

$$\langle E_x \rangle = \frac{\sqrt{6}}{N_0} \sum_N \sum_M \mathcal{A}'_N \mathcal{C}_M \int_0^R j_0(q_N r)j_1(k_M r)r - \frac{k_M}{3}\, j_0(q_N r)j_2(k_M r)r^2\mathrm{d}r =$$

$$= \frac{\sqrt{6}}{N_0} \sum_N \sum_M \mathcal{A}'_N \mathcal{C}_M \frac{k_M}{3} \int_0^R j_0(q_N r)j_0(k_M r)r^2\mathrm{d}r =$$

$$= \frac{\sqrt{6}}{N_0} \sum_N \sum_M \mathcal{A}'_N \mathcal{C}_M \frac{1}{3q_N} \int_0^R \sin(q_N r)\sin(k_M r)\mathrm{d}r \tag{9.58}$$

Considering conditions (9.23) and (9.30) we obtain

$$\int_0^R \sin(q_N r)\sin(k_M r)\mathrm{d}r = \frac{R}{2}\delta_{MN} \tag{9.59}$$

Then finally

$$\langle E_x \rangle = \frac{\sqrt{6}}{N_0} \frac{R}{6} \sum_M \frac{\mathcal{A}'_M \mathcal{C}_M}{q_M} \tag{9.60}$$

Obviously the mean field is frequency-dependent due to $\mathcal{C}_M = f(\omega)$.

Analogically, the classical averaging method gives

$$
\begin{aligned}
\langle E_x \rangle_c &= \frac{\sqrt{4\pi}\sqrt{6}}{V} \sum_M \mathcal{C}_M \int_0^R j_1(k_M r) r - \frac{k_M}{3} j_2(k_M r) r^2 \mathrm{d}r = \\
&= \frac{\sqrt{4\pi}\sqrt{6}}{V} \sum_M \mathcal{C}_M \frac{k_M}{3} \int_0^R j_0(k_M r) r^2 \mathrm{d}r = \\
&= \frac{\sqrt{4\pi}\sqrt{6}}{V} \sum_M \mathcal{C}_M \frac{1}{3} \int_0^R \sin(k_M r) r \mathrm{d}r
\end{aligned}
\tag{9.61}
$$

The radial part can be easily integrated by parts which gives

$$
\int_0^R \sin(k_M r) r \mathrm{d}r = (-1)^{M+1} \frac{R}{k_M}
\tag{9.62}
$$

and hence

$$
\langle E_x \rangle_c = \frac{\sqrt{4\pi}\sqrt{6}}{V} \frac{R}{3} \sum_M (-1)^{M+1} \frac{\mathcal{C}_M}{k_M}
\tag{9.63}
$$

9.3 Depolarization factor

For unitary local electric intensity $\mathbf{E}_{\mathrm{loc}} = 1$ (at given frequency ω), the definition relation of the depolarization factor L (7.14) simplifies to

$$
L = -\frac{\langle E_1 \rangle}{\Delta \chi}
\tag{9.64}
$$

We have already calculated the mean depolarization field $\langle E_1 \rangle$ above. The free electrons' contribution to the susceptibility $\Delta \chi$ can be obtained from the conductivity $\sigma(\omega)$ as in (6.1) through relation (3.11):

$$
\Delta \chi(\omega) = \frac{i\sigma(\omega)}{\omega \varepsilon_0}
\tag{9.65}
$$

The mean electric field $\langle E_1 \rangle$ turns out to have the same spectral dependence as the susceptibility $\Delta \chi$. That means the depolarization factor, as their ratio, is **real-valued** and **frequency-independent**. We shall distinguish between L and L_c, depending on the averaging used to calculate the mean field. The value of the depolarization factor while using the classical averaging is

$$
L_c = \frac{1}{3}
\tag{9.66}
$$

independent of size of the quantum dot or any other parameters. This result matches the classical theory.

The values of depolarization factor L obtained while using the weighted averaging, however, vary for different sizes, temperatures and charge densities. The dependence on size for various temperatures is plotted in fig. 9.2. We remind the notation from chapter 4: sphere(s) stands for a sphere with radius $R = s \left(\frac{3}{4\pi} \right)^{1/3}$ so that it has the same volume as a cube of size s. This is meant by size on the
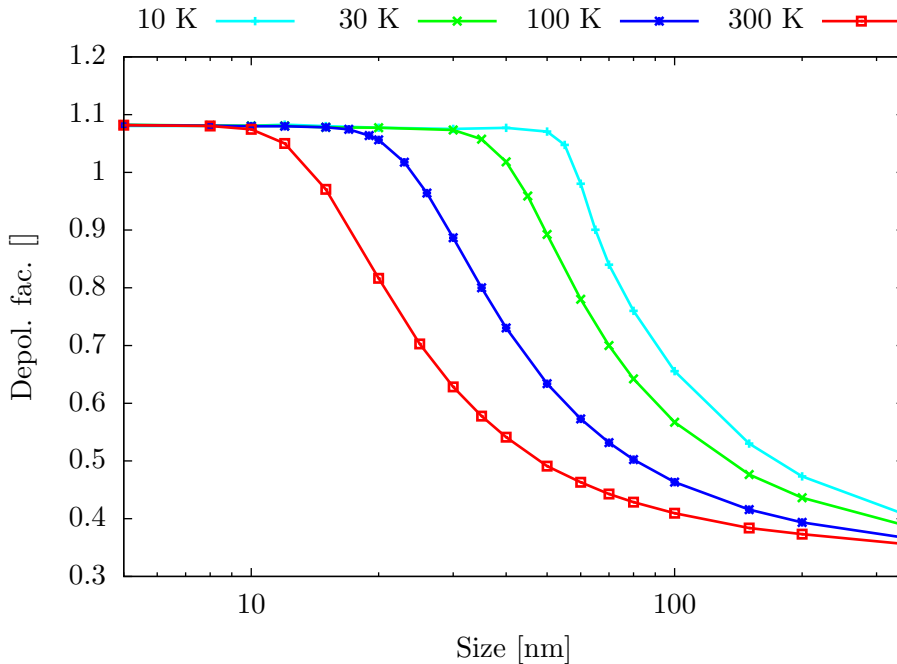
Figure 9.2: Dependence of the depolarization factor L on size of the spherical quantum dot for various temperatures. Density of electrons $n = 10^4 \ \mu\text{m}^{-3}$.

horizontal axis in the figure. The classical limit, i.e. for large sizes, high temperatures and densities, is $\frac{1}{3}$. That corresponds with the result of the classical theory. On the other hand, the saturation limit for the most non-classical cases $L_{\max}$ is elevated. We find the maximal depolarization factor $L_{\max}$ for the most non-classical case, analogically to our one-dimensional problem analysis, as

$$L_{\max} = L_c \frac{\langle E_x \rangle}{\langle E_x \rangle_c} \tag{9.67}$$

when only the ground state is occupied and only the transition from the ground to the first excited level occurs. The derivation is presented in the appendix B.1. Evaluating the exact expression returns value

$$\boxed{L_{\max} \approx 1.08164} \tag{9.68}$$

For our demonstration material GaAs, we have analyzed the dependence of the depolarization factor on the size, temperature and carrier density, and we have derived an approximate analytic formula. These material-specific results are shown in appendix B.2.

In general, we know that the depolarization factor reaches its maximum $L_{\max}$ in the most non-classical case when only the ground state is occupied. **We may identify a transition from a non-degenerate to a degenerate regime, where the depolarization effects start changing in quality.** For low concentration of conductive electrons, low temperature and small sizes, the system is non-degenerate. Adding more carriers (higher excitation pump intensity) that still occupy no excited levels increases magnitude of the response of the composite material to the external field, but does not cause any qualitative changes of the

response. On the other hand, when excited levels are occupied as well, the system becomes degenerate and the depolarization response is changing in quality, and hence the decreasing depolarization factor L. The transition between non-degenerate and degenerate regimes can be observed in fig. 9.2 where the bends are located.

9.4   Effective medium approximation

We adapt formula (3.5) for deployment of both classical L_c and the new L values of the depolarization factor where applicable. For the local field E_{loc} we obtain in the quantum approach

$$E_{\text{loc}} = E_0 \frac{\varepsilon_d}{\varepsilon_d(1 - L_c) + \varepsilon_s L_c + \Delta\chi(\omega)L(s,n,T)} \tag{9.69}$$

while in the classical way it remains

$$E_{\text{loc}} = E_0 \frac{\varepsilon_d}{\varepsilon_d(1 - L_c) + \varepsilon_s L_c + \Delta\chi(\omega)L_c} \tag{9.70}$$

In order to see the impact of modified values of the depolarization factor L on the permittivity of the composite material, we may express the contribution of the conductive electrons as

$$\Delta\varepsilon_{\text{eff}}(\omega) = \varepsilon_{\text{eff}}(\omega) - \varepsilon_g \tag{9.71}$$

We find both $\varepsilon_{\text{eff}}(\omega)$ and ε_g from the constitutive relation (3.2), for the former with the additive contribution of the free electrons susceptibility $\varepsilon_s + \Delta\chi$ obtained from the quantum formula for conductivity, and for the latter without, only ε_s. The output depends on which of the two formulas for the local field (9.69) or (9.70) we used while calculating $\varepsilon_{\text{eff}}(\omega)$. Both results are shown in fig. 9.3 and fig. 9.4 for sphere(50) and sphere(25) respectively. Parameters of the effective medium ε_g without the photoexcited free carriers are $\varepsilon_s = 12.85$ for the GaAs inclusions in GaInAs matrix $\varepsilon_d = 13.90$, filling fraction $f = 0.1$.

We may observe in the figures that the increased values of the non-classical depolarization factor L cause the susceptibility spectra to shift towards higher frequencies. We can also notice a certain decrease in magnitude. Larger depolarization factor means a stronger effective restoring force of the localized plasmonic oscillations. This force is also proportional to concentration of the displaced electrons. In order to demonstrate how the depolarization field affects the effective permittivity, we choose the carrier density $n = 10^5 \ \mu\text{m}^{-3}$ and we maximize the depolarization factor for given size by selecting low temperature $T = 10 \ K$. The apparent shift in frequency is about 1 THz to higher frequencies in both instances of sphere(50) and sphere(25).

(a) Real part.

(b) Imaginary part.

Figure 9.3: Contribution $\Delta\varepsilon_{\text{eff}}$ of conductive electrons to the total effective permittivity. Sphere(50), $T = 10$ K, $n = 10^5$ μm^{-3}, $L = 0.66$.

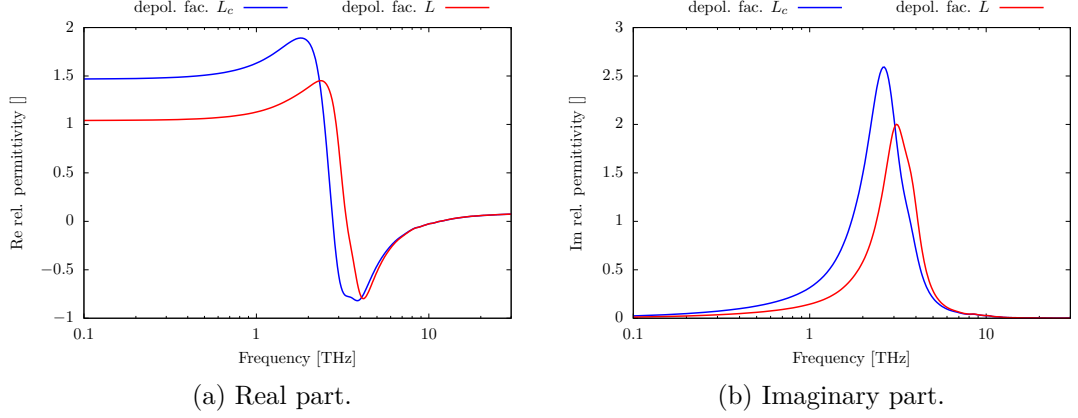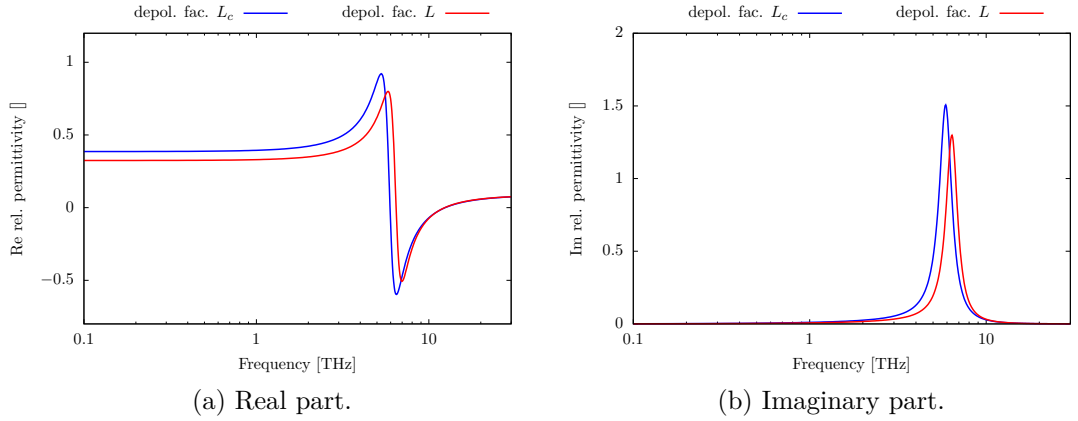(a) Real part.

(b) Imaginary part.

Figure 9.4: Contribution $\Delta\varepsilon_{\text{eff}}$ of conductive electrons to the total effective permittivity. Sphere(25), $T = 10$ K, $n = 10^5$ μm^{-3}, $L = 1.08$.

Effective volume

Let us define an effective susceptibility $\Delta\chi_{\text{eff}}$ which would give us the same result while using the classical value of the depolarization factor L_c as we get from the actual susceptibility $\Delta\chi$ and depolarization factor L: $L\Delta\chi = L_c\Delta\chi_{\text{eff}}$. Then

$$\frac{L}{L_c} = \frac{\Delta\chi_{\text{eff}}}{\Delta\chi} = \frac{\sigma_{\text{eff}}(\omega)}{\sigma(\omega)} = \frac{-e\mu(\omega)n_{\text{eff}}}{-e\mu(\omega)n} = \frac{n_{\text{eff}}}{n} = \frac{\frac{N}{V_{\text{eff}}}}{\frac{N}{V}} = \frac{V}{V_{\text{eff}}} \qquad (9.72)$$

For $L > L_c$, then $V_{\text{eff}} < V$. This can be interpreted that the same number of electrons is effectively confined in a smaller volume V_{eff}. The volume of inclusions does not enter the local field condition directly as a parameter, but the density of carriers n does enter through χ in (3.3). Then if we use $L_c\Delta\chi_{\text{eff}}$ instead of $L\Delta\chi$, it is mathematically equivalent to truncation of the spheres from V to V_{eff}. The outer area is then treated as part of the matrix. The dipole field the quantum dot generates in the matrix is neglected the same way as in the original Maxwell Garnett approximation. Obviously, a mathematical operation cannot change the

number of electrons in the system. Therefore one needs to lower the filling fraction f, as a parameter of the Maxwell Garnett mixing formula, accordingly.

10. Conclusion

We have revised the theoretical basics of quantum mechannics and electric conductivity in terahertz spectral range with particular attention given to composite materials.

We performed a direct comparison of densities of states of a quantum dot in chapter 4. We have shown that, despite differences in detailed structure, the asymptotic behaviour of densities of states is the same for various geometries, most notably a cube and a sphere, as long as they have the same volume. We also compared dipole moments of transitions between energy levels for a cube and a sphere in chapter 5 along with comparison of conductivity spectra in chapter 6. We have seen that the geometry doesn't play a crucial importance as opposed to volume. Although the spectra are not identical, we can say that the conductivities are the same, if we consider e.g. non-homogeneous broadening of the spectral lines by distribution of sizes in a sample. The different geometries are interchangeable in the scope of terahertz spectroscopy. That is handy, for we may choose an arbitrary geometry to simplify solving given problems.

In the strong confinement regime in nanostructures, the electrons are distributed in the volume according to the wavefunction, rather than to classical models. Therefore in chapter 7, we have derived the general way of finding the electric field generated by electrons displaced due to perturbation. In chapter 8 we have studied the depolarization effects in a one-dimensional case before moving on to a sphere in chapter 9. We have calculated the depolarization factor that varies largely from its classical value in nanoparticles, but converges to it in the classical limit. We have shown that the greater depolarization factor values affect spectra of the contribution of the conductive electrons to the total effective medium permittivity by shifting the plasmonic resonances towards higher frequencies.

This work contributes to theoretical models of terahertz conductivity in linear response regime. The conductivity of composite materials consisting of nanoparticles is affected by depolarization effects therein. We have shown that their strength is somewhat different from the one predicted by classical electrostatics approach. Along with the proposed correction to the depolarization factor, the Maxwell Garnett effective medium approximation formulates a comprehensive theory of dielectric properties of the composite materials with the inclusions sparsely distributed.

Appendix

A. Symmetry Groups Analysis

In this chapter we address symmetry of the quantum dots in a general manner. The symmetry of any object is independent of system of coordinates. Therefore reasoning based on symmetry allows for finding e.g. conserved integrals of motion or degeneracy of energy levels without the need to solve the actual equations of motion. We will be identifying allowed dipole transitions and non-zero elements of the conductivity tensor. We shall employ the formalism of symmetry groups and the theory of representations. We introduce only necessary basics of the formalism.

We keep in mind: **the response of a system coupled to an external field is always conditioned by its symmetry and by the symmetry of the field in question.**

A.1   Introduction to theory of representations

We may apply point operations to the geometry of a quantum dot transforming it in space. An operation of symmetry is called such, that it transforms a concerned object on itself. Physical properties must be invariant. Identity is always an operation of symmetry. Others may include the congruent transformations, i.e. rotations, reflections, point inversion or improper rotations. All of these operations always map one point to itself: the center of mass. Hence the name of point operations.

A *group* $\mathcal{G}$ is an algebraic structure consisting of a set of symmetry operations S, a binary operation $*$ and a relation of equivalence $=$.

$$\mathcal{G} = \{S, *, =\} \tag{A.1}$$

The group must satisfy four conditions: closure, associativity, include an identity operation and an inverse operation.

Let us consider a group of operations $\mathcal{G}$. Let there be a set of matrices M that represent the operations S in a given system of coordinates. let M form a group $\mathcal{M}$ with the matrix multiplication. As long as there is a *homomorphism* ϕ such that $\phi : \mathcal{M} \to \mathcal{G}$, we call $\mathcal{M}$ the matrix *representation* of the group $\mathcal{G}$.

For a symmetry group, *irreducible* representations Γ can be found. The irreducible representations of point groups, corresponding characters of operations and basis functions can be found in tables, see KOSTER [32]. There are exactly 32 crystallographic point groups. Irreducible representations can be in a sense compared to orthogonal basis of a vector space. The irreducible representations are often labeled by letters based on their dimensions d: A,B for 1, E for 2, T for 3 and so forth in case of the crystallographic point groups, whilst Σ for 1, Π for 2, Δ for 3 and so on for linear groups with at least one complete rotational symmetry. Further indexing denotes (anti-)symmetries under reflection or inversion.

A representation Γ_k describes the symmetry of its corresponding basis function ψ_k. Within a symmetry group $\mathcal{G}$, symmetry of a product of basis functions $\psi_k \times \psi_l$ is given by the *direct product* $\Gamma_k \otimes \Gamma_l$ of appropriate representations. A direct product of representations is also a representation of the group $\mathcal{G}$. It is not

however an irreducible representation in general. It can be expressed using the irreducible representations:

$$\Gamma_k \otimes \Gamma_l = a_1 \Gamma_1 \oplus a_2 \Gamma_2 \oplus a_3 \Gamma_3 \oplus ... \tag{A.2}$$

in the sense of equivalence. These decompositions can be found in the multiplication tables as well.

When evaluating an integral using calculus, we can determine if the integral is zero due to eventual odd parity of the integrand. In a similar fashion we will be able to decide whether a bra-ket (an integral) is zero based on the symmetries of the elements participating.

theorem: (Integral of basis function). *Let ψ_k be a kth basis function of representation Γ. $\forall k = 1, ..., d_\Gamma$ holds:*

$$\int \psi_k(x)\, \mathrm{d}^3x = 0 \tag{A.3}$$

unless Γ is the totally symmetric representation, often denoted Γ_1 or A_1, Σ^+.

Proof. We provide only an argument on this introduction's level of rigor. For the formal proof see e.g. WIGNER AND GRIFFIN [33]. First we realize that the operations of symmetry $\hat{R}$ have no effect on the resulting integral:

$$\int \psi_k(x)\, \mathrm{d}^3x = \hat{O}_R \int \psi_k(x)\, \mathrm{d}^3x = \int \hat{O}_R \psi_k(x)\, \mathrm{d}^3x$$

since it must be independent of choice of coordinate system. However, if ψ_k doesn't belong to the totally symmetric representation Γ_1, in general it changes under operations of symmetry of the group $\hat{O}_R \psi_k(x) \neq \psi_k(x)$ and hence also its non-zero integral would, which is a contradiction. Therefore $\int \psi_k(x)\, \mathrm{d}^3x = 0$ for $\Gamma \neq \Gamma_1$. **q.e.d.**

In other words the bra-ket

$$\left\langle \alpha \left| \hat{O}_\beta \right| \gamma \right\rangle = \int \psi_\alpha^*(x) \hat{O}_\beta \psi_\gamma(x)\, \mathrm{d}^3x \tag{A.4}$$

can be non-zero only if the product of representations contains the totally symmetric representation Γ_1, i.e. with $a_1 \neq 0$:

$$\Gamma_\alpha^* \otimes \Gamma_\beta \otimes \Gamma_\gamma = a_1 \Gamma_1 \oplus a_2 \Gamma_2 \oplus a_3 \Gamma_3 \oplus ... \tag{A.5}$$

This will help us in the next section to determine which dipole transitions are allowed.

A.2 Dipole moments

We are interested in the system's interaction with an external electric field. The group of symmetry of a homogeneous electric field is $\mathcal{C}_{\infty v}$. However that is not of a significant importance to us. We know the exact form of the dipole operator: $e\mathbf{r}$. For the purpose of the symmetry discussion we omit the electric elementary charge e. The operator then has form x, y, z^1 depending on the polarization of the field.

It is convenient that functions x, y, z are the basis functions of various irreducible representations of the point groups. Hence for a given quantum dot geometry, we only need to determine its group of symmetry and the rest can be read from tables.

The bra-ket under investigation is $\langle k \,|\, \mathbf{r} \,|\, l \rangle$. We will treat the components of the dipole moment vector separately: $\langle k \,|x|\, l \rangle$, $\langle k \,|y|\, l \rangle$, $\langle k \,|z|\, l \rangle$.

Cuboid

For instance, let us take a look at a cuboid geometry. Its group of symmetry is $\mathcal{D}_{2h}$. The representations to whom basis functions x, y, z belong are B_{3u}, B_{2u}, B_{1u} respectively. The 'u' from German *ungerade* stands for odd. First, let us suppose the initial state is the ground (totally symmetric) state $|l\rangle = A_g$, 'g' form *gerade* for even. The representation of symmetry of the bra-ket for x-polarization is then

$$\Gamma = \Gamma_{(k)}^* \otimes B_{3u} \otimes A_g \tag{A.6}$$

By a look into the multiplication table, in order to have Γ include A_g, the symmetry of the bra- needs to be $\Gamma_{(k)}^* = B_{3u}$, for $B_{3u} \otimes B_{3u} = A_g$. Apparently the the state of the system must change parity $g \to u$.

The electric field converted the ground state to a new state $|k\rangle = B_{3u}$. Let us apply the field again. For $\langle q \,|x|\, k \rangle$ we now get

$$\Gamma = \Gamma_{(q)}^* \otimes B_{3u} \otimes B_{3u} \tag{A.7}$$

which only allows for $|q\rangle = A_g$ that has the same symmetry as the ground state. It doesn't necessarily mean the system *is* in the ground state though.

For a change, let us apply y-polarized field to the first excited state we obtained by the x-polarized pulse:

$$\Gamma = \Gamma_{(q')}^* \otimes B_{2u} \otimes B_{3u} = \Gamma_{(q')}^* \otimes B_{1g} \tag{A.8}$$

The only viable evolution of the system – other than no interaction at all – is $|q'\rangle = B_{1g}$. The basis function is the axial vector S_z. The system changes parity again, but its symmetry is no longer that of the ground state.

Sphere

In the preceding part, we chose an asymmetric cuboid over a cube and thus we have avoided degeneracy. To contrast that we now choose a sphere, whose group $\mathcal{K}$ has the full rotational symmetry. The representations are Σ with total symmetry, Π with dimension of 3 indicating three-fold degeneracy, Δ, Φ,... The basis functions are the spherical harmonics Y_{lm}. The symmetry $\mathcal{C}_{\infty v}$ of both the

---

[1]A photon also has group of symmetry $\mathcal{C}_{\infty v}$. Say it propagates along axis z. As a boson with spin s=1, its corresponding representation is Π and the tabular basis functions are x, y based on polarization, which is in agreement with the results for the field.

field (or the photon) and the spherical harmonics for $l = 1$ lets us make choice

$$x \to \frac{1}{\sqrt{2}} \left(Y_{1,1} - Y_{1,-1} \right)$$

$$y \to \frac{1}{\sqrt{2}} \left(Y_{1,1} + Y_{1,-1} \right) \tag{A.9}$$

$$z \to Y_{1,0}$$

Let us begin with $\langle k \,|z|\, l \rangle$ where the initial state is the ground state $|l\rangle = \Sigma^+ = Y_{0,0}$. Let us express the integrand with basis functions directly

$$\psi_k^* Y_{1,0} Y_{0,0} = \psi_k^* Y_{1,0} \tag{A.10}$$

From tables follows that only the choice $\psi_k^* = Y_{1,0}$ gives a result containing $\Sigma^+ = Y_{0,0}$, for:

$$Y_{1,0} Y_{1,0} = -\frac{1}{\sqrt{3}} Y_{0,0} + \sqrt{\frac{2}{3}} Y_{2,0} \tag{A.11}$$

Only the first term contributes to non-zero dipole moment. Once more the change of parity from Σ^+ to Π_z^-.

Applying the field to the system again, coupled by $\langle q \,|z|\, k \rangle$, we obtain

$$\psi_q^* Y_{1,0} Y_{1,0} = \psi_k^* \left\{ -\frac{1}{\sqrt{3}} Y_{0,0} + \sqrt{\frac{2}{3}} Y_{2,0} \right\} \tag{A.12}$$

which allows for ψ_q^* become either $Y_{0,0}$ or $Y_{2,0}$ which yield non-zero coefficient for $Y_{0,0}$ in the decomposition of the product.

We can see that interaction with z-polarization of the field is allowed for $\Delta l = \pm 1, \Delta m = 0$. It can be shown that for x and y polarizations the transitions are allowed for $\Delta l = \pm 1, \Delta m = \pm 1$. The seeming difference between z as opposed to x and y polarizations is not caused by any physical symmetry breaking, but only by our choice of coordinates for mathematical description of the spherical harmonics. The physical properties are independent of the coordinate system.

The result from this section is following. **The parity of the state of the system must change so that a dipole transition can occur.** Although this is not the only requirement for the dipole transition to happen. The initial and final orbitals must overlap and the energy of photons must be close to resonance with the energy difference of the two levels.[2]

We note that clearly the selection rules are identical for geometries sharing the same symmetry group. There is no way that radial structure of a studied object is affected by point operations of symmetry. Therefore within this analysis the following shapes are equivalent: e.g. a cylinder, a rotational ellipsoid, a tube and even a toroid with group $\mathcal{D}_{\infty,h}$.

---

[2]This analysis based on groups of symmetry is not exhaustive. We will continue the investigation of dipole moments in chapter 5.

A.3 Conductivity tensor

As follows from (2.28), the dependence of the tensor of conductivity on symmetry of the quantum dot is characterized by the product of two dipole moments. Both of the bra-kets need to be non-zero in order to produce a non-zero element of the conductivity tensor

$$\sigma_{\lambda\mu} \propto \left\langle k \left| x_\lambda \right| l \right\rangle \left\langle l \left| x_\mu \right| k \right\rangle \tag{A.13}$$

We suppose no magnetic fields and thus no loops of electric current. We also don't take spin representations into account. The structure of multiplication tables of representations and their basis functions is such that the totally symmetric representation Γ_1 only appears on the diagonal. Therefore in the coordinate system given by the choice of basis functions one cannot obtain a non-zero off-diagonal element of the conductivity tensor. The conductivity tensor can be always diagonalized; the basis functions of the group representations determine the axes along which the tensor is diagonal.

The question stands, whether it is possible to find a coordinate system in which the tensor is non-diagonal for a given point group. It is very well possible to rotate the coordinate system and find non-zero off-diagonal elements if the diagonal elements in the initial basis have not all the same value, i.e. if we are dealing with anisotropic material/object. We can decide whether the diagonal elements have the same values or not based on eventual degeneracy of levels.

In the linear response regime, we assume the initial state of the system is the ground state $|k\rangle = \Gamma_1$. Then let bra-kets $\langle k|x|l\rangle\langle l|x|k\rangle$ yield non-zero product. There is only one[3] such representation basis function $|l\rangle$ – and it is indeed different from $|m\rangle$ – that yields non-zero product of $\langle k|x|m\rangle\langle m|x|k\rangle$. Contribution of these bra-ket products to the conductivity are weighted by a factor of form $\frac{1}{\omega+\omega_{k\nu}+i\gamma}$, see (2.28), where ν stands for either l or m. The contribution to diagonal conductivity elements can be the same only if $\omega_{kl} = \omega_{km}$, which implies degeneracy of the states.

As an exemplary geometry let us pick a square-base pyramid. The corresponding point group is $\mathcal{C}_{4v}$. Functions x, y form basis of a representation E of a two-fold degenerated state, while function z forms a basis of the totally symmetric representation A_1. Therefore $\sigma_{xx} = \sigma_{yy} \neq \sigma_{zz}$. Let us rotate the coordinate system about the axis z by an angle α. The off-diagonal elements are

$$\sigma_{x'y'} = -\sigma_{xx}\cos(\alpha)\sin(\alpha) + \sigma_{yy}\sin(\alpha)\cos(\alpha) = 0 \tag{A.14}$$
$$\sigma_{y'x'} = -\sigma_{xx}\sin(\alpha)\cos(\alpha) + \sigma_{yy}\cos(\alpha)\sin(\alpha) = 0 \tag{A.15}$$

for $\sigma_{xx} = \sigma_{yy}$. That is not surprising because we only rotated the system in the plane spanned by the basis functions x and y of a degenerated state. Let us now in contrast rotate around axis y. Then

$$\sigma_{x'z'} = \sin(\alpha)\cos(\alpha)(-\sigma_{xx} + \sigma_{zz}) \tag{A.16}$$
$$\sigma_{z'x'} = \sin(\alpha)\cos(\alpha)(-\sigma_{xx} + \sigma_{zz}) \tag{A.17}$$

which are non-zero.

Let us suppose a cube, point group $\mathcal{O}_h$. All three functions x, y, z form basis of the same representation T_{1u} of three-fold degenerated states. Within the linear

---

[3]Recall the diagonal structure of multiplication tables.

response, there is no coordinate system in which the conductivity tensor acquired any non-zero off-diagonal elements. However by a pump pulse preceding the probing pulse for non-linear response measurement, we would break the degeneracy in at least one direction. Then the diagonal elements begin to differ from each other and a coordinate system can be found, in which non-zero off-diagonal elements arise.

B. Depolarization Factor Analysis

In chapter 9, we have calculated the depolarization factor L by evaluating the quantum formula for electric current while simultaneously solving the Poisson's equation with the perturbation distribution of electrons. Here we provide the derivation of the exact value of the maximum L_{max}.

Calculation the depolarization factor is a formidable task, therefore we will be looking for an approximate analytic expression that would yield – for given size s, carrier density n and temperature T – the correct value of the depolarization factor $L(s, n, T)$ directly.

B.1 Exact maximum

In analogy to our one-dimensional problem analysis, we find the maximal depolarization factor L_{max} for the most non-classical case as

$$L_{\text{max}} = L_c \frac{\langle E_x \rangle}{\langle E_x \rangle_c} \tag{B.1}$$

when only the ground state is occupied, i.e. $f_{1,0} = N_0$ while $f_{nl} = 0$ otherwise, and only the transition from the ground to the first excited level occurs, i.e. $|n = 1, l = 0, m = 0\rangle \to |n' = 1, l' = 1, m' = \pm 1\rangle$. Using (9.60) and (9.63) we obtain

$$L_{\text{max}} = L_c \frac{V}{2\sqrt{4\pi} N_0} \frac{\sum\limits_N \dfrac{\mathcal{A}'_N \mathcal{C}_N}{q_N}}{\sum\limits_M (-1)^{M+1} \dfrac{\mathcal{C}_M}{k_M}} \tag{B.2}$$

Equilibrium expansion coefficients

When only the ground state is occupied, the expansion coefficients for the equilibrium density are

$$
\begin{aligned}
\mathcal{A}'_N &= \frac{N_0}{\sqrt{4\pi}} \mathcal{N}_N^2 \mathcal{N}_{1,0}^2 \int_0^R j_0(q_N r) j_0^2(k_{1,0} r) r^2 \mathrm{d}r = \\
&= \frac{N_0}{\sqrt{4\pi}} \mathcal{N}_N^2 \mathcal{N}_{1,0}^2 \frac{1}{q_N k_{1,0}^2} \int_0^R \frac{\sin(q_N r) \sin^2(k_{1,0} r)}{r} \mathrm{d}r
\end{aligned} \tag{B.3}
$$

The integral can be expressed analytically using the sine integral function Si as follows

$$
\begin{aligned}
\int_0^R &\frac{\sin(q_N r) \sin^2(k_{1,0} r)}{r} \mathrm{d}r = \\
&= \frac{1}{4} \Big[2\mathrm{Si}(q_N R) + \mathrm{Si}(2k_{1,0} R - q_N R) - \mathrm{Si}(2k_{1,0} R + q_N R) \Big]
\end{aligned} \tag{B.4}
$$

The sine integral Si is defined as

$$\mathrm{Si}(z) = \int_0^z \frac{\sin(x)}{x} \mathrm{d}x \tag{B.5}$$

which can be evaluated to arbitrary precision. Considering $q_N = \frac{N\pi}{R}$, $k_{1,0} = \frac{\pi}{R}$ and $\mathcal{N}_N^2 = \frac{2N^2\pi^2}{R^3}$, $\mathcal{N}_{1,0}^2 = \frac{2\pi^2}{R^3}$, we may simplify the expression for the coefficients

$$\mathcal{A}_N' = \frac{N_0}{\sqrt{4\pi}}\frac{\pi}{R^3}N\mathcal{S}_N \tag{B.6}$$

where we introduced

$$\mathcal{S}_N = \left[2\mathrm{Si}(N\pi) + \mathrm{Si}(2\pi - N\pi) - \mathrm{Si}(2\pi + N\pi)\right] \tag{B.7}$$

We also recall that $k_M = \frac{M\pi}{R}$ and hence the upper bound for for the depolarization factor $L_{\max}$ is

$$L_{\max} = L_c\frac{\pi}{6}\frac{\displaystyle\sum_N \mathcal{S}_N\,\mathcal{C}_N}{\displaystyle\sum_M \frac{(-1)^{M+1}}{M}\,\mathcal{C}_M} \tag{B.8}$$

Unlike in the one-dimensional case, here we will not be able to divide the sums without finding the expansion coefficients of the electric field $\mathcal{C}_N, \mathcal{C}_M$ respectively.

Perturbation expansion coefficients

Only the transition from the ground to the first excited level taken into consideration, the coefficients are

$$\mathcal{C}_N = \frac{\alpha_{1,0,1,1}}{2}\frac{e}{\varepsilon_0 k_N^2}\mathcal{M}_N^2\mathcal{N}_{1,0}\mathcal{N}_{1,1}\int_0^R j_1(k_N r)j_0(k_{1,0}r)j_1(k_{1,1}r)r^2\mathrm{d}r\times$$
$$\times\int_0^{2\pi}\int_0^\pi \sin(\theta)\times$$
$$\times\Big[\langle 1,0,0|x|1,1,1\rangle\left(Y_{1,1}^*(\theta,\phi) - Y_{1,-1}^*(\theta,\phi)\right)Y_{0,0}^*(\theta,\phi)Y_{1,1}(\theta,\phi)+$$
$$+\langle 1,0,0|x|1,1,-1\rangle\left(Y_{1,1}^*(\theta,\phi) - Y_{1,-1}^*(\theta,\phi)\right)Y_{0,0}^*(\theta,\phi)Y_{1,-1}(\theta,\phi)\Big]\,\mathrm{d}\theta\mathrm{d}\phi \tag{B.9}$$

Using the explicit form of $Y_{0,0} = \frac{1}{\sqrt{4\pi}}$, the angular part reduces to orthogonality relation for the spherical harmonics

$$\int_0^{2\pi}\int_0^\pi\left(Y_{1,1}^* - Y_{1,-1}^*\right)Y_{1,\pm 1}\sin(\theta)\mathrm{d}\theta\mathrm{d}\phi = \delta_{1,1}\delta_{1,\pm 1} - \delta_{1,1}\delta_{-1,\pm 1} \tag{B.10}$$

Exploiting that and knowing $\langle 1,0,0|x|1,1,-1\rangle = -\langle 1,0,0|x|1,1,1\rangle$, one obtains

$$\mathcal{C}_N = \frac{\alpha_{1,0,1,1}}{2}\frac{e}{\varepsilon_0}\frac{\mathcal{M}_N^2}{k_N^2}\mathcal{N}_{1,0}\mathcal{N}_{1,1}\frac{2}{\sqrt{4\pi}}\langle 1,0,0|x|1,1,1\rangle\times$$
$$\times\int_0^R j_1(k_N r)j_0(k_{1,0}r)j_1(k_{1,1}r)r^2\mathrm{d}r \tag{B.11}$$

Recalling $\mathcal{M}_N^2 = \frac{2N^2\pi^2}{R^3}$ and $k_N = \frac{N\pi}{R}$, and therefore

$$\frac{\mathcal{M}_N^2}{k_N^2} = \frac{2}{R} \tag{B.12}$$

One can see the only part of $\mathcal{C}_N$ that depends on N is the radial integral.

We know the wavevectors $k_N = \frac{N\pi}{R}$ and $k_{1,0} = \frac{\pi}{R}$, but we cannot express $k_{1,1}$ explicitly. k satisfying the boundary condition $j_1(kR) = 0$ are solutions to transcendent equation

$$\tan(kR) - kR = 0 \tag{B.13}$$

The zeros can be approximated by zeros of the cosine for large n, but for $n = 1$ the relative error is large. Therefore $k_{1,1}$ is to be found numerically. We employ at least the explicit forms of k_N and $k_{1,0}$ in order to facilitate the integration:

$$\int_0^R j_1(k_N r) j_0(k_{1,0} r) j_1(k_{1,1} r) r^2 \mathrm{d}r = \frac{R}{8k_{1,1}^2 \pi^3} \frac{k_{1,1}^2 R^2 + (N^2 - 1)\pi^2}{N^2} \, \mathcal{U}_N \tag{B.14}$$

where we introduced

$$\mathcal{U}_N = \Big[\mathrm{Si}(k_{1,1}R + (N-1)\pi) + \mathrm{Si}(k_{1,1}R - (N-1)\pi) - $$
$$- \mathrm{Si}(k_{1,1}R + (N+1)\pi) - \mathrm{Si}(k_{1,1}R - (N+1)\pi) \Big] \tag{B.15}$$

The coefficients $\mathcal{C}_N$ can be now expressed as

$$C_N = c \, \frac{k_{1,1}^2 R^2 + (N^2 - 1)\pi^2}{N^2} \, \mathcal{U}_N \tag{B.16}$$

where c is a constant independent of N that will cancel when calculating $L_{\max}$.

Results

$$L_{\max} = L_c \frac{\pi}{6} \frac{\displaystyle\sum_N \frac{k_{1,1}^2 R^2 + (N^2 - 1)\pi^2}{N^2} \, \mathcal{U}_N \, \mathcal{S}_N}{\displaystyle\sum_M \frac{k_{1,1}^2 R^2 + (M^2 - 1)\pi^2}{M^2} \, \mathcal{U}_M \, \frac{(-1)^{M+1}}{M}} \tag{B.17}$$

For sufficiently large N, all the sine integrals obtained above can be approximated by $\mathrm{Si}(\pm M\pi)$ and converge to its either positive or negative limit. Then, due to their structure, coefficients $\mathcal{S}_N$ and $\mathcal{U}_N$ approach zero for increasing N, and so do the entire summands. The sums in both numerator and denominator are convergent. Evaluated numerically, the saturation limit of the depolarization factor in the most non-classical case is

$$\boxed{L_{\max} \approx 1.08164} \tag{B.18}$$

$L_{\max}$ is the saturation limit of the depolarization factor for non-degenerate regime of the system of conductive electrons in a sphere.

B.2 Approximate analytic formula

We have shown that $L_{\max} \approx 1.08164$. For convenience, here we set its value to $13/12 = 1.08\overline{3}$

$$L_{\max} \quad \approx \quad \frac{13}{12} = \frac{13}{4} L_c \tag{B.19}$$

$$\Delta L_{\max} \quad \approx \quad \frac{3}{4} = \frac{9}{4} L_c \tag{B.20}$$

We remind the notation used throughout the thesis: s corresponds to radius $R = s \left(\frac{3}{4\pi}\right)^{1/3}$ so that the sphere has the same volume as a cube of size s.

Functional form

The additive correction to the classical depolarization factor $\Delta L = L - L_c$ can be seen in fig. B.1 in the log-log scale for certain temperatures and el. concentrations. The slope of the decreasing values of additions to the depolarization factor after the bend is $\frac{\Delta y}{\Delta x} = -1$. Such slope in the log-log scale means the dependence is reciprocal $\Delta L \sim s^{-1}$. Therefore the data are fitted using function

$$\Delta L(s, n, T) = \frac{\alpha(n, T)}{s - \beta(n, T)} \tag{B.21}$$

An eventual additive constant is zero, for ΔL has to vanish in the classical limit $s \to \infty$. The shift β on the x-axis causes the deformation of the straight lines of x^{-1} in the log-log plot. The fitted values of α and β show certain correlation within the fit error in most cases

$$\alpha = 2\beta \tag{B.22}$$

Fit using the single-parameter function

$$\Delta L(s, n, T) = \frac{2\beta(n, T)}{s - \beta(n, T)} \tag{B.23}$$

is also performed. Both fits are also plotted in the fig. B.1. For simplicity, we use the single-parameter fitting function henceforth. The results appear as sufficiently precise within our approximation.
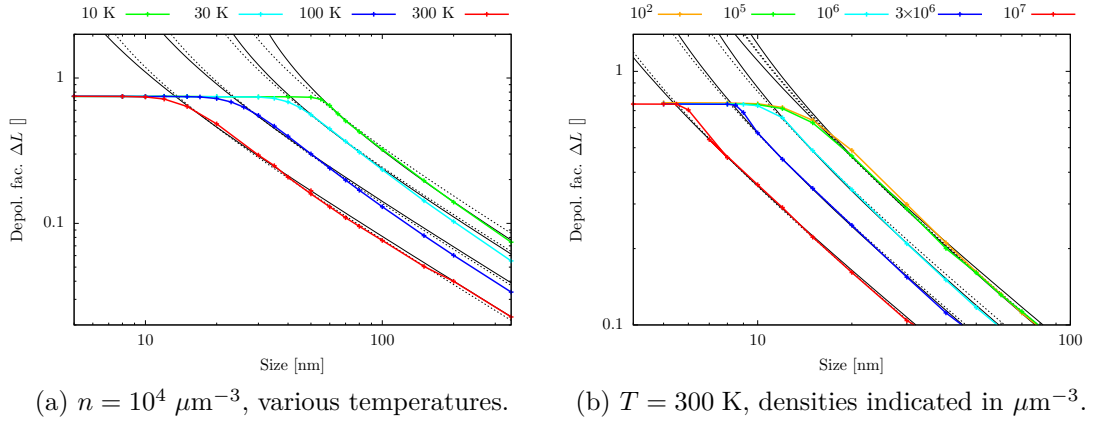

(a) $n = 10^4 \ \mu\text{m}^{-3}$, various temperatures.   (b) $T = 300$ K, densities indicated in μm^{-3}.

Figure B.1: The additive correction to the classical depolarization factor ΔL dependence on size s in the log-log scale. Solid black lines are fitted via two parameters; dotted lines are fitted using a single parameter.

The parameter β controls the position of the bend s_0 in the dependence of the depolarization factor on size of the sphere. We define the bend position as the intersection of the fitted dependence $\Delta L(s, n, T)$ with the $\Delta L = \Delta L_{\text{max}}$

$$\frac{2\beta(n, T)}{s_0(n, T) - \beta(n, T)} = \frac{3}{4} \tag{B.24}$$

which gives

$$s_0(n, T) = \frac{11}{3} \beta(n, T) \tag{B.25}$$

Note that for $\beta \to 0$ and $s \to s_0$ (i.e. zero as well), the depolarization factor correction as given by eq. (B.23) is well defined and yields $\Delta L \to \Delta L_{\max}$, which holds true also for $\alpha = 2\beta$ and hence supports the ansatz, although strictly speaking it only requires that for $\beta \to 0$ also $\alpha \to 0$.

Asymptotes

The dependence of the parameter $\beta(n, T)$ on carrier density n and temperature T is shown in fig. B.2. We observe that both temperature and density impose an upper limit for β independently of each other. We can see that for low concentrations of conductive electrons the parameter β depends solely on temperature, while for concentrations large enough it depends on concentration indifferent of temperature. Similarly for low temperatures the parameter β depends on concentration, while for high temperatures the concentration dependence becomes less significant. In this manner the influence of concentration and temperature is symmetric. The asymptotes of the density $\beta_n(n)$ and temperature dependence $\beta_T(T)$ are fitted in fig. B.2a and fig. B.2b respectively.

(a) Density dependence, various temperatures. (b) Temp. dependence, various densities.
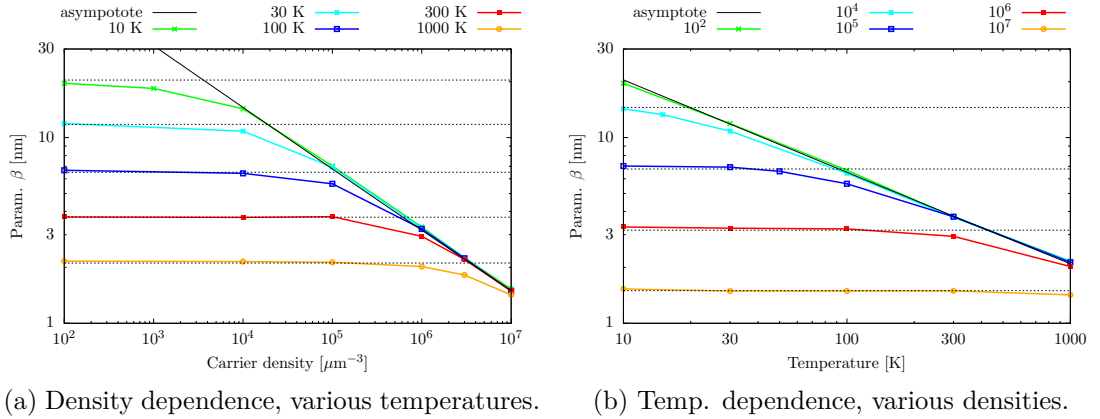
Figure B.2: Parameter $\beta(n, T)$. Solid lines represent the asymptotes fitted in the plot, dotted lines represent values of the asymptotes from the other plot.

The function form of the asymptotes is as follows. From fig. B.2a we can determine the slope in the log-log scale $\frac{\Delta y}{\Delta x} = -\frac{1}{3}$, therefore $\beta_n(n) \sim n^{-1/3}$. Similarly in fig. B.2b we observe $\frac{\Delta y}{\Delta x} = -\frac{1}{2}$ and thus $\beta_T(T) \sim T^{-1/2}$.

$$\beta_n(n) = \frac{\gamma}{n^{\frac{1}{3}} + \lambda} + \kappa \tag{B.26}$$

$$\beta_T(T) = \frac{\delta}{T^{\frac{1}{2}} + \lambda} + \kappa \tag{B.27}$$

The exponents (and dimensions of γ and δ seen below) can also be justified by the underlying physics. The bend position s_0 shifts to the largest size of the quantum dot, for which the electrons inside occupy the ground state only

(or, more accurately, the excited states occupation can be neglected) for given concentration n and temperature T. The ground energy level can accommodate up to two electrons (due to the spin degeneracy). The number of electrons in the quantum dot is given by $N_0 = nV_0$. By taking the cube root we obtain const. $= n^{1/3} s_0$ and hence $\beta \sim s_0 \sim n^{-1/3}$. Also for s_0, the *width* of the Fermi-Dirac distribution given by $k_B T$ must scale with the separation of the ground and excited energy levels ΔE proportional to s^{-2}. Therefore we find that $k_B T \sim s_0^{-2}$ which yields $\beta \sim s_0 \sim T^{-1/2}$.

Furthermore the parameters κ and λ must be zero having considered the following limits. For arbitrary finite n and T, one can find sufficiently small size s of a potential well so that the number of electrons N inside is low enough and the separation of energy levels ΔE is high enough for only the ground state to be occupied. As we established earlier, that is the most non-classical case corresponding to the saturation limit of the depolarization factor $L_{\max}$. An analytic continuation for $n \to \infty$ and/or $T \to \infty$ gives $s_0(n, T) \to 0$, and so $\beta(n, T) \to 0$, leaving $\kappa = 0$. Concerning λ, $\beta(n, T)$ needs to be well defined for $n \to 0$ and $T \to 0$ and also in the limit only the ground state will be occupied for arbitrarily large s, so it cannot shift the asymptote to the right nor to the left on the x-axis, setting $\lambda = 0$. We are left with the asymptotes in the form of

$$\beta_n(n) = 0.312\, n^{-\frac{1}{3}} \tag{B.28}$$

$$\beta_T(T) = 64.5\, T^{-\frac{1}{2}} \tag{B.29}$$

where the values of the non-zero parameters $\gamma = 0.312 \pm 0.004$ (dimensionless) and $\delta = 64.5 \pm 0.7$ nm K$^{1/2}$ have been determined by the fit in fig. B.2a and fig. B.2b respectively.

The unifying parameter to dependencies on size, temperature and density of electrons appears to be the relative occupation of ground and excited energy levels. That is, however, not an input parameter of the model. Instead, we derived $L(s, n, T)$ formula as follows

$$L(s, n, T) = \min \left[L_{\max}; L_c + \frac{2 \min\left[\beta_n(n); \beta_T(T) \right]}{s - \min\left[\beta_n(n); \beta_T(T) \right]} \right] \tag{B.30}$$

This formula holds at least approximately. Certain errors appear in the vicinity of points where the asymptotic values meet and where the actually correct dependencies bend smoothly, i.e. when $\beta_n(n) \approx \beta_T(T)$ and also $L(s, n, T) \approx L_{\max}$. The errors can be seen in fig. B.3. The latter is inherent to all size dependencies. The case of $\beta_n(n) \approx \beta_T(T)$ is observed for 30 K in the figure. The smooth bend, see the $T = 30$ K, $n = 10^4$ μm^{-3} point (fig. B.2), is not accounted for. The asymptotic value of $\beta_T(30)$ is used instead and hence the offset. The size dependencies in the fig. B.3 for 300 K and 100 K correspond well to the asymptotic values of $\beta_T(T)$, while for 10 K it follows the $\beta_n(n)$ asymptote.
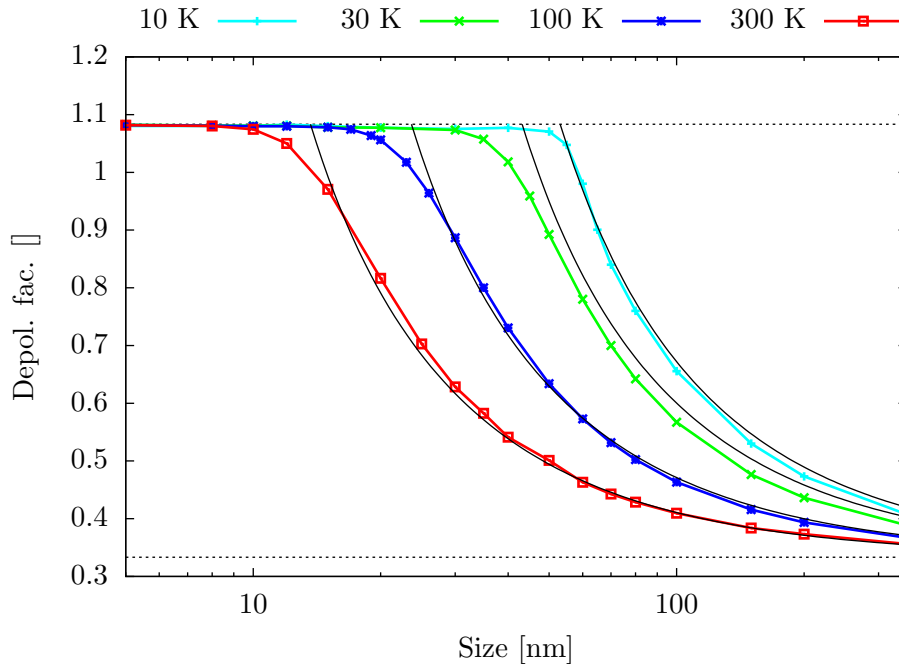
Figure B.3: Dependence of the depolarization factor L on size of the spherical quantum dot for various temperatures. Density of electrons $n = 10^4$ μm^{-3}. Horizontal dotted lines show values $L = L_c$ and $L = L_{max}$. The black solid lines show the estimated depolarization factor based on our formula $L(s, n, T)$.

Different materials

The depolarization factor values used for fitting in this analysis have been calculated specifically for our demonstration material GaAs. Its convenient properties like isotropic effective mass, holes significantly heavier then electrons and single energy minimum in the conduction band facilitate the analysis, but are not common to most materials. Therefore the derivation presented above is not universally applicable, but may serve as a guideline for such analysis in other materials.

Different material properties would lead to different fitted values of parameters γ and δ. Changing the effective mass of electrons will affect mostly parameter δ, for it controls separation of energy levels. Anisotropy of the effective mass would, presumably, cause anisotropy of the depolarization factor as well, in a similar manner as breaking of the symmetry of the shape of inclusions does. Eventual multiple minima of the energy bands most probably scale parameter γ, as they effectively increase degeneracy of the energy levels. Finally, while performing this analysis for materials in which the effective mass approximation is not applicable at all, one must handle the density of states as needed.

Bibliography

[1] J. Lloyd-Hughes and Tae-In Jeon. A review of the terahertz conductivity of bulk and nano-materials. *Journal of Infrared, Millimeter, and Terahertz Waves*, 33(9):871–925, 2012.

[2] H. Němec, V. Zajac, P. Kužel, P. Malý, S. Gutsch, D. Hiller, and M. Zacharias. Charge transport in silicon nanocrystal superlattices in the terahertz regime. *Phys. Rev. B*, 91:195443, May 2015. doi: 10.1103/PhysRevB. 91.195443.

[3] H. B. Callen. *Thermodynamics and an Introduction to Thermostatistics.* Wiley, 1985. ISBN 9780471862567.

[4] M. P. Marder. *Condensed matter physics.* Wiley-Interscience. John Wiley, 2000. ISBN 9780471177791.

[5] V. Pushkarev, T. Ostatnický, H. Němec, T. Chlouba, F. Trojánek, P. Malý, M. Zacharias, S. Gutsch, D. Hiller, and P. Kužel. Quantum behavior of terahertz photoconductivity in silicon nanocrystals networks. *Phys. Rev. B*, 95:125424, Mar 2017. doi: 10.1103/PhysRevB.95.125424.

[6] C. Cohen-Tannoudji, B. Diu, and F. Laloë. *Quantum mechanics.* Quantum Mechanics. Wiley, 1977. ISBN 9780471164333.

[7] J. R. Chelikowsky and S. G. Louie. *Quantum Theory of Real Materials.* The Springer International Series in Engineering and Computer Science. Springer US, 1996. ISBN 9780792396666.

[8] J. C. Maxwell Garnett. Colours in metal glasses and in metallic films. *Philosophical Transactions of the Royal Society of London A: Mathematical, Physical and Engineering Sciences*, 203(359-371):385–420, 1904. ISSN 0264-3952. doi: 10.1098/rsta.1904.0024.

[9] D. A. G. Bruggeman. Berechnung verschiedener physikalischer Konstanten von heterogenen Substanzen. I. Dielektrizitätskonstanten und Leitfähigkeiten der Mischkörper aus isotropen Substanzen. *Annalen der Physik*, 416:636–664, 1935. doi: 10.1002/andp.19354160705.

[10] L. D. Landau, E. M. Lifshitz, and L. P. Pitaevskiĭ. *Electrodynamics of continuous media.* Course of theoretical physics. Pergamon, 1984. ISBN 9780080302751.

[11] P. Drude. Zur Elektronentheorie der Metalle. *Annalen der Physik*, 306: 566–613, 1900. doi: 10.1002/andp.19003060312.

[12] Han-Kwang Nienhuys and Villy Sundström. Influence of plasmons on terahertz conductivity measurements. *Applied Physics Letters*, 87(1):3–012101, 2005. ISSN 0003-6951.

[13] J. M. Pitarke, V. M. Silkin, E. V. Chulkov, and P. M. Echenique. Theory of surface plasmons and surface-plasmon polaritons. *Reports on Progress in Physics*, 70(1):1, 2007.

[14] N. V. Smith. Classical generalization of the Drude formula for the optical conductivity. *Phys. Rev. B*, 64(15):155106, October 2001. doi: 10.1103/PhysRevB.64.155106.

[15] T. L. Cocker, D. Baillie, M. Buruma, L. V. Titova, R. D. Sydora, F. Marsiglio, and F. A. Hegmann. Microscopic origin of the drude-smith model. *Phys. Rev. B*, 96:205439, Nov 2017. doi: 10.1103/PhysRevB.96.205439.

[16] H. Němec, P. Kužel, and V. Sundström. Far-infrared response of free charge carriers localized in semiconductor nanoparticles. *Phys. Rev. B*, 79:115309, Mar 2009. doi: 10.1103/PhysRevB.79.115309.

[17] R. A. Dunlap. *An Introduction to the Physics of Nuclei and Particles*. Thomson/Brooks-Cole, 2004. ISBN 9780534392949.

[18] F. W. Olver, D. W. Lozier, R. F. Boisvert, and C. W. Clark. *NIST Handbook of Mathematical Functions*. Cambridge University Press, New York, NY, USA, 1st edition, 2010. ISBN 0521140633, 9780521140638.

[19] X. Leyronas and M. Combescot. Quantum wells, wires and dots with finite barrier: analytical expressions for the bound states. *Solid State Communications*, 119:631–635, August 2001. doi: 10.1016/S0038-1098(01)00288-5.

[20] G. J. Bauhuis, P. Mulder, and H. van Kempen. Tip formation of micrometer scale GaAs pyramid structures grown by MOCVD. *Journal of Crystal Growth*, 240:104–111, April 2002. doi: 10.1016/S0022-0248(02)00905-3.

[21] Y. Vorobiev, V. Vieira, P. Ribeiro, V. Gorley, P. Horley, J. González-Hernández, and T. Torchynska. Energy spectra of an electron in a pyramid-shaped quantum dot in effective mass approximation with even mirror boundary conditions. In *Proceeding of 10th WSEAS International Conference on Electronics, Hardware, Wireless and Optical Communications*, NE-HIPISIC'11, pages 127–131, Stevens Point, Wisconsin, USA, 2011. World Scientific and Engineering Academy and Society (WSEAS). ISBN 978-960-474-276-9.

[22] L. F. Shampine. Vectorized adaptive quadrature in matlab. *Journal of Computational and Applied Mathematics*, 211(2):131 – 140, 2008. ISSN 0377-0427. doi: 10.1016/j.cam.2006.11.021.

[23] U. Rössler. *Solid State Theory: An Introduction*. Advanced Texts in Physics. Springer Berlin Heidelberg, 2004. ISBN 9783540222446.

[24] T. Ostatnický, V. Pushkarev, H. Němec, and P. Kužel. Quantum theory of terahertz conductivity of semiconductor nanostructures. *Phys. Rev. B*, 97:085426, feb 2018. doi: 10.1103/PhysRevB.97.085426.

[25] M. Kazhdan, T. Funkhouser, and S. Rusinkiewicz. Rotation invariant spherical harmonic representation of 3D shape descriptors. In *Symposium on Geometry Processing*, pages 167–175, June 2003.

[26] F. Lacava. *Classical Electrodynamics: From Image Charges to the Photon Mass and Magnetic Monopoles.* Undergraduate Lecture Notes in Physics. Springer International Publishing, 2016. ISBN 9783319394749.

[27] G. B. Arfken, H. J. Weber, and F. E. Harris. *Mathematical Methods for Physicists: A Comprehensive Guide.* Elsevier, 2012. ISBN 9780123846549.

[28] I. I. H. Chen. Modified fourier-bessel series and finite spherical hankel transform. *International Journal of Mathematical Education in Science and Technology*, 13(3):281–283, 1982. doi: 10.1080/0020739820130307.

[29] N. N. Lebedev and R. A. Silverman. *Special Functions and Their Applications.* Dover Books on Mathematics. Dover Publications, 1972. ISBN 9780486606248.

[30] W. J. Thompson. *Angular Momentum: An Illustrated Guide to Rotational Symmetries for Physical Systems.* Number sv. 1 in A Wiley-Interscience publication. Wiley, 1994. ISBN 9780471552642.

[31] M. Abramowitz and I. A. Stegun. *Handbook of Mathematical Functions: With Formulas, Graphs, and Mathematical Tables.* Applied mathematics series. Dover Publications, 1964. ISBN 9780486612720.

[32] G. F. Koster. *Properties of the thirty-two point groups.* Massachusetts institute of technology press research monograph. M.I.T. Press, 1963.

[33] E. P. Wigner and J. J. Griffin. *Group Theory and Its Application to the Quantum Mechanics of Atomic Spectra.* Pure and applied Physics. Academic Press, 1959.